3. SITE 418: BERMUDA RISE[1]

Shipboard Scientific Party[2]

HOLE 418A

Date re-occupied: 21 March 1985 (2000L)

Date departed: 8 April 1985 (1348L)

Time on hole: 17 days, 17 hr, 48 min

Position: 25°02.10′N, 68°03.44′W

Water depth (sea level; corrected m, echo-sounding): 5511

Water depth (rig floor; corrected m, echo-sounding): 5520.5

Bottom of open hole (rig floor; m, drill pipe): 6389

Tools run	Sub-bottom interval (m)	Data quality
Temperature probes; water sampler	52–81, 81	Good
Temperature probes; water sampler	624–649, 649	Good
Velocity; induction; natural gamma; spherically focused log; caliper	327–788	Good
Density; porosity; spectral gamma	0–462	Poor to fair
	462–790	Good
Resistivity; natural gamma	490–785	Good
Magnetic susceptibility; conductivity	295–800	Good to poor
Three-axis magnetometer; gradiometer	465–790	Good
Multichannel sonic: Vp, Vs	365–800	Good
Borehole seismometer	343, 366, 406,	None to good
	555, 655, 755	Good
Packer	347, 465, 517	None
Borehole televiewer	344–690	Poor

Principal results: Hole 418A was reentered 8 yr after it was originally drilled to retrieve a logging tool lost in the hole on DSDP Leg 53 and to conduct logging and geophysical experiments in the well in an effort to determine for the first time the *in-situ* geophysical behavior of old oceanic basement. Although extensive bridges had developed in the uncased sediments during the interim, we succeeded in reopening the hole to total depth (868 m below seafloor [mbsf], 544 m sub-basement). The tool was not in the hole.

Because the hole was thought to have been isolated from the water column by cavings for the past 8 yr, a limited temperature-measurement and water-sampling program was conducted in the hole immediately after reentry. The temperature measurements, conducted in the sediments between 52 and 81 mbsf and in the basement between 624 and 649 m, indicate that heat transfer is conductive at the site. The water sample taken in the basement at 649 m is strongly enriched in Ca^{2+} and depleted in Mg^{2+} and K^{+}, suggesting exchange with basement water.

The hole was nearly to gauge (10 in.) throughout (which is itself unusual), allowing virtually all of the tools to operate flawlessly. The only exceptions were the deep Laterolog, which was improperly calibrated; the packer, which failed to seat; and the borehole televiewer, which caught on a ledge in the open hole, just below the pipe. The only limitations experienced were those imposed by a bridge at 399 mbsf, which required that the hole be logged in stages, and those imposed by time constraints, which prevented us from running several tools in the upper third of the basement and from logging the bottom 79 m after it was reopened toward the end of the leg.

In general, the logs confirm and refine the calculations, defined during DSDP Legs 52 and 53 on the basis of petrology, of the thicknesses of lithologic units; the log values of velocity, density, porosity, and magnetic susceptibility commonly approach or match laboratory values obtained on core material. In particular, the massive basalts of Units 9 and 10 (676–687 mbsf on the basis of logs, 672–686 mbsf on the basis of core) display average compressional wave velocities of 5.1–5.9 km/s, shear wave velocities as high as 3.3 km/s, high Vp and Vs semblance values, average densities of 2.7 and 2.9 g/cm^3, and resistivities exceeding 1000 ohm-m. On the other hand, the pillow basalts, which dominate the section, display average compressional and shear wave velocities ranging, respectively, from 4.5 to 5.4 km/s and from 2.6 to 3.3 km/s, lower values of semblance, average densities of 2.5–2.8 g/cm^3, and average resistivities of 60–350 ohm-m. Although distinct from massive basalts, the pillow basalts in Hole 418A also behave differently from pillow basalts in young crust: the velocities and densities are much higher and the porosities are lower, suggesting the infilling and sealing of interpillow voids by alteration products. Since the compressional wave velocity throughout the section matches that of Layer 2B, but the natural gamma count in the top 200 m is high, we conclude that the upper part of the section was once much more porous and represents paleo-Layer 2A. Interestingly, the boundary between this unit and the rest of the section is also marked by a thick smectite-sealed breccia (Subunit 6A), a sharp magnetic polarity reversal, and a pronounced decrease in magnetic susceptibility from an average apparent value of about 1.5×10^{-3} m cgs units to about 0.5×10^{-3} m cgs units. Below 610 m, however, the susceptibility climbs sharply again to values exceeding 2.0×10^{-3} m cgs units; several thin zones are in the range of $4.0–4.5 \times 10^{-3}$ cgs units.

In addition to conducting measurements of the borehole wall, a major two-ship seismic experiment was conducted on Leg 102 in which the R/V *Fred H. Moore* shot radial and circular lines around the site while a borehole seismometer was clamped at different levels in the hole. The objectives of the study were to determine the velocity structure of the upper crust and to determine azimuthal variations in velocity and attenuation.

---

[1] Salisbury, M. H., Scott, J. H., Auroux, C. A., et al., *Proc., Init. Repts. (Pt. A), ODP*, 102.

[2] Matthew H. Salisbury (Co-Chief Scientist), University of California, San Diego, La Jolla, CA 92093 (current address: Centre for Marine Geology, Dalhousie University, Halifax, Nova Scotia, Canada); James H. Scott (Co-Chief Scientist), U.S. Geological Survey, M.S. 964, Box 25046, Denver Federal Center, Denver, CO 80225; Christian Auroux, Ocean Drilling Program, Texas A&M University, College Station, TX 77843-3469; Keir Becker, Geological Research Division A-031, Scripps Institution of Oceanography, La Jolla, CA 92093; Wilhelm Bosum, Federal Institute for Geosciences and Natural Resources, D-3000 Hannover 51, P.O. Box 51 01 53, Federal Republic of Germany; Cristina Broglia, Lamont-Doherty Geological Observatory, Palisades, NY 10964; Rick Carlson, Department of Geophysics, Texas A&M University, College Station, TX 77843; Andrew Fisher, Rosenstiel School of Marine and Atmospheric Sciences, University of Miami, Miami, FL 33149; Joris Gieskes, Ocean Research Division—A-015, Scripps Institution of Oceanography, University of California, La Jolla, CA 92093; Mary Anne Holmes, 433 Morrill Hall, Department of Geology, University of Nebraska, Lincoln, NE 68588-0340; Hartley Hoskins, Ocean Industries Program, Woods Hole Oceanographic Institution, Woods Hole, MA 02543; Jacques Legrand, Département Systemes et Projets, IFREMER B.P. 337, Brest 29273, France; Dan Moos, Lamont-Doherty Geological Observatory, Palisades, NY 10964; Domenico Rio, Istituto di Geologia, Via Kennedy, 4, 43100 Parma, Italy; Ralph A. Stephen, Department of Geology and Geophysics, Woods Hole Oceanographic Institution, Woods Hole, MA 02543; Roy Wilkens, Earth Resources Laboratory, E34-404, Massachusetts Institute of Technology, Cambridge, MA 02139.

BACKGROUND AND OBJECTIVES

During the first 15 yr of the drilling program, significant basement penetration (>500 m) was achieved at several sites in the ocean basins, but comprehensive borehole geophysical measurements were successfully conducted at only two sites, Holes 395A and 504B, both in young crust (Table 1). These measurements have been of landmark importance. The results from Hole 504B, for example (Anderson, Honnorez, et al., 1985), demonstrate the following:

1. Layers 2A, 2B, and 2C correspond, respectively, to rubble, pillow basalts, and sheeted dikes.
2. Borehole measurements indicate that the permeability of the crust decreases by several orders of magnitude in the upper 1 km of Layer 2, in response to a tenfold decrease in porosity.
3. The formation porosity in Layers 2A and 2B (the upper 600 m of the basement) averages 10%; below this, the porosity decreases to 1%–2% (i.e., grain boundary values) in the dikes, and the relatively narrow (about 100-m-thick) dike/pillow-basalt transition zone displays intermediate values.
4. Young crust is commonly underpressured by 1–10 bars. Temperature measurements conducted in Hole 504B at different times during drilling indicate that seawater was flowing down the hole into permeable aquifers in the upper basement at rates decreasing from 7000 to 150 L/hr over a period of 3.5 yr. Modeling studies suggest that underpressures measured in the crust are dynamically maintained by convection.
5. Convection in the basement near Hole 504B is confined to the high-permeability zone near the top of the extrusive material; in the dikes, where fracture porosity approaches zero, temperature gradients imply conductive heat flow.
6. The velocity structure of Layer 2 is controlled not by petrology but by variations in porosity with depth.
7. The maximum horizontal compressive stress, sigma 1, is realigned subperpendicular to the ridge axis in relatively young crust.

Similarly, the measurements conducted in Hole 395A, although less extensive, confirm that the extrusive material is underpressured and extremely porous and that the permeability is negligible below 500 m sub-basement.

Although it is tempting to extrapolate these results to the ocean crust as a whole, we must remember that they were taken exclusively on young crustal sites. Strong evidence exists (Houtz and Ewing, 1976) that old crust is profoundly different (the absence of Layer 2A and the predominance of conductive heat flow) from young crust, but, before Leg 102, no comparable set of borehole geophysical measurements had been made in old crust (that from Hole 462A, though old, is not considered representative of old crust because the basement section drilled consists of Cretaceous sills).

Leg 102 was planned for reentry of one of the two deep basement holes (Hole 417D or 418A) drilled on Legs 51–53 in 110-m.y.-old crust in the western Atlantic (Donnelly et al., 1979; Figs. 1–4). These sites, plus Sites 395 and 396, were drilled as

Table 1. DSDP holes penetrating more than 500 m into basement.

Leg	Hole	Basement penetration (m)	Age (Ma)	Borehole measurement	Quality[a]	References
37	332B	583	3.5	—		Aumento, Melson, et al., 1977
45, 78B	395A	580	7	T-probe	G	Melson, Rabinowitz, et al., 1978
				Water samples	P	Hyndman, Salisbury, et al., 1984
				[b]HRT, delta T	G	
				Caliper	G	
				Density	F	
				Natural gamma	G	
				P-wave velocity	P	
				Resistivity	G	
				Porosity	P	
				Magnetometer	G	
				Susceptibility	G	
				Televiewer	F	
				Packer	G	
				Seismometer	G	
52, 53	418A	544	110	—		Donnelly et al., 1980
61, 89	462A	645	115	Caliper	G	Larson, Schlanger, et al., 1981
				Porosity	G	Moberly and Schlanger, in press
				Natural gamma	F	
				P-wave velocity	G	
				HRT	G	
69, 70	504B	1075	5.9	T-probe	G	Cann et al., 1983; Honnorez,
83, 92				Water sample	G	Von Herzen, et al., 1983;
				HRT, delta T	G	Anderson, Honnorez, et al., 1985;
				Caliper	G	Leinen and Rea, in press
				Density	F	
				Natural gamma	F	
				P-wave velocity	G	
				Resistivity	G	
				Porosity	G	
				Large resistivity	G	
				Seismometer	G	
				Packer	G	
				Televiewer	F	
				Magnetometer	G	

[a] G = good, F = fair, P = poor.
[b] High resolution temperature.

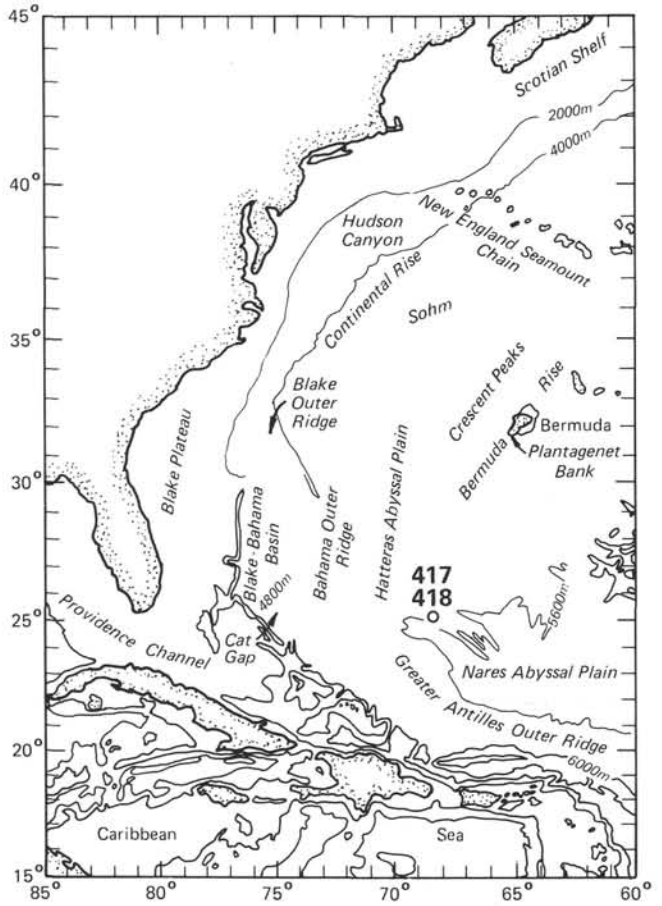

Figure 1. Location of DSDP Sites 417 and 418.

part of a basement-age transect during the early years of the International Phase of Ocean Drilling (IPOD). The objective on Leg 102 was to acquire a comprehensive base-line suite of borehole geophysical data in old oceanic crust. The following were specific scientific objectives of Leg 102:

1. To determine *in-situ* velocity structure at a site in old crust. To determine whether Layers 2A, 2B, and 2C are present and whether they correspond to the same lithologies as in Hole 504B.
2. To determine the permeability of old oceanic crust.
3. To determine the porosity-vs.-depth function of the site. These data, together with those from Hole 504B, were thought to make possible determination of whether or not the extrusive section has become sealed by alteration products and to determine the porosity–permeability and porosity–velocity systematics for Layer 2.
4. To determine the thickness of the magnetic layer in old crust.
5. To determine whether or not convection and underpressures persist in old crust.
6. To sample and determine the chemistry of water in equilibrium with old basement.
7. To determine the direction and magnitude of *in-situ* stress.
8. To determine the temperature profile in old crust and thus infer whether heat transfer in old oceanic basement is by convection or conduction.
9. To determine the eruptive history of the Layer 2 extrusive pile from variations in magnetic susceptibility and natural remanent magnetization (NRM) intensity, inclination, and declination vs. depth.
10. To determine the magnitude, direction, and origin of seismic anisotropy in Layer 2.
11. To determine whether or not sub-basement seismic reflectors are present in the crust.

Consequently, the ship returned to Hole 418A, which was drilled through sediments, pillow basalts, massive basalts, and into the top of the dike transition zone to a sub-basement depth of 544 m on Legs 52 and 53 (see Fig. 4 and Tables 2 and 3), and which was thought to contain a lost logging tool in overlying sediments. If the tool could be retrieved, a suite of experiments similar to those run in Hole 504B would be run in Hole 418A. A further objective of the leg also would then have been achieved: the reopening of a second deep basement hole, similar to Hole 504B but in old crust, for eventual deepening. Finally, we planned to run a downhole bit-motion indicator on the logging line in conjunction with the ship's heave sensor to determine the amount by which the logging line had to be heave-compensated.

Specifics of the experiments scheduled at 418A included the following:

Conventional logging (Lamont-Doherty Geological Observatory/Schlumberger). Standard industry tools were to be run to determine the velocity, density, porosity, resistivity, and natural gamma radioactivity structure of the section. Tools and instrumentation that were operated and that were available included the following: (1) long-spaced sonic (first-arrival delta-t, full waveform), (2) dual induction, (3) spherically focused resistivity, (4) compensated gamma-gamma density, (5) compensated neutron porosity, (6) caliper, (7) natural gamma-ray (spectral and total count), (8) Laterolog, (9) pore-fluid sampler, and (10) injection flowmeter (tracer).

Multichannel sonic logging (Lamont-Doherty Geological Observatory). A 12-channel sonic tool was to be run to determine the propagation characteristics of compressional, shear, and Stoneley waves in the section.

Vertical seismic profile/oblique seismic experiment (Woods Hole Oceanographic Institution). A combined vertical seismic profile (VSP)/oblique seismic experiment (OSE), using a three-component borehole seismometer, air gun, and explosive sources and the R/V *Fred H. Moore* as the shooting ship, was to be conducted to determine interval velocities, compressional and shear wave velocity gradients, seismic anisotropy, attenuation, and the presence of sub-basement reflectors near the site. This was to be the first full-scale test of VSP technology by the Ocean Drilling Program. In addition, the R/V *Fred H. Moore* was to conduct an extensive seismic-reflection survey near the hole so that the OSE data might be corrected for topography.

Large-scale resistivity experiment (Scripps Institution of Oceanography). This experiment was to be run to determine the large-scale porosity of the crust.

Packer tests (Scripps Institution of Oceanography). Packer tests were to be run at several depths in the hole to determine permeability, pore pressure, and *in-situ* stress. This was to be the first full-scale use of a straddle packer in the drilling program.

Borehole televiewer observations (Lamont-Doherty Geological Observatory). A borehole televiewer (BHTV) was to be run downhole to observe mesoscopic features, such as fractures and dikes in the borehole wall, and to determine the orientation of the *in-situ* stress field from breakouts.

Three-axis magnetometer measurements (Bundesanstalt für Geowissenschaften und Rohstoffe). A three-axis gyroscope-oriented borehole magnetometer was to be run to determine the vertical field intensity, the natural remanent magnetization, and the magnetic inclination and declination vs. depth in the hole. This tool also was to provide a borehole-drift survey as a byproduct of probe-orientation measurements needed for analysis of the magnetometer measurements.

Magnetic-susceptibility measurements (U.S. Geological Survey). A magnetic-susceptibility tool was to be run downhole to study susceptibility vs. depth and alteration in the crust.

Temperature–heat-flow measurements (Texas A&M University). The Von Herzen hydraulic piston core (HPC) heat-flow tool and the Barnes/Uyeda tool were to be deployed to measure the temperature gradient

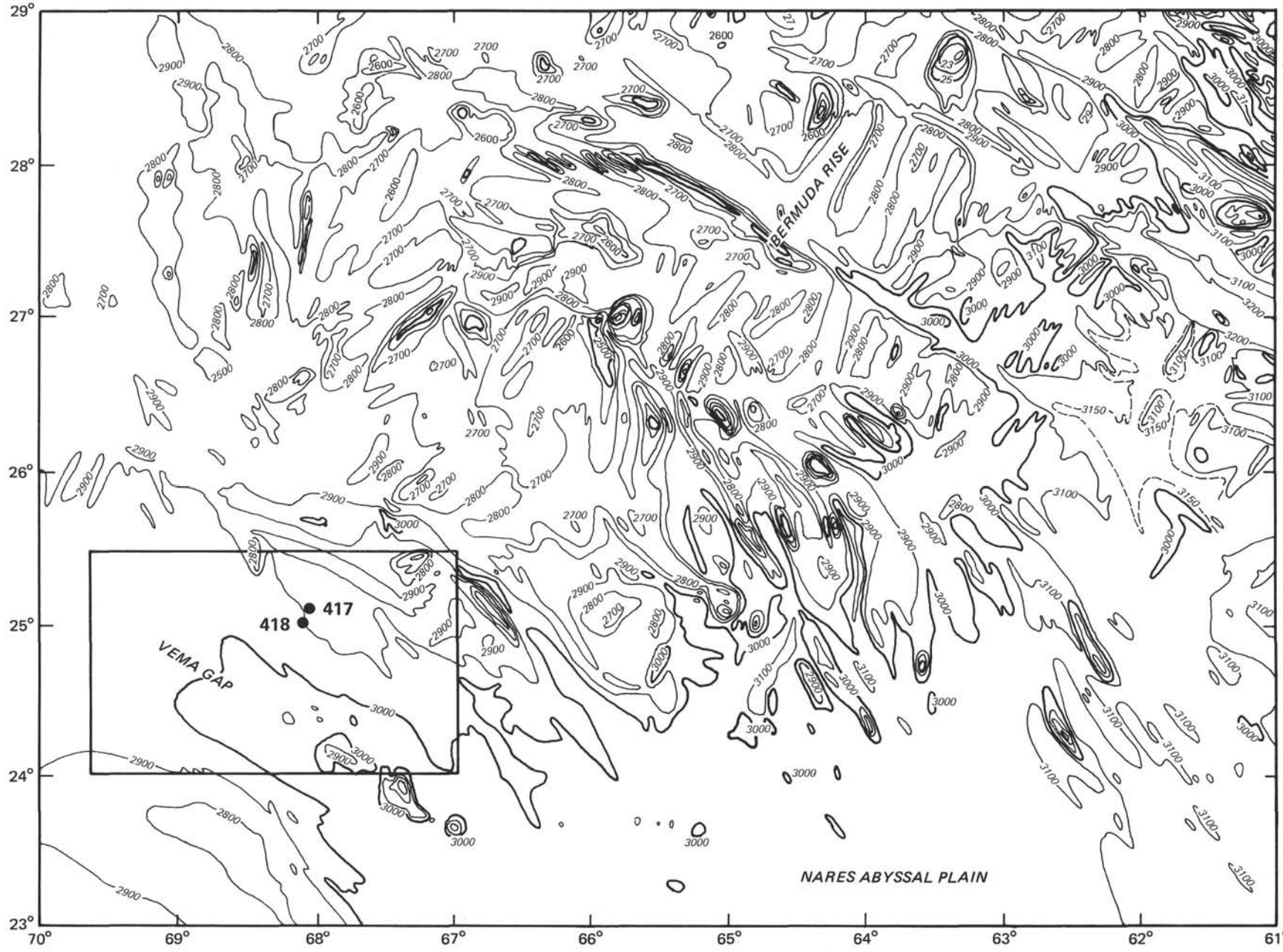

Figure 2. Bathymetric map of the southern part of the Bermuda Rise (after Vogt and Johnson, 1971). Depths are in units of 1/400-s traveltime (nominal fathoms).

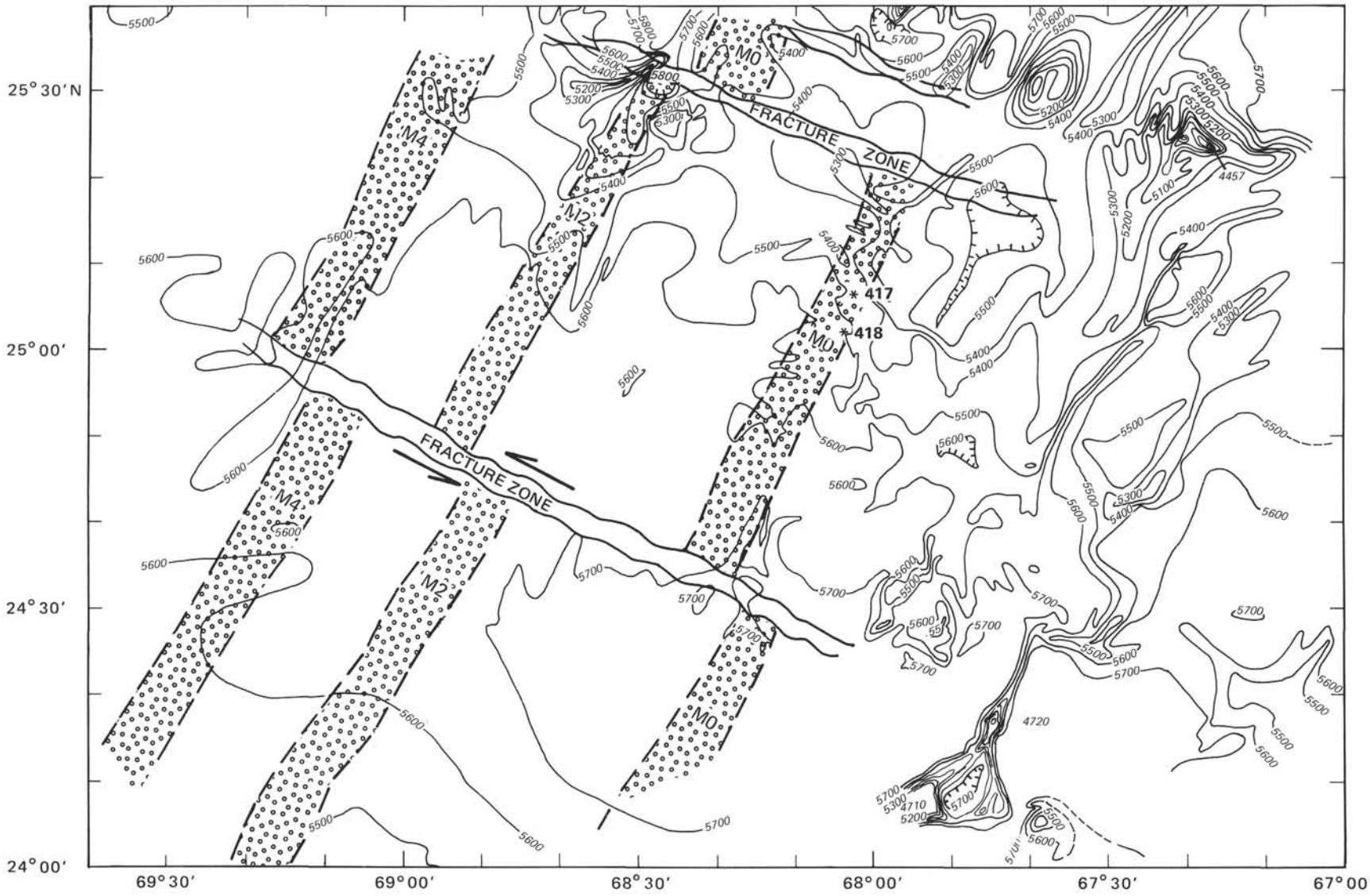

Figure 3. Bathymetry and positions of magnetic source bodies near Sites 417 and 418 (Rabinowitz et al., 1979). Depths contoured in 100-m intervals.

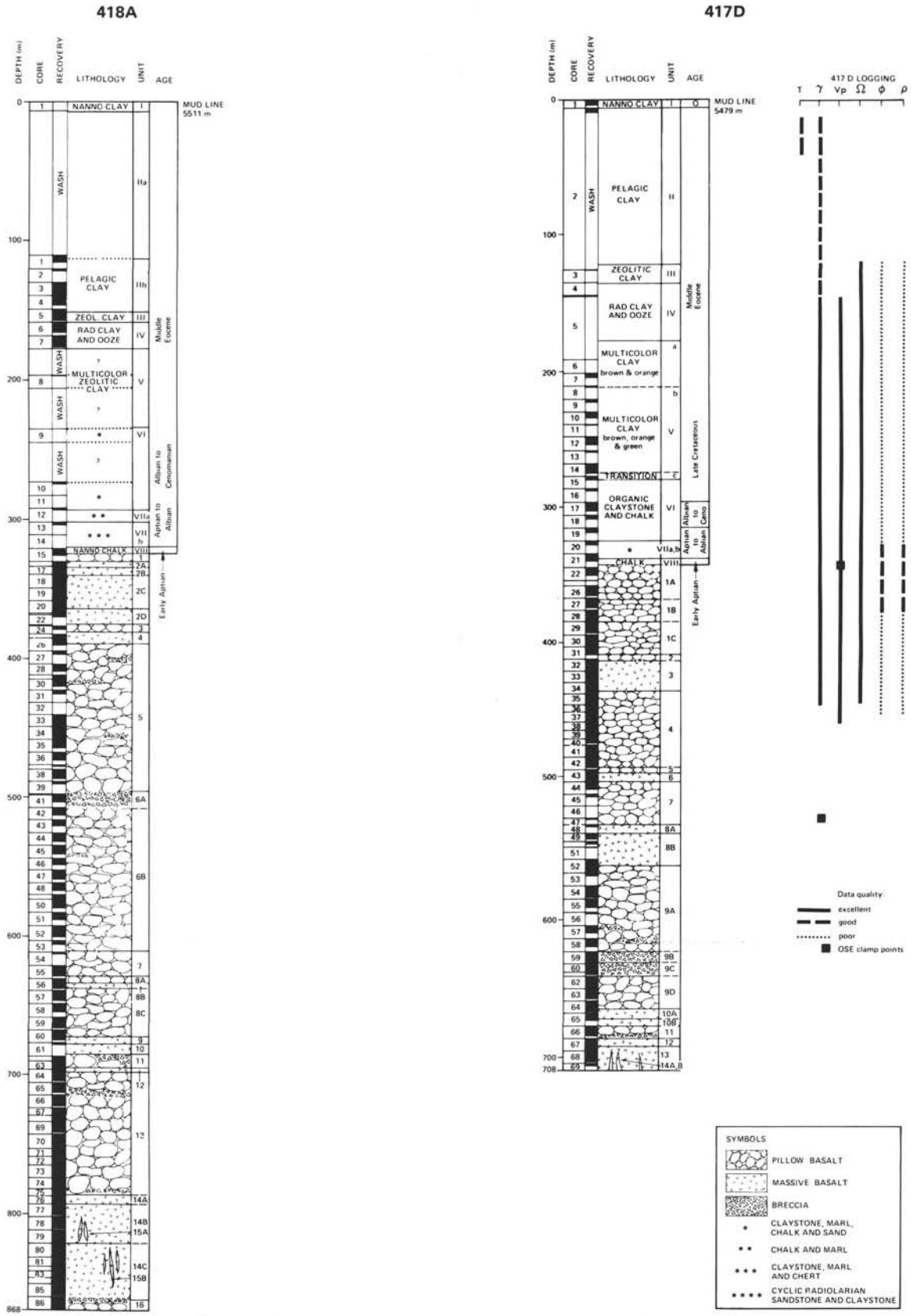

Figure 4. Lithology vs. depth in Holes 417D and 418A (from Donnelly et al., 1980). Shown also are the intervals logged in Hole 417D on Leg 51 and the positions of the geophone during the oblique seismic experiment on DSDP Leg 52. T, γ, Vp, Ω, ϕ, and ρ stand for the temperature, natural gamma-ray, velocity, resistivity, porosity, and density logs, respectively.

Table 2. Sedimentary lithologic units—Site 418 (Donnelly et al., 1980).

Unit/ subunit	Lithology	Chronostratigraphy	Holes 418 and 418A			Hole 418B		
			Depth (mbsf)	Thickness (m)	Core, section, interval	Depth (mbsf)	Thickness (m)	Core, section, interval
I	Brown pelagic clay with nannofossil horizons (10YR 4/2)	Quaternary	[a]0.0–6.0	6.0	418-1	0–16.3	~16.3	418B-1 418B-2
II	Pelagic clay: Yellow brown to pale yellow gray, grayish orange (10YR 7/4) to light olive brown (2.5Y 5/4)	Miocene/Oligocene(?)	[b]111.0–151.2 or 6.0–151.2	40.2(?) or 145.2 to base of Core 1	418A-1 to 418A-2	16.3–139.1	122.8	418B-3-1 to 418B-15, CC
IIA	Yellow brown					16.3–73.3	57	418B-3-1 to 418B-8, CC
IIB	Pale orange					73.3–139.1	65.8	418B-9-1 to 418B-15, CC
III	Dark gray brown pelagic clay Some pale zeolitic interbeds	?	151.2–159.3	~8.1	418A-5-2 to 418A-6-1	139.1–158	18.9	418B-16-1 to 418B-17, CC
IV	Dark gray brown to red brown pelagic clay with radiolarians (2.4Y 4/2)	Middle Eocene	159.3–177.5	~18.2	418A-6-1 to 418A-7, CC	158.0–177.2	19.2	418B-18-1 to 418B-19, CC
VA	Dark gray brown to red brown pelagic clay (5YR2 5/2)	?	[c]177.5–206	~29.0	418A-7, CC to 418A-8, CC	177.2–196.3	19.1	418B-19, CC to 418B-21, CC
VB	Multicolored zeolite clay Pale orange, brown to pale green	Upper Cretaceous	[c]—			196.3–236	39.7	418B-22-1 to 418B-26-1, 90 cm
VI	Green, black, light to olive gray, blue green claystones, marls, nannofossil chalks, and radiolarian sands including pyrite, chert, and organics (black-clay facies)	Albian to Cenomanian	[d]234.5–291.0	~56.4	418A-9 to 418A-11, CC	236–291.6	55.6	418B-26, CC to 418B-32-1, 20 cm
VII	Pale to dark red brown, pink, and pale green Radiolarian claystones, clays, marls, and nannofossil chalks and black to green clay including chert	Upper Aptian to Albian	[e]291.5–324.0	~32.5	418A-12-1 to 418A-15-1	[e]291.6–319.5	28.1	418B-32-1, 30 cm to 418-34-1, 60 cm
VIIA	Pale to dark red brown nannofossil chalks to radiolarian marls	Upper Aptian to lower Albian	291.5–303.3	11.8	418A-12-1 to 418A-13-2, 80 cm	291.6–301.6	10	418B-32-1, 30 cm to 418B-33-1, 60 cm
VIIB	Black and green claystones, marls, and chert		303.3–320.0	16.7	418A-13-2, 80 cm to 418A-14, CC	[e]301.6–319.5 (311.1)	18.1 (9.5)	418B-33-1, 60 cm to 418B-34-1, 60 cm
VIII	Gray nannofossil chalk	Lower Aptian	[e]323.8–324.0 or (320.0–320.2)	20 cm recovered above basalt	418A-15-1, 0–20 cm		Not recovered	
IX	Basalt with interpillow limestone							

[a] Core 1 at Hole 418; no coring until 111 mbsf at Hole 418A.
[b] No coring before 111 mbsf.
[c] Washed intervals = 177.5–196.5 = 19 m; 206–234.5 = 28.5 m.
[d] Washed after 244.0 to 272.5 = 28.5 m.
[e] Based on driller's depth to basalt.

Table 3. Basement lithologic units, Hole 418A, from results of Legs 52 and 53 (Donnelly et al., 1980).

Unit/ subunit	Top[a] (mbsf)	Base[a] (mbsf)	Thickness (m)	Type of cooling unit	Phenocryst assemblage[b]	Interval (core, section, cm)
1	324.0	329.6	5.6	Pillow basalt	Plag-(Oliv)	15-1, 20 to 16-1, 10
2A	329.6	331.7	2.1	Massive basalt	Plag-(Oliv)	16-1, 10 to 16-2, 105
2B	331.7	339.0	7.3	Massive basalt	Plag-(Oliv)	16-2, 105 to 17-4, 150
2C	339.0	363.1	24.1	Massive basalt	Plag-(Oliv)	18-1, 0 to 20-5, 81
2D	363.1	376.6	13.5	Massive basalt	Plag-(Oliv)-[Cpx]	20-5, 81 to 24-1, 57
3	376.6	383.3	6.7	Pillow basalt	Plag-(Oliv)-[Cpx]	24-1, 57 to 25-2, 60
4	383.3	387.1	3.8	Massive basalt	Plag-(Oliv)-[Cpx]	25-2, 60 to 26-2, 110
5	387.1	498.5	111.4	Pillow basalt and breccia	Plag-(Oliv)-[Cpx]	26-2, 110 to 40-3, 47
6A	498.5	510.5	12.0	Breccia	Plag-Oliv-(Sp)-[Cpx]	41-1, 0 to 42-2, 150
6B	510.5	611.0	100.5	Pillow basalt	Plag-Oliv-(Sp)-[Cpx]	42-3, 0 to 53-3, 150
7	611.0	629.2	18.2	Pillow basalt	Plag-Oliv-Cpx	54-1, 0 to 55-7, 70
8A	629.2	632.9	3.7	Pillow basalt	Plag-Oliv-Cpx	55-7, 70 to 56-3, 45
8B	632.9	636.3	3.4	Massive(?) basalt	Plag-Oliv-Cpx	56-3, 45 to 56-5, 125
8C	636.3	671.8	35.5	Pillow basalt	Plag-Oliv-Cpx	56-5, 125 to 60-4, 33
9	671.8	676.5	4.7	Massive, vesicular basalt	Plag	60-4, 33 to 60-6, 66
10	676.5	686.0	9.5	Massive basalt	Plag	61-1, 0 to 61 bit, 95
11	686.0	695.5	9.5	Pillow basalt	Plag-Cpx-Oliv	62-1, 0 to 63-5, 119
12	695.5	698.2	2.7	Massive(?) basalt	Plag-Cpx-Oliv	64-1, 0 to 64-2, 122
13	698.2	786.5	88.3	Pillow basalt and breccia	Plag-Cpx-Oliv	64-2, 122 to 75-4, 150
14A	786.5	793.6	7.1	Massive basalt	Plag-Cpx-Oliv	75-5, 0 to 77-1, 50
14B	793.6	821.5	27.9	Massive basalt	Plag-Cpx-Oliv	77-1, 50 to 79-7, 124
14C	821.5	859.8	38.3	Massive basalt	Plag-Cpx-Oliv	80-1, 0 to 86-1, 25
15A	[c]—	—	—	Basalt dikes	Plag-Oliv-Cpx	79-1, 75 to 79-1, 110 79-2, 78 to 79-2, 105 79-3, 105 to 79-4, 95
15B	—	—	—	Basalt dikes	Plag-Oliv	80-2, 117 to 80-3, 127 80-4, 2 to 80-4, 42 80-4, 107 to 80-5, 110
16	859.8	868.0	8.2	Pillow basalt and breccia	Plag-Oliv-Cpx-Sp	86-1, 25 to 86-6, 55

[a] Depths corrected for spacers.
[b] Plag = plagioclase; Oliv = olivine; Cpx = clinopyroxene; Sp = spinel.
[c] Undetermined.

in the basement and, if time allowed, in the sediments adjacent to the hole. The temperature data also were to be used to determine whether or not water is flowing down the hole. For measuring very low flow rates, the Schlumberger tracer was to be used.

Water sampling (Scripps Institution of Oceanography). A sediment bridge near the sediment/basement contact in Hole 418A was thought to have sealed off the basement from bottom-water invasion since the time 8 yr earlier when the hole was drilled. If the logging tool could be removed and the bridge penetrated, the Barnes sampler and/or the Schlumberger sampler was to be used to collect samples of water in equilibrium with the basement.

Downhole bit-motion indicator (Texas A&M University). The JOIDES Downhole Measurements Panel had expressed concern that drill-ship motion would degrade logging data obtained from the *JOIDES Resolution*. To assess the magnitude of the problem, a downhole bit-motion indicator (DBMI) developed by DSDP was to be deployed on the end of the wireline and monitored at the same time as the ship's heave sensor. The tool also was to be attached to the BHTV so that the televiewer data could be corrected.

If Hole 418A could not be reopened, the ship was to proceed to Hole 417D, which was still presumed to be open to 270 m sub-basement, and the same experiments would be performed there. (A limited downhole-measurements program was attempted in Hole 417D during Legs 51 and 52, but only the oblique seismic experiment and two logging runs near the top of the hole were successful.)

OPERATIONS

The *JOIDES Resolution* departed Miami, Florida, at 0815 local time (L) on 19 March 1985 and began steaming at full speed toward Site 418 after clearing the harbor entrance. We deployed no underway geophysical gear since it would have only slowed the ship when the time was needed on site and since the R/V *Fred H. Moore* would be surveying in our wake. The ship traveled without incident at an average speed of 12.7 kt until 0515L on 21 March, when the ship was slowed to about 6 kt to acquire several satellite navigation passes on the final approach to the site. At 1633L, a 15.5-kHz beacon was released as the ship passed over the site, but the beacon died within 20 min, causing us to lose position. By dead reckoning and monitoring the water depth, however, we were able to stay approximately on station until a new satellite pass at 2000 hr indicated that we had drifted 2 mi to the northwest. We then steamed to the new location, dropped a 14.5-kHz beacon, and began making up a bottom-hole assembly (BHA).

At 0645 hr on 22 March, after offsetting the ship 4000 ft to the west on the basis of integrated satellite navigation data and making several repairs on the rig floor, we started to lower the pipe. At 0300 hr on 23 March, the pipe was on bottom, and we started to rig up the Mesotech reentry tool. The tool was started down the pipe at 0700 hr and appeared to be operating properly until it hit an obstruction at 5473 m in the telescopic section of the BHA (bumper sub). During attempts to retrieve the tool, it became caught in a transition stand of 5½-in. pipe, and the wireline parted at the weak point of the cable head. The tool, subsequently recovered on the sand line, was damaged but operable. After testing the pressure integrity of the pipe with a hydraulic bit release (HBR) go-devil, we rigged up an EDO sonar tool and started it down the pipe at 0200 hr on 24 March. When the tool reached bottom and scanning was initiated at 0650 hr, the reentry cone was observed at a range of 270 m. At 0900 hr,

while positioning to reenter, we lost rotation of the EDO and had to recover the tool. A second EDO tool was rigged and lowered down the pipe at 1330 hr. Scanning was initiated at 1645 hr, and the cone was stabbed at 1823 hr, when the tool was recovered and reentry verified by lowering an additional stand.

Between 2145 and 0300 hr on 25 March, the pipe was lowered into the casing without pumping, and a series of temperature measurements was made in the bottom of the casing and out through the end, using a combined HPC/Barnes-Uyeda probe at sub-bottom depths of 52, 62, 72, and 81 m (Fig. 5 and Table 4). In addition, a water sample was taken at 81 m. During this operation, we noted that the bit began to take weight just before leaving the casing, suggesting that the uppermost sediments had sloughed into the hole.

After the temperature run was completed, the hole was cleaned to 6142 m below rig floor (mbrf), the last 20 m without rotation or circulation to minimize thermal disturbance of the water column. Tight spots were encountered between 5734 and 5776 m, but the hole was open below 5776 m. Between 0330 and 0645 hr on 26 March, a second temperature run was made in the basement at sub-bottom depths of 624, 634, 644, and 649 m, and a water sample was taken at the last station in an attempt to acquire a sample that had been isolated from seawater and had begun to exchange with water in the basement or to react with the basalt when the sediments slumped into the hole at the end of Leg 53.

Upon completion of the temperature run, the hole was cleared to 6332 mbrf (812 m sub-bottom, 488 m sub-basement), where solid contact was made with an obstruction in the hole, yet circulation was not lost. On the assumption that we had finally made contact with the lost tool and that a wad of cable was obstructing the hole, we decided to log the hole from a point 42 m above the sediment/basalt contact (282 mbsf) to 32 m above the obstruction, an interval that encompassed all the basalt except the top of the dike-transition zone. Since some of the old logging cable could have spiraled in the hole above the lost tool, we decided to run the magnetic-susceptibility tool first because it could sense the cable, if present. After some jockeying of drill pipe to get the susceptibility probe rigged up, we started the tool down the pipe at 1625 hr and logged downhole in moderate seas from 295 to 337 mbsf, or 13 m sub-basement, where a bridge stopped the tool unexpectedly. We then pulled in the logging tool, ran in two stands, cleaned the hole, and pulled back a stand so that the bottom of the pipe was just below the sediment/basalt contact. At 0535 hr on 27 March, we picked up the susceptibility tool again and lowered it to 5990 mbsl (480 mbsf), where it lodged on another bridge about one-third of the way into the basement. We then logged uphole from 5990 to 5831 m, or just above the basement, by pulling in a stand, and then we brought the tool back to the surface.

Since the susceptibility tool was relatively short and light, we next decided to run a heavier, longer tool and try to push through the bridge. The Schlumberger sonic-induction-SFL-caliper-natural-gamma combination tool was accordingly rigged up and started down the hole at 1245 hr, but it also stopped at 480 mbsf at the same bridge, so we logged uphole to 327 mbsf and then recovered the tool. It should be noted that although mud had occasionally been used to clean the hole, mud-cake accumulation was probably minimal since we pumped after each pull.

During these operations, the R/V *Fred H. Moore* arrived on site at 1820 hr to begin reflection profiling near the hole in preparation for the oblique seismic experiment. A small amount of equipment was transferred between ships, but no personnel could be transferred because of a heavy swell.

Since the hole was known to be open below the bridge to a depth of 6332 mbrf (812 mbsf), we cleaned the hole to the bottom from 2130 to 0330 hr on 28 March and then raised the pipe to 6004 m so that we could log the bottom two-thirds of the hole with impunity and then raise the pipe by a stand to log through the bridge. When this operation was completed, we logged the interval from 5975 to 6298 mbsl with the sonic-induction-SFL-caliper-natural-gamma tool, going downhole and uphole from 6298 to 5968 m between 0330 and 1115 hr. We then logged the interval from 5972 to 6300 m in the same fashion with the gamma-gamma-density-neutron-porosity-spectral-gamma-ray tool between 1115 and 2100 hr. When the tool reentered the pipe, however, we continued to log through the pipe wall to the mud line before pulling the tool out of the hole.

After the Schlumberger nuclear tool was on deck, we rigged up the BGR three-axis magnetometer, oriented the gyroscope with respect to the ship's heading, and started the tool down the hole at 2100 hr. The hole was logged downhole from 6004 to 6300 m, the vertical component being recorded continuously, and all three components being recorded in the stationary mode at 5-m intervals. Short repeat sections were recorded at selected intervals on the way up, and the section straddling the bridge from 6004 to 5975 m was logged in the continuous and stationary modes after the pipe was raised by one stand. After the tool was received on deck at 1500 hr on 29 March, the orientation of the gyroscope with respect to the ship's heading was recorded, and the gyroscope was allowed to stop before releasing the tool. During this operation, Ralph Stephen transferred over from the R/V *Fred H. Moore* to begin setting up the oblique seismic experiment.

Between 1500 and 2345 hr, the Schlumberger dual Laterolog was rigged up and the hole logged uphole from 6295 to 6000 mbsl. Owing to a misunderstanding concerning the depth of the pipe, the tool was inadvertently left on after it was brought into the pipe, resulting in damage to the tool. Although the data acquired before this incident were unaffected and appear to be reasonable, a calibration check immediately before logging up the hole indicated that the deep Laterolog was operating just outside of specifications.

Once the Laterolog was on deck, the LDGO multichannel sonic tool was rigged up and run in to 6310 mbsl. The tool was then logged uphole to 5875 m, tripped to the surface, and rigged down by 0745 hr on 30 March. We then rigged up the U.S. Geological Survey magnetic-susceptibility tool again and logged going downhole from 6004 to 6310 m, where the tool took weight. Because no wire in the hole was detected, we concluded that approximately 12 m of fill had fallen to the bottom of the hole and covered the tool since the beginning of logging. We then pulled a stand of pipe, logged uphole to 5975 m, and then logged down again to 6004 m to determine whether the bridge, which had stopped the tool previously at 5990 m, was still present. Since no bridge was detected, we concluded that subsequent operations could be run with the bottom of the pipe set just below the sediment/basalt contact. We then brought the tool back to the surface, where it arrived on deck at 1600 hr, and pulled out of the hole to 5859 mbrf.

Between 1815 and 2100 hr, we rigged up the Woods Hole borehole seismometer and ran it past the bridge to 6265 mbsl, where it was clamped in the hole. After several hours of troubleshooting and monitoring test shots from the R/V *Fred H. Moore*, we began recording the first of the planned seismic lines (pattern 1, Fig. 6) at 2300 hr. Between 2300 hr on 30 March and 0231 hr on 1 April, we shot patterns 1 and 2, using 15-lb explosives every 3 min, and patterns 3 and 4, firing two 2000-in.^{3} air guns once per min. We then unclamped the tool, raised it to 6165 m, and reshot the pattern shown in Figure 6 between 0300 hr on 1 April and 0330 hr on 2 April, the sole difference being that the 6-km circle in pattern 3 was shot using air guns instead of explosives. After raising the tool to 6065 m, we shot the pattern once again between 0409 and 0845 hr on 3 April.

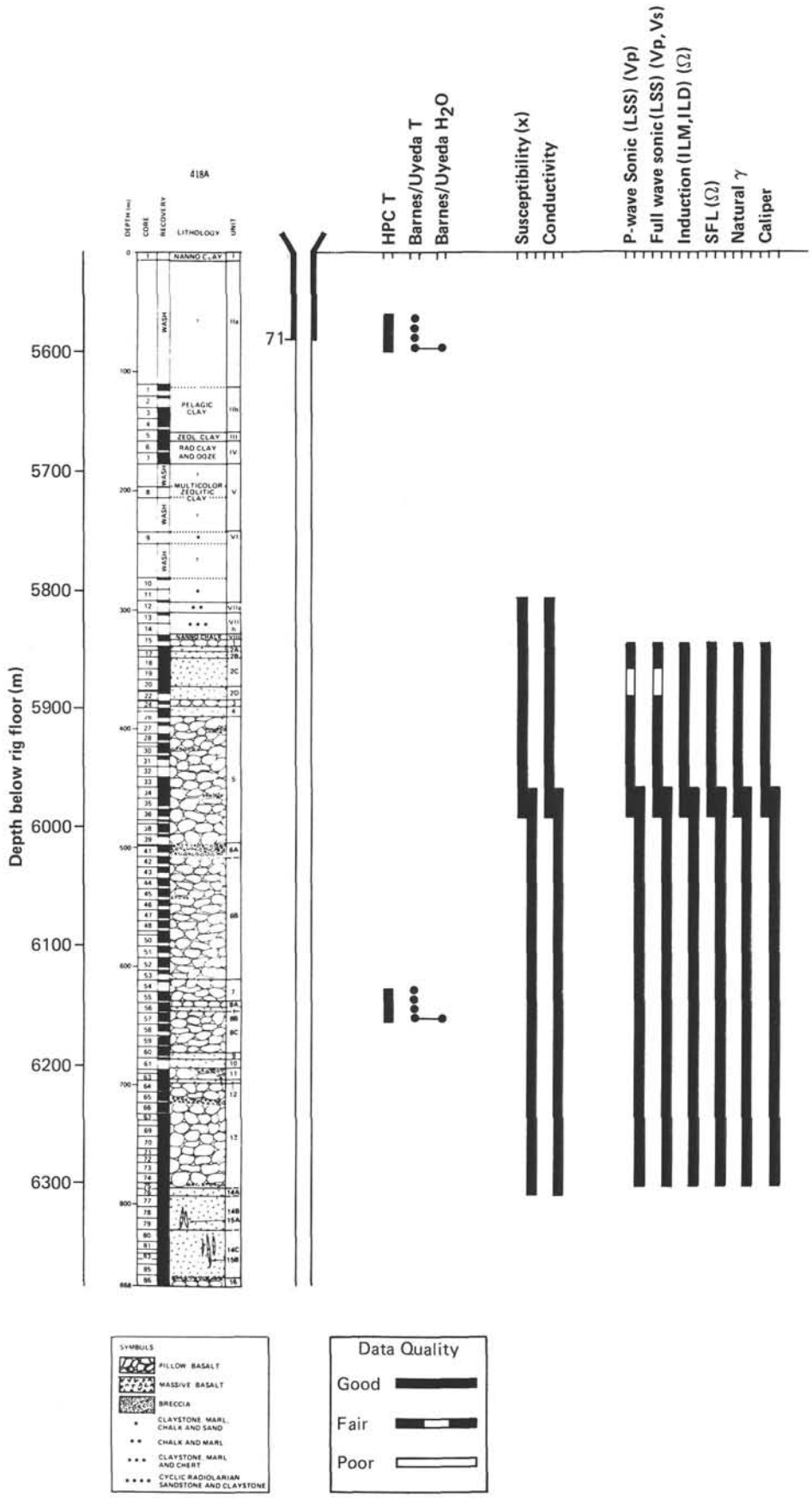

Figure 5. Leg 102 downhole-operations summary.

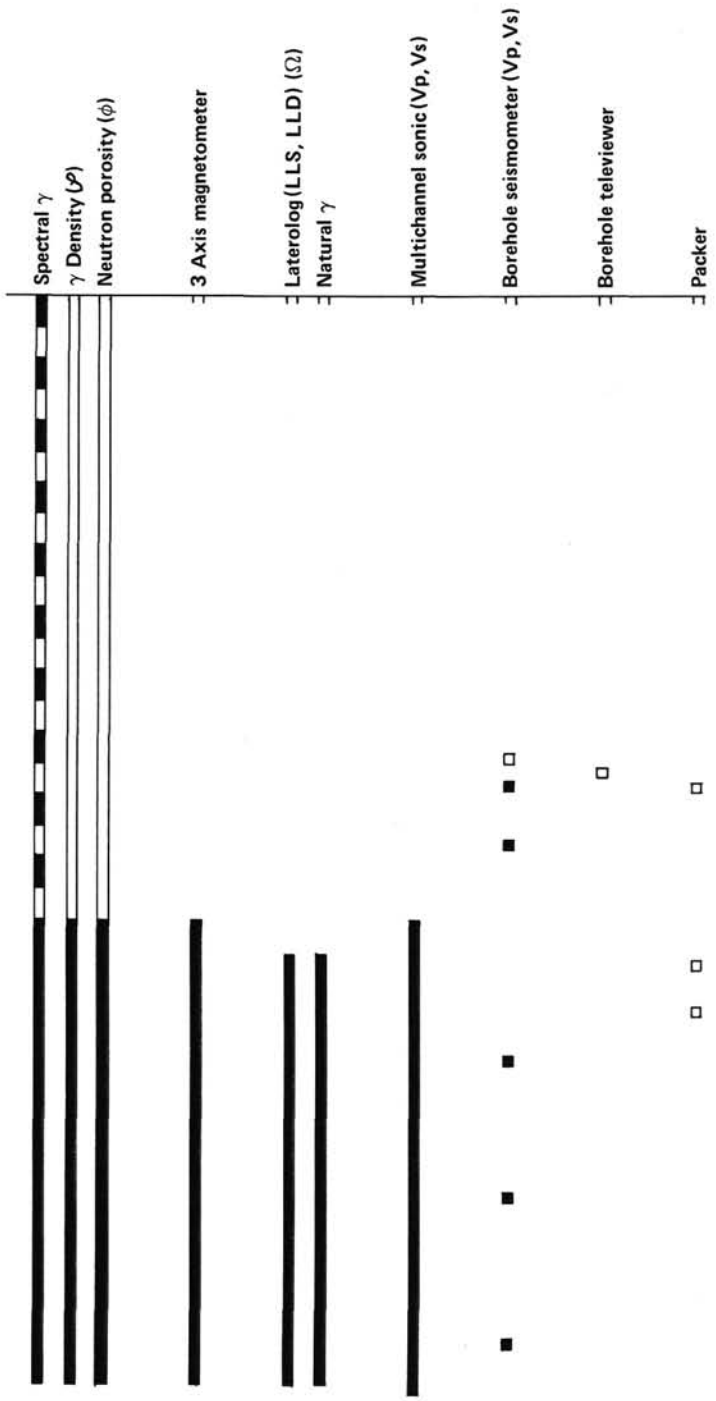

Figure 5 (continued).

After shooting to the three-deep positions had been completed, the seismometer was raised to 5916 m, and pattern 3 minus the 65°–245° and 155°–335° lines was shot using air guns, and pattern 2 was shot using explosives. At 2034 hr, the tool was raised to 5876 m, where a 6-km-radius circle (the inner circle of pattern 2) was shot using explosives. The 20°–200° line in pattern one was then shot to 10 km using explosives until 0026 hr on 4 April. The tool was then raised to 5853 m, or just below the bottom of the pipe, where a short developed in the cable; thus, we brought the tool to the surface. When the tool came on deck at 0430 hr, we found that a kink had developed in the torpedo, probably in response to pipe heave.

Since only a few hours remained of the time allotted for the oblique seismic experiment, and it was estimated that the time would be largely consumed by tool trips, repairs, and calibration if we attempted to relower the borehole seismometer, we decided to terminate the seismic experiment and fish the Leg 53 sonic tool from the hole before tripping the pipe to the surface for the packer. Accordingly, we lowered the pipe to 6303 mbrf and then washed past 6332 m, where the bit had taken weight

Table 4. Leg 102 downhole-operations summary, Hole 418A.

Run	Date	Time (hr)	Depth below rig floor (m)	Depth (mbsf)	Logging direction	Tool/test[a]	Data quality	Remarks
HPC temperature probe-Barnes/Uyeda temperature probe-water sampler								
1	3/24/85	2145-2400	[b]5571-5600	52-81	Down	HPC temperature	Good	
						Uyeda temperature	Good	
	3/25/85	0000-0300				Barnes water sampler	Good	Sampled at 81 m
2	3/26/85	0330-0645	[b]6143-6167	624-649	Down	HPC temperature	Good	
						Uyeda temperature	Good	
						Barnes water sampler	Good	Sampled at 649 m
USGS magnetic susceptibility tool								
1	3/26/85	1625-2400	[c]5805-5847	295-337	Down	Susceptibility	Good	Tool temperature
	3/27/85	0000-0320				Conductivity	Poor	too low
2	3/27/85	0535-1200	[c]5831-5990	321-480	Down, up	Susceptibility	Good	Tool temperature too
						Conductivity	Poor	low (down only)
Downhole logging								
1	3/27/85	1245-2130	[c]5837-5990	327-480	Up	Vp	Good	
						Sonic waveform	Good	
						ΩILM	Good	
						ILD	Good	
						SFL	Good	
						γ	Good	
						Caliper	Good	
2	3/28/85	0330-1115	[c]5968-6298	458-788	Down, up	Vp	Good	
						Sonic waveform	Good	
						ΩILM	Good	
						ILD	Good	
						SFL	Good	
						γ	Good	
						Caliper	Good	
3	3/28/85	1115-2100	[c]5510-5972	0-462	Up	Spectral γ	Fair	Through pipe
			5972-6300	462-790	Down, up		Good	
			5510-5972	0-462	Up	γ-density	Poor	Through pipe
			5972-6300	462-790	Down, up		Good	
			5510-5972	0-462	Up	Neutron porosity	Poor	Through pipe
			5972-6300	462-790	Down, up		Good	
German three-axis magnetometer								
1	3/28/85	2100-2400	[c]5975-6300	465-790	Down, up	$H_{x,y,z}$	Good	
	3/29/85	2400-1500						
Downhole logging								
4	3/29/85	1500-2345	[c]6000-6295	490-785	Up	Ω Laterolog LLS	Good	
						LLD	Fair	Out of calibration
LDGO multichannel sonic tool								
1	3/30/85	0100-0745	[c]5875-6310	365-800	Down, up	Vp, Vs	Good	
USGS magnetic susceptibility tool								
3	3/30/85	0745-1600	[c]5975-6310	465-800	Down, up	Susceptibility	Good	Tool temperature too
						Conductivity	Poor	low (down only)
WHOI borehole seismometer								
1	3/30/85	1815-2400	6065, 6165,	555, 655,	Stationary	Vp, Vsv, Vsh	Good	Shooting conducted
	3/31/85	0000-2400	[c]6265	755		Anisotropy		by *Moore*
	4/1/85	0000-2400						
	4/2/85	0000-2400						
	4/3/85	0000-2400	5853, 5876,	343, 366,	Stationary	Evanescent waves	Good	Cable failed to
	4/4/85	0000-0430	[c]5916	406				5853-m position
Packer								
	4/6/85	1625-2400	5867, 5985,	347, 465,	Stationary	Pore pressure,	—	Packer would not
	4/7/85	0000-0930	[c]6037	517		permeability		seat
L-DGO borehole televiewer								
	4/7/85	1200-2300	[c]5870	360	Down	Borehole imagery	Fair	Slow sweep;
						Acoustic caliper	Fair	tool caught on ledge

[a] See text and Table 6 for specifications.
[b] Subtract 10 m to obtain depth below sea level.
[c] Equals depth below sea level (rig-floor height and cable stretch cancel each other, by coincidence).

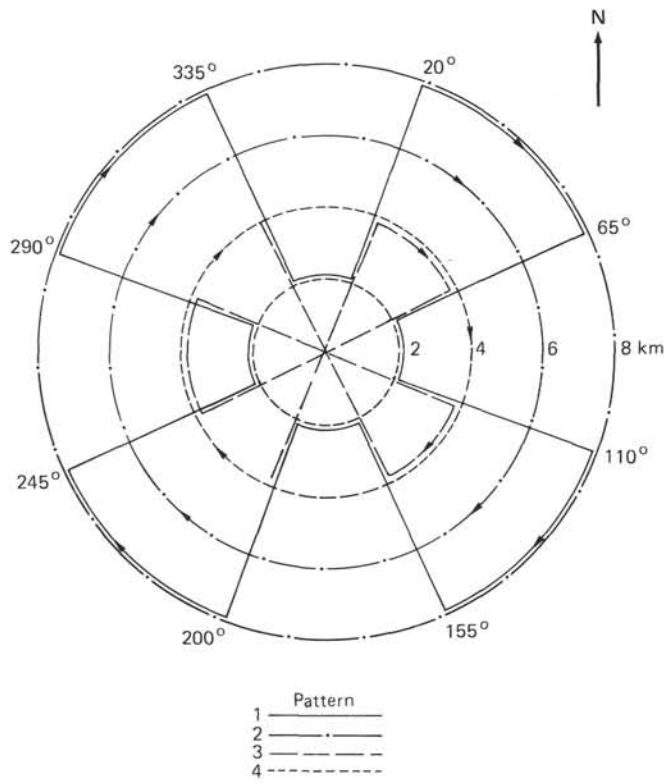

Figure 6. Shot patterns conducted around the *JOIDES Resolution* by the R/V *Fred H. Moore* during the oblique seismic experiment.

previously, to 6389 m, or total depth, which we reached at 1130 hr. Although torquing was observed, the bit did not take weight, and the tool was not in the hole. Evidently the tool had fallen off into the sediments when the cable frayed during the last pipe trip to the surface 8 yr ago. Therefore, we cleaned the hole with mud and tripped the pipe to the surface, which was reached at 0800 hr on 5 April.

After rigging up the packer, we started lowering the pipe again at 1030 hr and reached the seafloor at 0115 hr on 6 April. The reentry tool was then rigged up and lowered to the bit by 0515 hr. Because of a heading-related offset error in the ship's dynamic-positioning system, we could not acquire the cone, even with the original offsets, until the ship was restored to the heading at which the cone was first acquired. Even when this was done, maneuvering problems delayed reentry until 1430 hr, when the cone was stabbed and the sonar tool brought back to the surface. After recovering the reentry tool at 1700 hr, we lowered the pipe to 5867 mbrf, turned on the Kuster recorders, and pumped them down in the go-devil to the packer.

After enough time had passed for the go-devil to seat and the Kusters to record the hydrostat, we attempted to inflate the packer but found it would create pressure only up to 800 psi because of air in the system. Once the air had been bled off, the packer took 1000 psi, as required, but would not seat. When the packer would not hold but kept sliding down the hole even at 2000 psi, we deflated the packer and lowered it to 6037 mbrf, where we tried again without success to get it to seat. After a third attempt to seat the packer just above the bridge at 5985 m failed, we attempted several times to retrieve the go-devil on the sand line to assess the problem. On the third attempt, at 0930 hr on 7 April, we recovered the go-devil and determined that it had seated and operated properly but had never sensed the pressure used to inflate the packer. Thus, the packer either was not inflating or was not holding onto the borehole wall. Since the tool appeared to be malfunctioning and we did not have enough time for another pipe trip to repair it, we decided to discontinue the packer tests and to use the time remaining for logging.

After disconnecting the plumbing associated with the packer tests, we rigged up the borehole televiewer by 1200 hr and attempted to log the hole, going downhole from 5849 to 6200 mbsl. The tool appeared to be operating (although at a slow rotation rate) when it left the pipe, but it caught on a bridge below the pipe, and several hundred meters of cable were spooled out on top of the tool, causing cable shortening. When the tool was subsequently recovered at 2300 hr, it was time to start tripping the pipe in preparation for departure.

Once the pipe was on deck, the ship departed the site at 1348 hr and began to steam slowly on a heading of 122°, while deploying underway geophysical gear. After steaming 6 n. mi on this heading, the ship made a Williamson turn at 1500 hr and returned to the site on a heading of 302°. When the ship passed over the site at 1600 hr, we began steaming at full speed for Norfolk, Virginia. Before our arrival on the morning of 11 April, an investigation of the packer indicated that it was still working and did not reveal why it had failed to seat downhole.

SEISMIC-LINE INTERPRETATION

Introduction

During Leg 102, a seismic survey was conducted with the R/V *Fred H. Moore,* using one 80-in.^{3} water gun and shooting every 20 s. The bounds of the survey area were 27°55′ to 25°08′N and 67°55′ to 68°11′W. This preliminary interpretation was done with nine seismic lines oriented N110°. Other seismic lines oriented N20° were recorded but were not available aboard the *JOIDES Resolution*. As shown in the navigation chart of Figure 7, four seismic lines lie south of the *Resolution*, and five lie to the north.

Most of the seafloor in the survey area lies at a depth between 5325 and 5550 m. The sediment cover is from 0.24 to 0.6 s thick, and the vertical exaggeration of the seismic lines is 3.4. The acoustic basement lies from 7.5 to 8 s below sea level (sbsl), and according to previous velocity estimates (see follow-

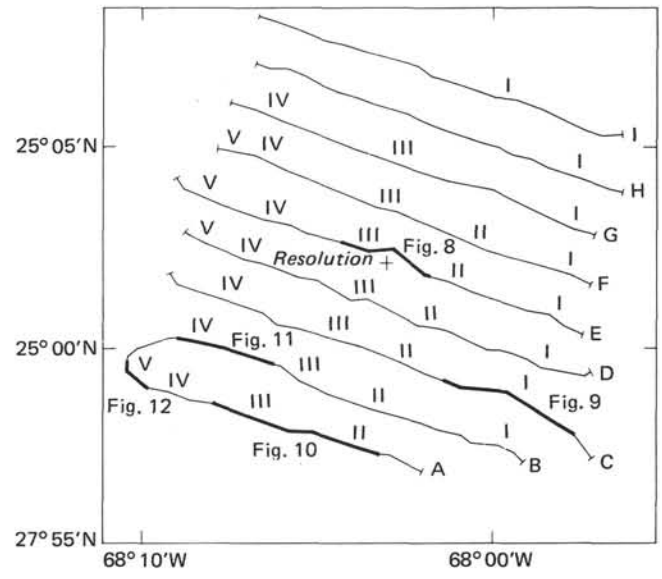

Figure 7. Detailed location map of R/V *Fred H. Moore* seismic-reflection lines (A, B, C, D, E, F, G, H, I). Note location of the seismic features (I, II, III, IV, V)

ing discussion), slopes of as much as 17% can be observed in the basement.

Because line E is near Hole 418A, correlations with the previously drilled lithologic column and with the previous seismic lines can be presented. Since the interval between seismic lines is small (2 km), preliminary mapping of five acoustic features can be shown.

Correlation with Hole 418A

Section E (Fig. 7) is near Hole 418A (the range is less than 600 m between shots 1600 and 1620, Fig. 8). The following reflectors can be observed: (1) the seafloor at 7.32 s (5490 mbsl), (2) a prominent sediment reflector at 0.22 sbsf, and (3) the acoustic basement at 0.4 sbsf.

These results are similar to the Legs 51–53 site-survey results (Rabinowitz et al., 1979). According to the previous Site 418 velocity evaluations (Donnelly et al., 1979), the reflector within the sediment is at 165 mbsf and can be attributed to the boundary between Unit II and Unit III (top of the middle Eocene) in the Hole 418A lithologic column. The acoustic basement lies at 320 mbsf and can be attributed to the basalt/sediment interface.

Description of Some Acoustic Events

Event I

Event I (Fig. 9), a 100-m bathymetric high, is 5 km wide. The seafloor slope is as much as 5% on the west side, and the basement slope is as great as 14%. The sedimentary layer is generally 0.4 s (320 m) thick. This structure is observed on nine recorded seismic lines and is oriented N15°–N20° (Fig. 7).

Event II

Event II (Fig. 10), present on seismic sections A, B, C, D, E, and F, is characterized by a strong basement reflection surmounted by two reflectors within the sedimentary layer. The layer is about 0.36 s thick, and the two reflectors are at 0.12 and 0.22 sbsf. This structure appears be relatively well aligned along a line oriented N20°–N25° (Fig. 7).

Event III

Event III (Fig. 10), on seismic sections A, B, C, D, E, F, and G, is a 1.5-km-wide strong basement reflection, which shows a slightly westward-dipping slope (2%–3%) terminated by a probable basement normal fault. The sediments obliterate these basement structures. These structures are relatively well aligned along a line oriented N20°–N25° (Fig. 7).

Event IV

Event IV (Fig. 11), on seismic sections A, B, C, D, E, F, and G, appears as an old valley in the basement and is 4.5 km wide and 0.28 s deep. The structure is aligned along two lines (Fig. 7): a line oriented N35° between seismic sections A and D, and a line oriented N05° between seismic sections D and G.

Event V

Event V (Fig. 12), on seismic sections A, D, E, and F, is a strong reflection, which lies at 0.25–0.30 sbsl and is 1.5 km wide. Without seismic processing, whether this reflection is within the sediment or within the sediment/basement interface is difficult to determine. This event appears on a line oriented N20°.

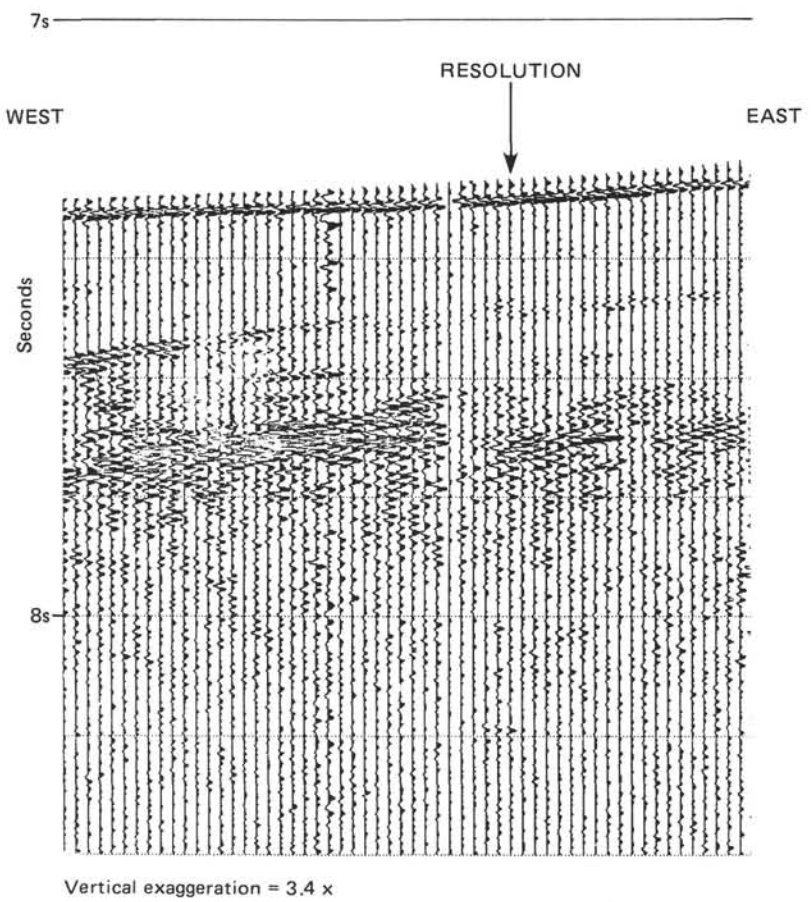

Figure 8. Seismic line E detail near the *JOIDES Resolution* (see location, Fig. 7). Vertical scale: two-way traveltime.

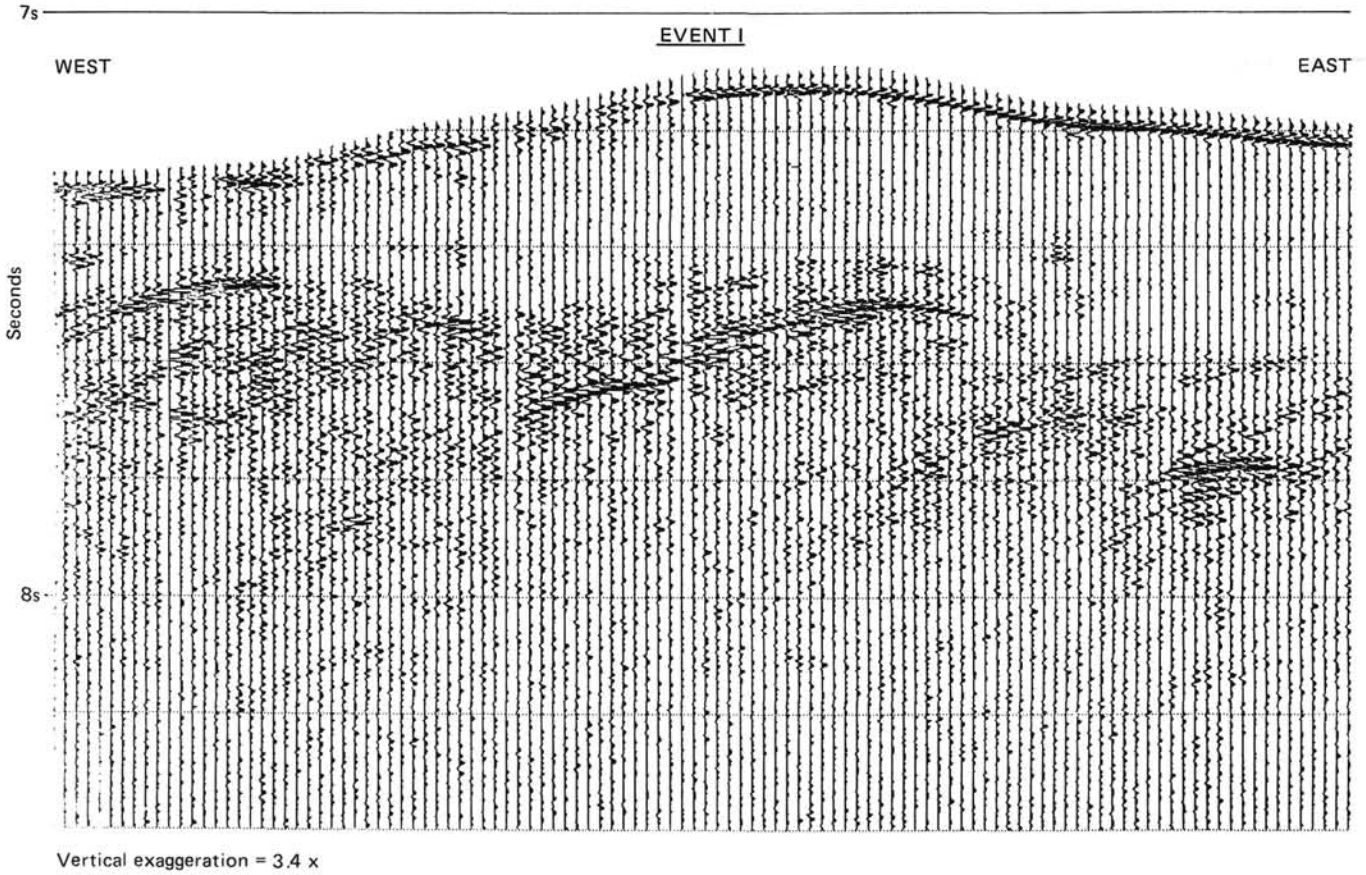

Figure 9. Seismic line C detail (see location, Fig. 7), showing acoustic event I. Vertical scale: two-way traveltime.

CONVENTIONAL LOGGING RESULTS

A full suite of Schlumberger electrical, nuclear, and sonic logs was recorded in the basement from 789 to 464 mbsf. Only the LSS-DIL-GR (sonic, induction, gamma) combination tool was run in the open hole from 476 to 325 mbsf after a failed attempt to get through a hole restriction in a breccia zone from 469 to 481 mbsf during the tool lowering. Therefore, the following procedure was followed for each run: after lowering the pipe string to 493 mbsf to permit the tool to get through the bridge and reach the bottom, the pipe was raised to 460 mbsf and the logs were run from 789 to 464 mbsf. Logs were not recorded from total depth (868 mbsf), since it was thought that a sonic tool and about 300 m of knotted cable lost during Legs 52 and 53 had probably slipped down to the bottom of the hole. The NGT and CNTG (natural gamma and neutron) logs were recorded through the pipe and the casing up to the mud line to get information about the sediments, the sediment/basement interface, and the upper part of the basement.

Runs 1–2: DIL-LSS-GR

The dual induction (DIL) tool records two resistivity curves with different depths of investigation, ILD (deep) and ILM (medium). The sonde also includes a shallow-focused device, the spherically focused log (SFL), that provides better vertical resolution (about 60 cm vs. 100–150 cm for ILD-ILM) and more reliable readings in the high-resistivity range than do the ILD-ILM logs. In fact, since the induction tool measures the conductivity of the formation (converted to resistivity), errors are negligible at low resistivity values but can increase as much as 20% when resistivity exceeds 100 ohm-m.

The long-spacing sonic (LSS) tool measures the time required by a sonic wave to travel through 1 ft of formation. The tool borehole compensates each reading by recalling the first traveltime reading and averaging it with a second reading after the sonde has been raised a fixed distance in the borehole. The LSS tool provides two curves (DT and DTL) with different depths of investigation. The long-spacing (10–12 ft) reading (DTL) is deeper and is not as severely influenced by altered or disturbed zones near the borehole, which cause a decrease of acoustic velocity on the DT curve. Full waveforms were also recorded for each receiver; in the field log, they are plotted 15 m below the midpoint of the source–receiver interval. Gamma-ray and three-arm caliper logs were also run. The latter provides a measurement of hole size and a check of borehole conditions. The tool specifications and the logged curves are listed in Tables 5 and 6.

Run 3: LDT-CNTG-NGT

The lithodensity tool (LDT) measures the bulk density of the formation (RHOB) and the photoelectric cross section (PEF). The former depends on electron density; the latter is related to the lithology. The dual-porosity compensated neutron tool (CNTG) provides two separate porosity curves (ENPH and TNPH) corresponding to epithermal (high) and thermal (low) neutron energy recordings. The difference between the two curves is related to the clay content, the epithermal log being less influenced and reading closer to the true formation porosity (Davis et al., 1981; Scott et al., 1982). Therefore, when used together, the two logs can help distinguish bound water from free water in rock. Since the epithermal curve had not been properly calibrated by Schlumberger, it is not presented in this report.

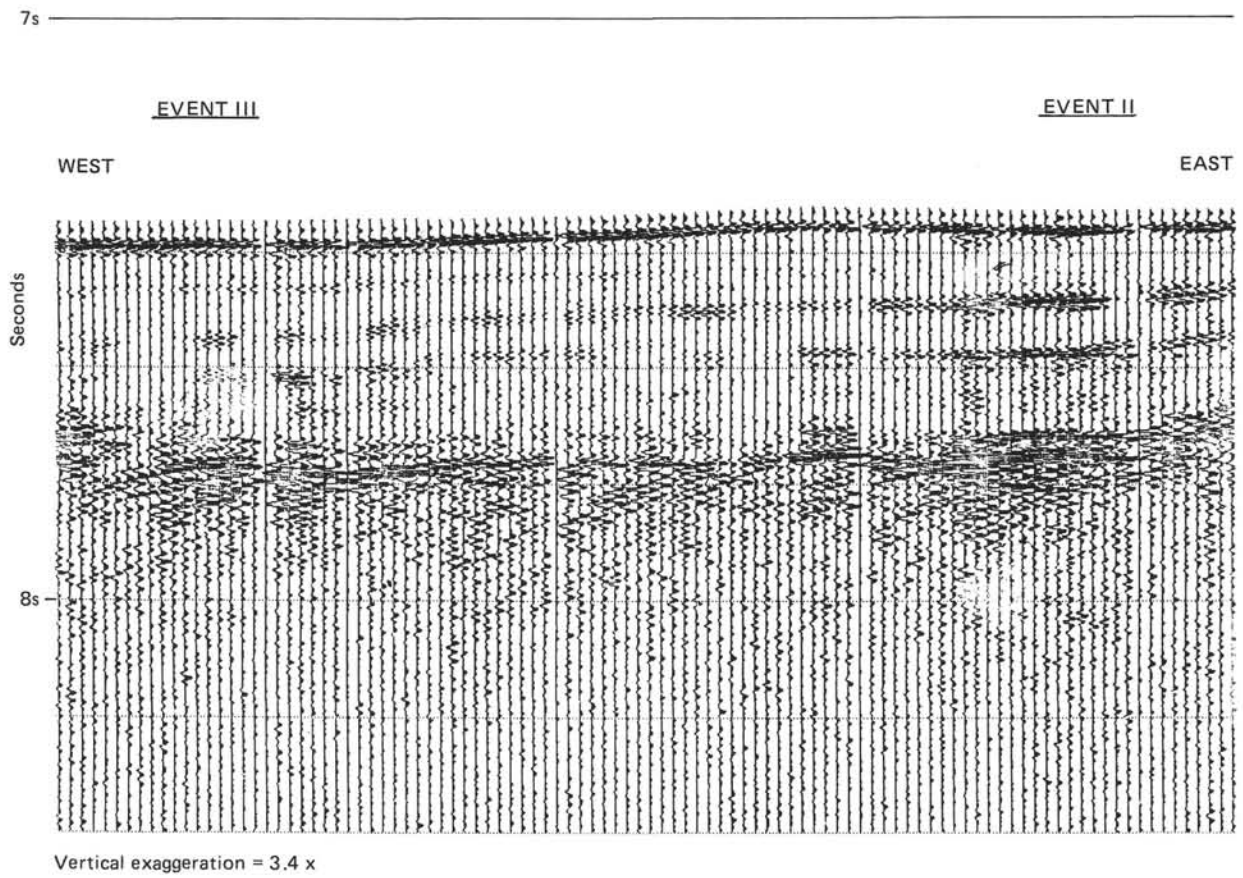

Figure 10. Seismic line A detail (see location, Fig. 7), showing acoustic events II and III. Vertical scale: two-way traveltime.

The natural gamma-ray spectrometry tool (NGT) detects natural gamma radiation in five energy bands, providing a quantitative determination of uranium (U), thorium (Th), and potassium (K) concentrations. Standard gamma ray (SGR) is the total-count gamma ray; computed gamma ray (CGR) does not include the uranium component and is a better indicator of formation "shaliness."

Run 4: DLL

The dual Laterolog is a focused-current resistivity log that measures the formation resistivity at two different depths, LLD (deep) and LLS (shallow), providing better vertical resolution than does the deep induction log (ILD) and more accurate readings in the high-resistivity range (>100 ohm-m). Because the deep resistivity measurement was not calibrated correctly and the large-scale resistivity experiment was not run, the LLS is the only reliable noninduction resistivity curve obtained in Hole 418A.

Results

The downhole logging at Site 418A had two objectives: first, to define and possibly revise the basement lithostratigraphy, particularly where unit boundaries are uncertain, owing to the poor core recovery during Legs 52 and 53; second, and more important, to define more precisely the physical properties of the rocks of the upper crust. The more limited suite of logs obtained in the sedimentary section was run to improve the lithostratigraphy of the sediments.

Because all the Schlumberger logging tools were designed for oil-field application, some of them may present certain limitations whenever they are not run in "standard lithologies" (sandstone, limestone, and dolomite). Currently, we do not know how much the response of the neutron tool is affected by the matrix in massive basalt or whether the equation relating electron density to bulk density is correct in basaltic rocks. Logs can be more effectively used in the study of the properties of the crust only after being calibrated through comparison with the physical properties of the cores. Therefore, the following results represent a preliminary interpretation of the original data.

Plates 1 through 4 (back pocket) show the primary logging results and a comparison of the log and core lithologic interpretations. Plate 1 shows ILD, ILM, SFLU, LLS, DT, and DTL curves recorded in the basement interval. LLS was recorded only from 789 to 489 mbsf. Plate 2 shows gamma-ray, caliper, neutron porosity, density, and sonic velocity for the basement section. In the interval from 464 to 324 mbsf, neutron porosity was recorded through the drill pipe. Plate 3 shows CGR, SGR, THOR, URAN, POTA, and PEF curves in the basement section. The interval from 464 to 324 mbsf was recorded through the drill pipe. Plate 4 shows the rest of the logging runs through drill pipe, recorded in the sediments from 324 mbsf to the mud line. This includes NPHI, CGR, SGR, URAN, THOR, and POTA curves. The various corrections applied to this logging data, which are necessary to provide readings corresponding to the condition under which the tools were calibrated, are described as follows.

The GR was corrected for hole size using the caliper log. This correction ranges from 0.3 to 8.5 GAPI. No correction was applied for mud weight because the borehole fluid was seawater (8.8 lb/gal), and the correction is necessary only when the mud weight exceeds 10 lb/gal. Corrections for hole size, mud cake (in the restricted zone from 469 to 481 mbsf), and pressure were applied to the neutron curve from 789 to 464 mbsf (open hole). The hole-size correction, based on the caliper curve recorded

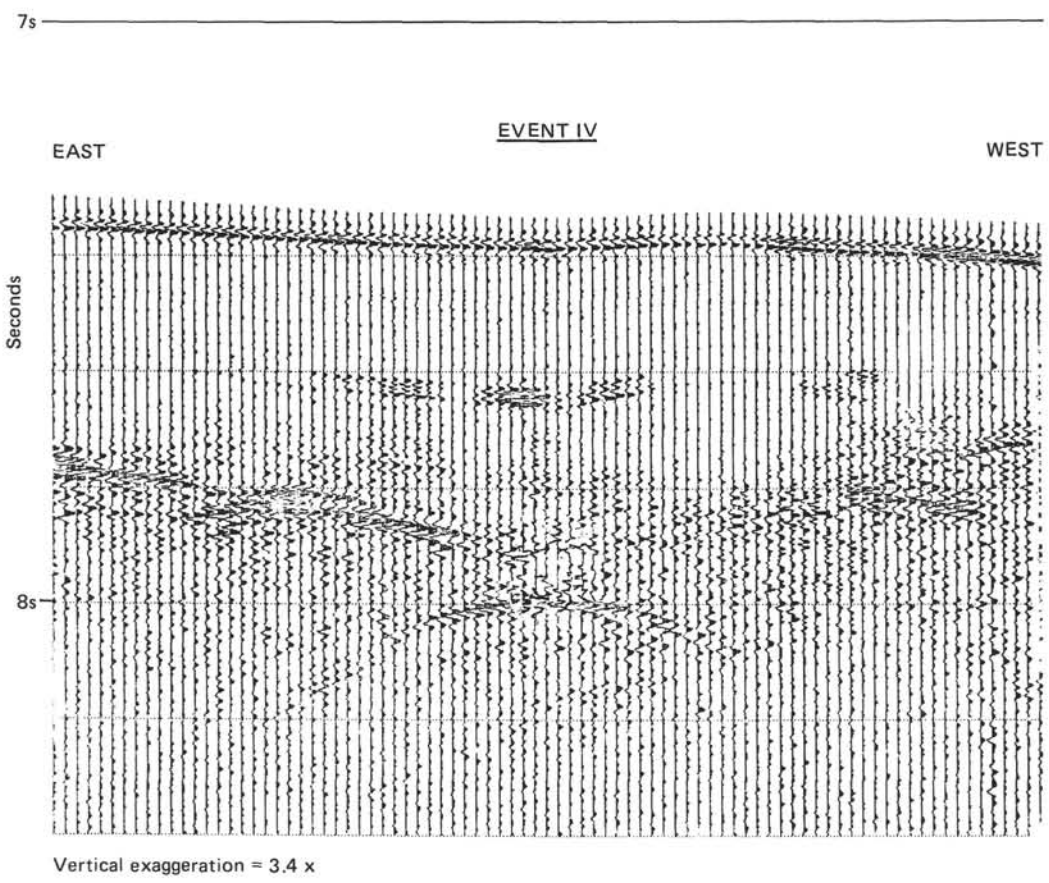

Figure 11. Seismic line B detail (see location, Fig. 7), showing acoustic event IV. Vertical scale: two-way traveltime.

during Run 2 (DIL/LSS/GR), replaced the correction applied by the Schlumberger engineer at the well site, which assumed a constant borehole diameter. No temperature correction was performed because the range of temperatures measured in the well (5°–22°C) is close to the standard temperature (24°C). No mud-weight or salinity correction was necessary, as the borehole and formation fluids are similar. The total correction ranges from −1.0% to −13.1%. From 464 mbsf up to the mud line, a correction for offset of the ship was also calculated, partly to reduce the effect of neutron absorption by the pipe and the casing. This correction is significant, ranging from −4.3% to −15.5%. Corrections to the SFL/LLS curves were not required, as these are necessary only when the hole exceeds 12 in. in diameter. Corrections to ILD and ILM were not necessary either, as these are needed only if the borehole fluid is highly conductive (i.e., if the salinity of the borehole fluid exceeds 70,000 ppm). The density curve was automatically corrected for borehole rugosity and mud-cake accumulation during the recording process by electronic application of relationships based on a spine and rib chart (Schlumberger, Inc., 1972). Table 7 is a summary of the environmental corrections applied in Hole 418A. After these borehole corrections were applied, all the curves were smoothed using a five-point running average (0.75-m depth interval).

Interpretation of the Basement Interval

The interpretation of the upper part of basement is based on the DIL-LSS curves (open hole) and the NGT-CNTG logs, recorded through the pipe up to the mud line. The DIL-LSS-GR logs were run up to 325 mbsf, just below the sediment/basalt boundary, but the natural spectrometry log and neutron curve show a kick at 324 mbsf, at the sediment/basement contact (Plates 2 and 3).

The hole conditions (as shown by the caliper log) are poor between 323 and 389 mbsf (Units 1 through 4) and, combined with the ship's heave, make the response of both the DT and DTL logs meaningless in this interval. However, a first interpretation based on the resistivity, gamma-ray, and neutron curves substantiates the lithologic boundaries indicated by cores.

A sharp decrease in the velocity and resistivity values marks the top of the pillow basalts and breccia of Unit 5 (388–503.6 mbsf), the latter corresponding to higher GR values (up to 49.0 GAPI) and lower velocities (2.5 km/s). Density in the lower part of the unit ranges from 2.00 to 2.77 g/cm^3 (2.56 ± 0.14 g/cm^3). Between 469 and 481 mbsf, the caliper curve shows values of about 9¾ in. (bit size = 10.25 in.), which correspond to the bridge encountered during tool lowering.

Subunit 6A, consisting of a breccia, is clearly delineated by the logs, which allow for a precise definition of the top and bottom of the unit: high GR values (28.0 ± 4.0 GAPI), low resistivity (41 ± 8 ohm-m), and low velocity (4.5 ± 0.4 km/s). The bulk-density and neutron curves reflect the presence of smectite (2.45 g/cm^3 from lab measurements) in the matrix. The high neutron porosity values throughout the well were caused by the limestone matrix scale used during recording and by the high content of bound water in smectite (Fertl and Frost, 1980), which result in an overestimate of rock porosity. Only a proper calibration of the neutron log against core values and a correction for the "shaliness" could reduce this error and provide porosity values closer to the lab measurements. The bottom of Subunit 6A (513.7 mbsf) is marked by a sharp drop in the GR curve, from 30 to about 10 GAPI.

Subunits/Units 6B, 7, 8A, 8C, 11, 13A, and 13C all consist of pillow basalts and show similar features on the logs. The bulk density ranges from 2.00 to 2.97 g/cm^3, negative deflec-

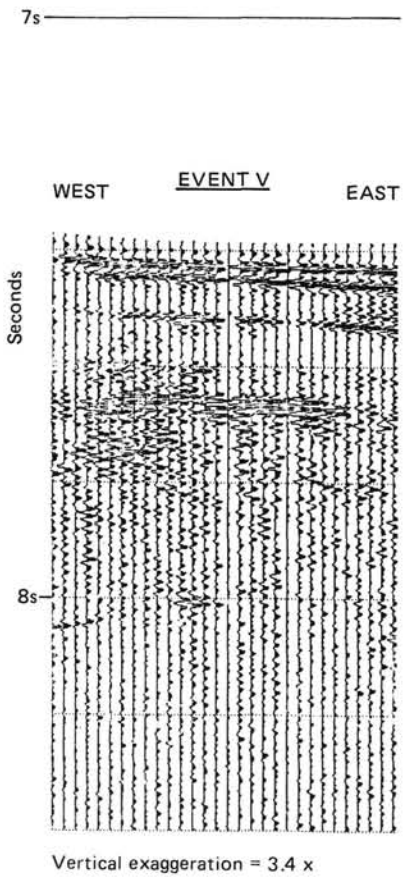

Figure 12. Seismic line A detail (see location, Fig. 7), showing acoustic event V. Vertical scale: two-way traveltime.

tions being opposite altered zones. Resistivity drops in the more porous and shaly intervals, and sonic velocity increases to a maximum of 6.8 km/s in the more homogeneous intervals. Low density readings (down to 1.60 g/cm^3) were recorded between 539 and 589 mbsf and are due to cavities and rugosity of the borehole wall (see caliper log on Plate 2), which prevented the pad of the lithodensity tool from making contact with the formation. The poor hole conditions are also confirmed by the response of the MCS and resistivity logs, the latter being very spiky in this part of the hole. No data are available for the lower part of Subunit 13C below 788 mbsf or for the contact with the underlying massive basalts. Unfortunately, all recordings started between 788 and 773 mbsf, and none of them cross this contact. A homogeneous interval can be observed between 731.5 and 743.8 mbsf (Subunit 13B), which shows features similar to the overlying massive basalts: high bulk density (2.81 ± 0.08 g/cm^3), lower porosity (12.0% ± 3.6%), high resistivity (402 ± 572 ohm-m), and very high velocity (6.0 ± 0.4 km/s).

Subunits/Units 8B, 9, 10, and 12 correspond to massive basalt. Their main feature is the absolute uniformity of log readings. Unit 10 (679.8–686.5 mbsf) is the thickest unit and shows the most typical values: a velocity of 5.9 ± 0.1 km/s, a bulk density of 2.86 ± 0.04 g/cm^3, neutron porosity constant and lower than in the adjacent units (as low as 7.5%), very low gamma-ray response (5.7 ± 1.0 GAPI), and high resistivity (as much as 2000 ohm-m). The core recovery in Unit 10 was poor (19.1%), but the uniformity of log readings confirms the massiveness of the rock and the lack of altered zones. A summary of the lithologic boundaries and of the properties of the basement section made from well logs is shown in Table 8.

Interpretation of the Sedimentary Interval

Plate 4 shows the logs recorded through pipe in the sedimentary section of Hole 418A. The data recorded in the sedimentary section extend from the sediment/basement interface at 324 mbsf to the mud line. Although the full complement of nuclear logs was recorded in this interval, the density is unreliable, as the pad of the lithodensity tool was not in contact with the for-

Table 5. Specifications of the Schlumberger tools run in Hole 418A.

Tool	Source	Transmitters	Detectors (receivers)	Spacing (ft)	Outside diameter (in.)	Length (in.)	Weight (lb)	Maximum temp. (°F)	Maximum press. (psi)
CALI (caliper)	—	—	—	—	3-3/8	60	120	350	20,000
CNTG (dual porosity compensated neutron tool)	Am/Be241	—	4	—	3-3/8	153	213	350	20,000
GR (gamma ray)	—	—	1	—	3-3/8	60	125	350	20,000
LDT (lithodensity tool)	Ce137	—	2	—	3-3/8	245	381	350	20,000
LSS (long-spacing sonic)	—	2	2	10-8 12-10	3-3/8	309	441	350	20,000
NGT (natural gamma-ray spectrometry tool)	—	—	1	—	3-3/8	100	165	350	20,000

Tool	Electrodes	Outside diameter (in.)	Length (in.)	Weight (lb)	Maximum temp. (°F)	Maximum press. (psi)
DIL (dual induction log)	9	3-3/8	346	335	350	20,000
DLL (dual laterolog)	10	3-5/8	368	474	350	20,000

Table 6. Summary of Schlumberger log curves.

Run 1-2 (LSS-DIL-GR)		Unit
CALI	Three-arm caliper	in.
GR	Gamma ray	GAPI
ILD	Deep induction log	ohm-m
ILM	Medium induction log	ohm-m
SFLU	Spherically focused log	ohm-m
DT	Sonic (delay time)	μsec/ft
DTL	Sonic long-spacing (delay time)	μsec/ft
Run 3 (LDT-CNTG-NGT)		
RHOB	Bulk density	g/cm^3
NPHI	Thermal neutron porosity (equals TNPH)	%
PEF	Photoelectric effect	barns/electron
DRHO	Density correction	g/cm^3
SGR	Standard gamma ray (U + Th + K)	GAPI
CGR	Computed gamma ray (U + Th)	GAPI
THOR	Thorium component	ppm
URAN	Uranium component	ppm
POTA	Potassium component	%
Run 4 (DLL)		
GR	Gamma ray	GAPI
LLS	Laterolog shallow	ohm-m
LLD	Laterolog deep	ohm-m

Table 7. Summary of the environmental corrections, Hole 418A.

Curve	Depth interval (mbsf)	Correction
GR	324–788	Hole size
NPHI	0–464	Standoff + pressure
NPHI	464–788	Hole size + pressure
NPHI	469–481	Mud cake
RHOB	464–788	Hole size
ILD		No correction
ILM		No correction
SFLU		No correction
LLS		No correction
SGR		No correction
CGR		No correction

mation. The remaining logs (neutron porosity and natural gamma spectrometry) were also affected by the log being obtained with the tool inside the drill pipe. The corrections are described in previous text.

Tentative correlations between these logs and the core lithologic units were made on the basis of variations in the relative amounts of U, Th, and K. The neutron log was not particularly diagnostic of lithologic variations in the sediment column. The K-U-Th variations probably are due to differences between the carbonate/clay ratio of the individual units. We synthesized a complete lithologic column on the basis of core recovered in both Holes 418A and 418B because neither hole was cored continuously.

Differences between Unit I (a noncalcareous soft pelagic clay) and Unit II, which is similar, are subtle. The boundary was selected at about 19.5 m sub-bottom, where both K and Th contents increase. Subunits IIa and IIb were differentiated primarily on the basis of color on Legs 52 and 53, although the presence of zeolites in Subunit IIa suggests a higher radionuclide content.

Because an abrupt increase in K and Th and an abrupt decrease in U occurs at 124 mbsf, the Layer IIa/IIb contact was placed at this depth. The Subunit IIb/UnitIII boundary corresponds to the K and Th decrease and U increase at 144 mbsf. Units III and IV could not be differentiated on the basis of the logs. The base of Unit IV was placed at 179 mbsf, at a minimum in K and Th and an abrupt decrease in U content. This interval may be equivalent to the calcareous material recovered in Core 418B-19. Subunits Va (179–199 mbsf) and Vb (199–244 mbsf) are differentiated on the basis of U content, which is low in Subunit Va and shows a gradational increase in uppermost Subunit Vb. The lower contact of Unit V was placed at 244 mbsf. K and Th contents in Unit V are both high. At 231 to 235 mbsf, low K and Th levels indicate the presence of a calcareous zone just above the base of this unit.

Unit VI is described as an interbedded claystone, marl, chalk, and sand. The log unit extends from 244 to 294 mbsf. Log response suggests a possible subdivision of Unit VI on the basis of the relative levels of radionuclides into Subunits VIa (244–264 mbsf) and VIb (264–294 mbsf). An abrupt decrease in K, Th, and U levels characterizes the Unit VI/Unit VII contact.

Core recovery in Unit VII was poor, and on the basis of the logs, the interval appears to be much thinner than initially reported in the core descriptions (Donnelly et al., 1979). Subunit VIIa is a 4-m-thick chalk; the log response in Subunit VIIb is similar to the response in Unit VI. The Unit VII/Unit VIII boundary is characterized by an abrupt decrease in K and Th and an increase in U. The unit extends from 305 mbsf to basement, although the Unit VII/Unit VIII boundary was originally placed at the top of Core 418B-15 (320 mbsf). Poor core recovery in this interval makes this reinterpretation reasonable.

Some of our log unit boundaries apparently conflict with boundaries assigned on the basis of core analysis. This is not surprising, as generally no direct relationship exists between the primary core discriminant (color) and the log discriminants (chemical composition and petrophysical character). We would urge, therefore, that the reader avoid directly correlating the log and core unit boundaries.

Lithostratigraphic interpretations are summarized in Table 9.

MULTICHANNEL SONIC LOGGING RESULTS

The multichannel sonic (MCS) log, run in Hole 418A to measure the elastic properties of the basement section, complements the Schlumberger long-spaced sonic (LSS) log by providing a better measurement of compressional and shear velocity. The MCS log is inherently more accurate than the LSS because (1) 12 receivers are employed to compute the velocities, and (2) the spacing between the receivers is 15 cm, less than one-fourth of the interreceiver spacing of the LSS sonde. The greater number of receivers improves the statistical significance of the velocity measurement, whereas the shorter interreceiver spacing improves the correlation between individual arrivals in heterogeneous formations.

The MCS log has been run successfully in several wells on land and in DSDP Hole 504B. The sonde we deployed on Leg 102 is a modification of the sonde run in Hole 504B.

Tool Description

The multichannel sonic sonde operates from a single source and contains 12 receivers. The entire waveform at a single receiver is recorded every time the source is fired. The source-receiver pair and the downhole gain are selected before each source pulse. To produce the full 12-receiver suite, the source is fired 12 times, and the receivers are polled in order. The data are digitized at the surface and stored on magnetic tape.

The operation of the MCS log is controlled by a Masscomp 561 computer, which monitors the depth and triggers the source to record a full suite of data at fixed intervals in the well. The data are digitized at a user-selected rate (typically 2 microseconds/sample) and stored in real time. Compressional and shear wave velocities are computed after the log is complete by semblance analysis of the recorded waveforms. The logging speed is

Table 8. Properties of basement units, Hole 418A, from well logs.

Unit/ subunit	Lithology	Depth (mbsf)	Bulk density (g/cm^3)	Neutron porosity[a] (%)	Sonic velocity (km/s)	Resistivity[b] (ohm-m)	Radioactivity (GAPI)
1	Pillow basalts	324–333		32.3 ± 6.0		350 ± 707	22.3 ± 7.4
2A	Massive basalts	333–335.5		30.3 ± 5.4		77 ± 14	10.1 ± 1.8
2B	Massive basalts	335.5–345.2		18.6 ± 7.5		290 ± 454	6.5 ± 3.5
2C	Massive basalts	345.2–366.7		14.0 ± 7.2		938 ± 777	3.9 ± 1.6
2D	Massive basalts	366.7–376.5		30.3 ± 12.6		325 ± 679	7.8 ± 5.5
3	Pillow basalts	376.5–385		26.6 ± 5.6	5.3 ± 0.1	79 ± 33	6.1 ± 0.7
4	Massive basalts	385–388		23.1 ± 4.3	5.6 ± 0.4	551 ± 858	6.9 ± 4.5
5	Pillow basalts and breccia	388–503.8	2.56 ± 0.14	28.3 ± 6.3	4.5 ± 0.6	59 ± 173	23.1 ± 8.6
6A	Breccia	503–513.7	2.25 ± 0.15	35.2 ± 3.5	4.5 ± 0.4	41 ± 8	28.0 ± 4.0
6B	Pillow basalts	[c]513.7–614	2.56 ± 0.18	21.4 ± 6.9	5.3 ± 0.5	147–305	7.2 ± 2.9
7	Pillow basalts	614–632	2.67 ± 0.19	23.1 ± 8.9	5.2 ± 0.8	100 ± 296	7.6 ± 2.6
8A	Pillow basalts	632–636	2.72 ± 0.09	21.5 ± 4.7	5.4 ± 0.5	77 ± 85	6.8 ± 1.5
8B	Massive basalts	636–639	2.75 ± 0.03	16.9 ± 3.9	5.8 ± 0.5	100 ± 57	5.3 ± 0.7
8C	Pillow basalts	639–676	2.65 ± 0.11	22.3 ± 5.6	5.3 ± 0.4	115 ± 254	7.4 ± 1.5
9	Massive vesicular basalts	676–679	2.74 ± 0.08	21.2 ± 3.3	5.1 ± 0.4	67 ± 8	8.7 ± 1.7
10	Massive basalts	679–686.5	2.86 ± 0.04	10.1 ± 2.7	5.9 ± 0.1	430 ± 444	5.7 ± 1.0
11	Pillow basalts	686.5–703.5	2.54 ± 0.17	24.8 ± 5.0	5.1 ± 0.5	61 ± 38	10.4 ± 1.4
12	Massive basalts	703.5–707.5	2.70 ± 0.03	13.7 ± 3.0	5.7 ± 0.4	75 ± 23	7.1 ± 1.0
13A	Pillow basalts	707.5–731.5	2.61 ± 0.10	22.0 ± 5.0	5.2 ± 0.4	53 ± 25	8.8 ± 2.0
13B	Massive pillow basalts	731.5–743.8	2.81 ± 0.08	12.0 ± 3.6	6.0 ± 0.4	402 ± 572	5.8 ± 0.04
13C	Pillow basalts	743.8–788	2.70 ± 0.16	15.7 ± 5.7	5.7 ± 0.4	195 ± 303	5.9 ± 1.1

[a] Recorded through the pipe from 464 to 324 mbsf.
[b] From spherically focused log (SFLU).
[c] Does not include data affected by bad hole conditions.

Table 9. Properties of sedimentary units, Hole 418A, from well logs.[a]

Unit/ subunit	Depth (mbsf)	Lithology	Neutron porosity (%)	Radioactivity		U (ppm)	Th (ppm)	K (%)
				Computed (GAPI)	Standard (GAPI)			
I	0.0–19.5	Pelagic clay	67.2 ± 11.8	27.1 ± 5.7	30.3 ± 6.6	0.35 ± 0.38	3.62 ± 0.99	0.65 ± 0.12
IIA	19.5–124.0	Pelagic clay	68.5 ± 7.1	31.7 ± 4.8	37.0 ± 5.7	0.59 ± 0.45	4.45 ± 0.86	0.71 ± 0.15
IIB	124.0–144.0	Pelagic clay	68.8 ± 6.3	35.4 ± 5.7	37.3 ± 4.3	0.22 ± 0.25	5.04 ± 0.91	0.77 ± 0.14
III–IV	144.0–179.0	Pelagic clay	66.3 ± 5.7	32.7 ± 6.1	39.1 ± 6.2	0.72 ± 0.54	4.51 ± 0.88	0.75 ± 0.20
VA	179.0–199.0	Pelagic clay	63.8 ± 5.1	51.6 ± 7.5	52.0 ± 7.4	0.04 ± 0.25	6.85 ± 1.39	1.26 ± 0.16
VB	199.0–244.0	Zeolite clay	62.5 ± 7.1	46.0 ± 10.5	49.9 ± 10.9	0.44 ± 0.33	5.57 ± 1.28	1.24 ± 0.35
VIA	244.0–264.0	Claystones, marls, chalks, and sands	69.6 ± 6.1	15.2 ± 4.8	21.4 ± 8.7	0.70 ± 0.64	1.81 ± 0.62	0.41 ± 0.18
VIB	264.0–294.0	Claystones, marls, chalks, and sands	61.3 ± 6.3	28.7 ± 6.1	39.7 ± 10.1	1.24 ± 0.79	3.08 ± 0.90	0.87 ± 0.19
VIIA	294.0–298.0	Chalk	56.5 ± 4.8	22.0 ± 8.5	28.8 ± 6.8	0.77 ± 0.44	2.40 ± 1.17	0.67 ± 0.24
VIIB	298.0–305.0	Claystones, marls, and chert	59.0 ± 6.5	26.6 ± 7.4	32.6 ± 6.8	0.68 ± 0.61	3.11 ± 1.27	0.74 ± 0.19
VIII	305.0–324.0	Chalk	62.6 ± 10.6	13.3 ± 3.9	22.7 ± 5.4	1.05 ± 0.35	1.24 ± 0.45	0.44 ± 0.13

[a] Recorded through the pipe from 324 mbsf to the mud line.

determined by the depth interval between records. At 400 m/hr, one full suite can be recorded at approximately 0.4-m intervals.

A schematic diagram of the MCS tool is shown in Figure 13. The sonde has a maximum diameter of 3.5 in. and is split into three sections. The uppermost section contains the magnetostrictive source and the source-firing circuitry. The bottom section is the receiver array, an oil-filled tube surrounded by a fiberglass sheath, which provides lateral support. The 12 receivers are spaced 15 cm apart in an array that spans 1.65 m. The receiver array is separated from the source by a variable-length spacer, which acoustically isolates the receivers from the source. Two spacer sections are available, allowing the source to be separated by 2, 3, or 4 m from the first receiver, depending on the length of the spacer. The sonde is centered in the borehole by bow-spring centralizers at its upper and lower end. A 105-lb weight attached to the lower centralizer helps to prevent "floating" during the descent through the pipe.

The total length of the logging sonde is 7.63 m plus the length of the spacer section. During operations at Hole 418A, the 1-m spacer was used, resulting in a source-to-near-receiver separation of 2 m; the total length of the sonde was 8.63 m. The measuring point of the tool is the midpoint of the receiver array, which in this instance was 2.825 m below the source. Regardless of the length of the spacer section, the measuring point is 3.61 m above the bottom of the tool.

Operations

The MCS was the fifth logging tool run in Hole 418A. Previous logs included the upper part of the susceptibility log, run in two sections from 294 to 480 mbsf, the Schlumberger LSS-ILD-GR log, run in two sections from 325 to 789 mbsf, the Schlumberger NGT-CNTG-LDT, run in open hole from 464 to 789 mbsf and through pipe to the mud line, and the three-axis magnetometer, run from 464 to 789 mbsf. These logs are described in detail in the previous section.

Previous logging runs stopped at various points in the interval between 469 and 481 m log depth when the logging probes lodged on a ledge at 481 mbsf. The second section of the susceptibility log ended at 480 mbsf, where the tool lodged on the bridge. The LSS-ILD-GR encountered the same bridge. Subse-

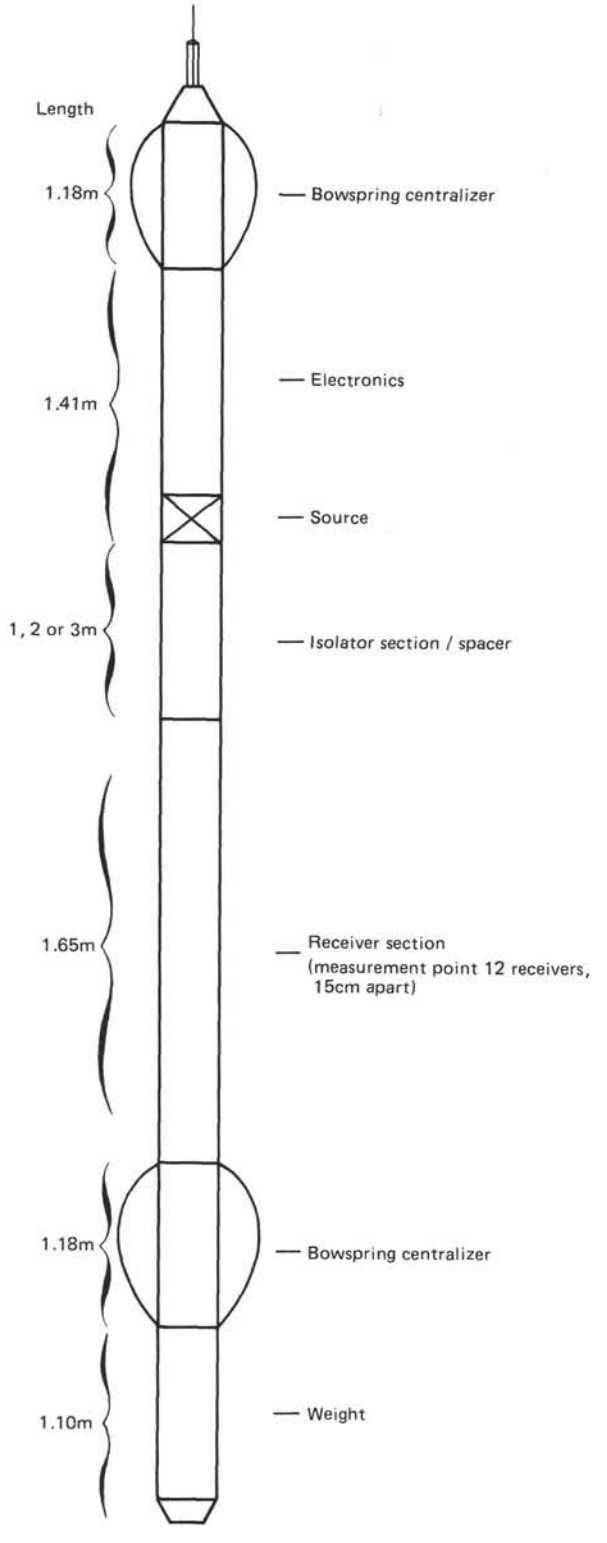

Figure 13. Schematic diagram of the multichannel sonic logging tool.

quent logs were recorded with the pipe straddling the bridge. Running into the well, the pipe was lowered to 493 mbsf and raised to 459 mbsf to log the bridged interval as each log was run. The MCS log was run using the same procedure, resulting in an open-hole interval that extended from 797 to 459 mbsf.

The MCS tool was run into the well at 0100 hr, 30 March 1985. The tool left the pipe at 0315 hr, and a downgoing log was recorded at 460 m/hr. A full suite of 12 channels was recorded every 0.5 m over the interval from 491 to 767 mbsf. Gaps in the downgoing log occur at 577–592 and 615–620 mbsf, where the recording parameters were modified during the downgoing run. The tool was then lowered to 797 mbsf, and an upgoing log was recorded at 270 m/hr at a 0.3-m sample interval from 796 to 449 mbsf, about 10 m into the pipe. The upgoing logging run was completed at 0503 hr. During the run out of the hole, waveforms were recorded in the pipe until it reached 3 m above seafloor. In all, more than 2200 suites of 12 waveforms were recorded during the 2.5 hr of open-hole operations. The tool was on deck at the conclusion of the experiment at 0745 hr, 30 March 1985.

The depth measurements were recorded from a Comprobe EDC-1 digital decoder driven by one of the two Schlumberger encoders on the logging winch. Depths read from the EDC-1 during the downgoing log were about 6 m less than depths read at the winch cab. These depths were corrected to true depth by adding 6 m to the recorded depth. Before starting up, the depth counter output was corrected to correspond to the depths read at the winch. All depths were measured at the center of the tool, using the drilling stool (0.4 m above the rig floor) as a zero mark. Depths were corrected to depths below seafloor using depth ties to the Schlumberger logs at the top of the Subunit 6A breccia and the Unit 10 massive basalt.

Characteristics of the Full Waveforms

During the operation of the MCS tool, suites of waveforms were recorded at fixed depth intervals and stored on magnetic tape. An example of a waveform suite recorded in granodiorite in a test well on land is shown in Figure 14, where waveforms recorded at the 12 receivers are displayed at offsets corresponding to the receiver positions. To emphasize the characteristics of the waveforms, the same suite appears on the left and right at two different time scales.

This record is an exceptional example of the features of the recorded waveforms in "fast" formations (that is, where the shear velocity of the formation is higher than the compressional velocity of the fluid). In such formations, the borehole supports two refracted waves, a series of normal modes and a Stoneley or tube wave. The first arrival is the refracted compressional wave, followed in some formations by a ringed coda of "leaky P" energy, owing to multiple reflected energy in the annulus between the sonde and the borehole wall. The second arrival is a refracted converted shear wave, which commonly is higher in amplitude than is the compressional arrival. The first normal mode, sometimes called the pseudo-Rayleigh wave, travels at a velocity just below that of the refracted shear wave. This mode is characterized by a low-frequency cutoff related to the formation and fluid properties and to the size of the borehole. The pseudo-Rayleigh wave is highly ringed and can obscure the shear wave in some cases. Other borehole modes have cutoff frequencies that are multiples of the first normal mode cutoff (outside the range of frequencies excited by the source) and are seldom recorded. The last prominent arrival is the Stoneley wave, an interface wave that travels along the borehole wall at a velocity slightly below the compressional velocity of the borehole fluid.

The amplitudes and frequency contents of the arrivals shown here are typical of waveforms recorded in fast formations. Compressional and shear waves contain more high frequencies than does the Stoneley wave. The pseudo-Rayleigh wave is the high-frequency ringed arrival shortly after the shear wave.

Semblance Analysis

Velocities of the various phases are measured using a modified semblance technique. Semblance is computed on a set of recorded waveforms by multiplying the cross-correlation of each waveform pair (suitably time-shifted) and then normalizing this

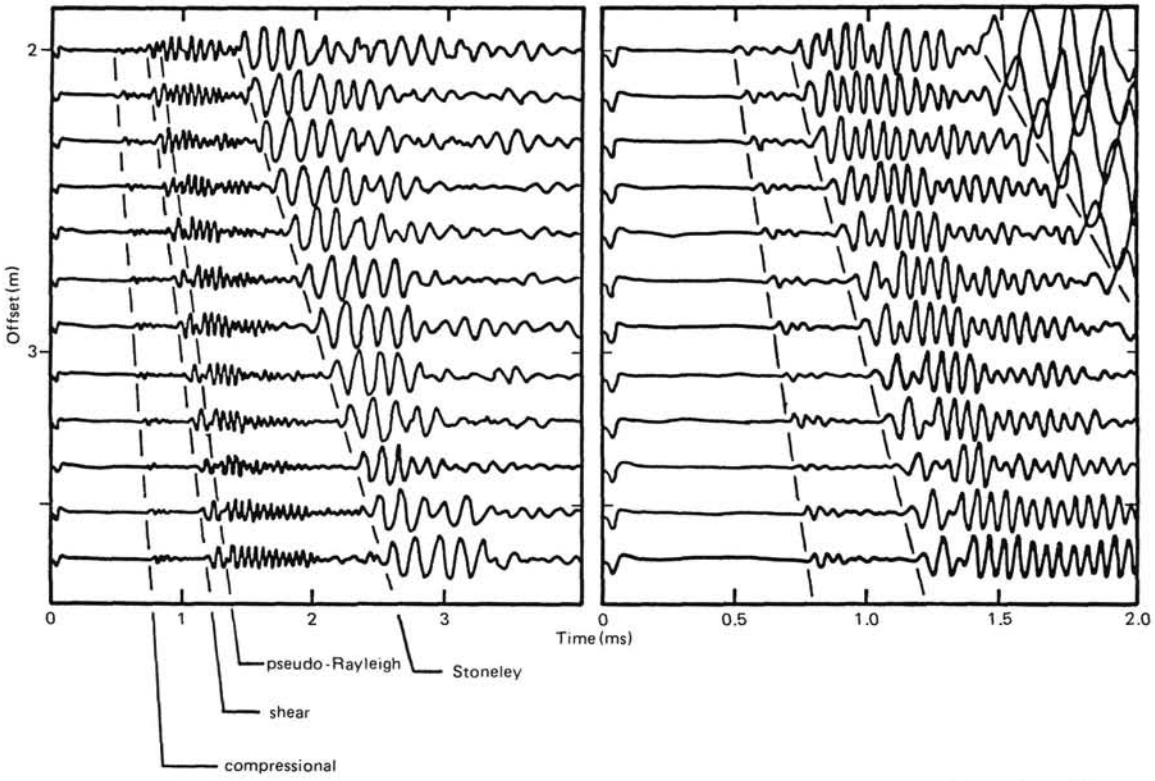

Figure 14. Sample suite of full waveform data from a borehole drilled through granodiorite. Characteristics of the full waveforms are described in the text.

product by the product of the auto-correlations of each trace. This produces a number (the semblance) that ranges between 0 and 1. Perfectly coherent arrivals result in a semblance value of 1. The time shift is computed by multiplying the relative offset between the receiver pair by the slowness (which is simply inverse velocity). For instance, if two receivers are separated by 1 m, and the slowness is 2 milliseconds/m, then the maximum semblance can be obtained by time-shifting the second trace by 2 milliseconds. If one or both of the traces contain noise or are contaminated by energy traveling at a different velocity, then the semblance value will decrease. Therefore, the maximum semblance will be attained when the chosen velocity is nearest the velocity at which most of the energy in the waveform is traveling.

Figure 15 displays semblance calculations for waveform suites recorded from 517 to 529 mbsf. On the right, the plot of the semblance values was calculated using slownesses from 40 to 90 microseconds/ft. The best-fit velocity for each waveform suite is simply the inverse of the slowness for which the semblance is greatest (marked by a cross on the right-hand curve); the corresponding velocity is plotted on the left in km/s. In the center is the semblance value calculated using this velocity. Here the semblance is greater than 0.5, indicating a relatively high level of waveform coherence.

Full Waveforms in Hole 418A

Plate 5 shows the waveforms recorded as a function of depth in Hole 418A at receiver 3, 2.45 m below the source depth and 0.375 m above the measurement point, delineating a constant offset section of the well. Plate 5 also shows Vp, Vs, Vp/Vs, and mean semblance computed from the upgoing log. Note first that the waveforms recorded from 791 to 796 mbsf are identical, suggesting that the bottom of the logging sonde touched down at 795 mbsf. Because the pipe touched down at about 6330 mbrf (817 mbsf) during the initial retrieval operations, approximately 22 m of detritus could have collected during the interval between the retrieval operation and the beginning of the upgoing MCS log.

The compressional, shear, and Stoneley wave arrivals are clear in the interval from 686.5 to 703.5 mbsf, a massive flow (Unit 10). Unit 9 (676 to 679 mbsf) is characterized by sharply lower compressional and shear amplitudes. The constricted zone at 481 mbsf causes a complete loss of transmitted energy if the interval is between the source and receiver (a log depth of 480–483 mbsf). Note also that the zone above 492 mbsf is different from the deeper sections; compressional and shear amplitudes are uniformly low, and the arrival times are highly variable.

The Stoneley wave is most sensitive to borehole-size changes but is also sensitive to rock properties. Interestingly, several units can be uniquely characterized on the sole basis of variations in the Stoneley wave amplitude and arrival time. For example, the amplitudes and arrival times of the Stoneley wave are highly consistent throughout the interval from 722 to 791 mbsf. This corresponds approximately to the extent of Unit 13. The loss of coherency in the uppermost part may be due somewhat to more alteration in the top of the unit than in the remaining section. Similarly, the Stoneley wave is highly coherent in the interval from 514 to 577 mbsf (the uppermost part of Subunit 6B). In the rest of the section, the Stoneley wave is more variable.

Figures 16 through 19 show the waveform suites recorded at various depths in Hole 418A. As in Figure 14, the phases can be identified in these figures by differences in their moveouts. The depths were selected to be representative of the characteristics of the waveforms in each of four different lithologies. Refer to the velocity logs (Figs. 20 and 21) for the discussion of velocities and semblance values.

Figure 16 shows the waveforms recorded at 745 mbsf in the borehole. This unit is a well-cemented pillow, having relatively

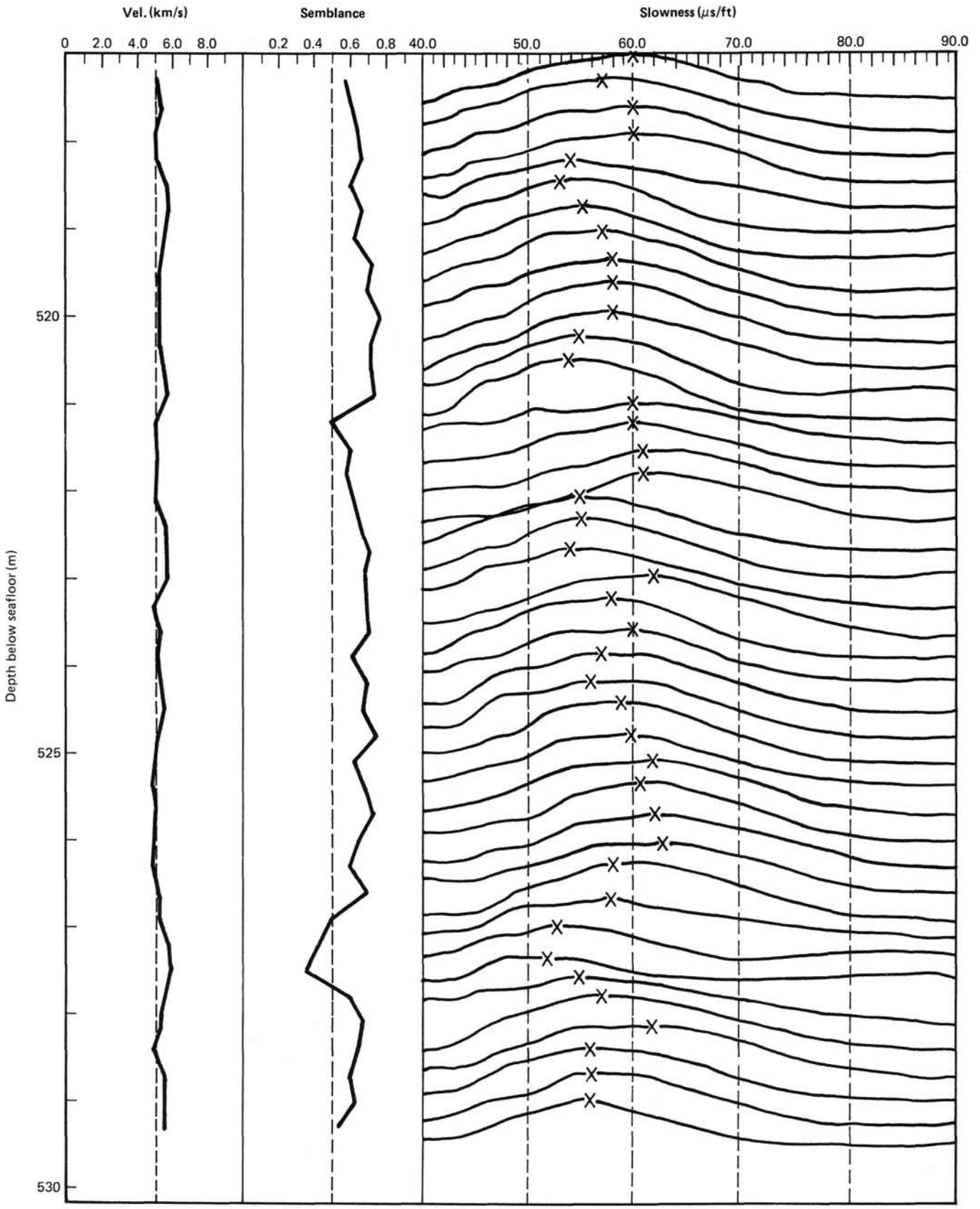

Figure 15. Initial results of the semblance calculation for the interval between 517 and 529 mbsf. Velocity is shown on the left. The center track is the maximum value of the semblance; the velocity used for this result is the group velocity of the arrival. On the right are the semblances calculated at each depth for a range of slowness (inverse velocity) values.

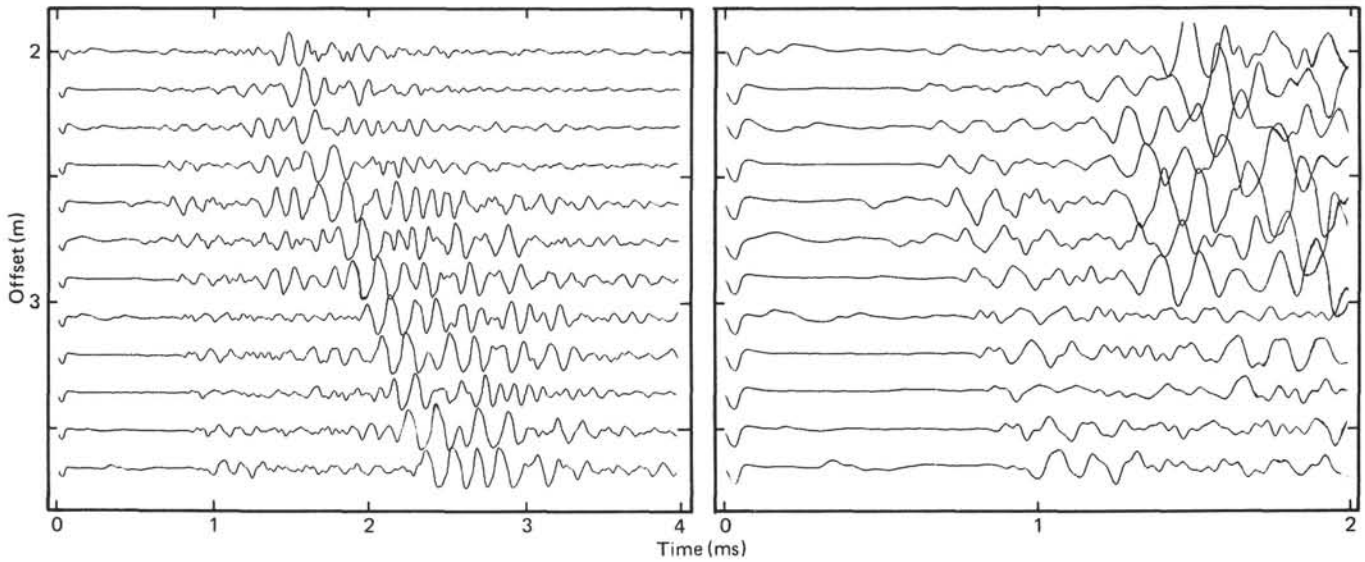

Figure 16. Waveform suite recorded at 745 mbsf, within the pillows of Unit 11, just below the massive basalt of Unit 10.

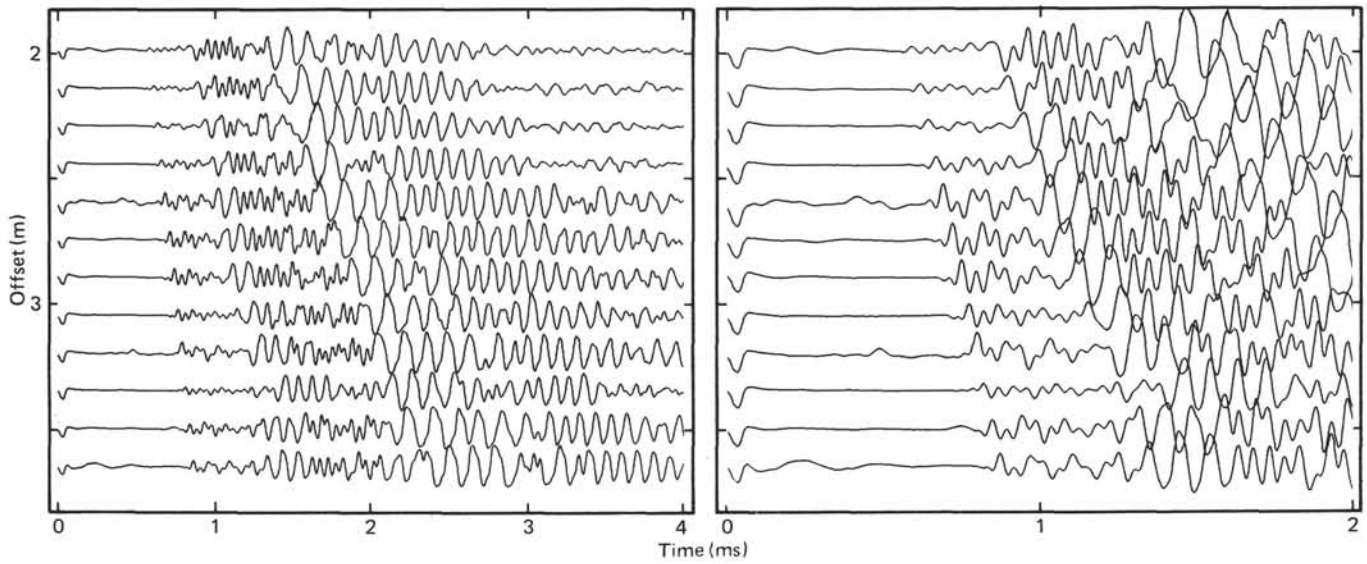

Figure 17. Waveform suite recorded at 682 mbsf, within the massive basalt of Unit 10.

high compressional and shear velocities and a Vp/Vs of about 1.8. Note that the compressional arrivals are somewhat incoherent and that the shear arrival is hard to distinguish from the rest of the waveform. The Stoneley arrival is clear, however. Compressional semblance is high in this interval; shear semblance is much lower.

Figure 17 shows the waveform suites in the massive flow at 682 mbsf. Compressional and shear arrivals are strong and coherent. The ringed configuration in the shear arrival is due to the arrival of the pseudo-Rayleigh wave. Again, the high-amplitude, low-frequency Stoneley wave is clear. This interval is characterized by very high compressional and shear velocities and a Vp/Vs of 1.75. Not unexpectedly, both shear and compressional semblance is very high.

Figure 18 shows the waveforms recorded in the breccia unit at about 512 mbsf. Compressional and shear velocities are low, but the strong, coherent arrivals are clear. The shear waveform is hard to distinguish from the Stoneley arrival because the frequency is much lower than in the pillows or flows and the shear wave velocity is about 2 km/s. Here Vp/Vs is about 2.0.

Figure 19 shows the waveforms recorded in the altered pillows at a depth of 486 mbsf. The compressional and shear amplitudes are low; only the Stoneley wave can be detected clearly. Compressional and shear velocities are low. Not unexpectedly, compressional and shear semblances are also low, suggesting that the quality of the velocity determination is poor. Vp/Vs is greater than 2.0.

Sonic Velocities and Semblance

Figure 20 shows the velocities and semblance values calculated from the waveforms recorded by the downgoing log; Figure 21 shows the results from the upgoing log. Figure 21 also depicts the locations of the waveform suites shown in Figures 16 through 19. These are labeled with the figure numbers for reference. A lithologic column determined from cores recovered during drilling is plotted on the left-hand edge of each figure. The

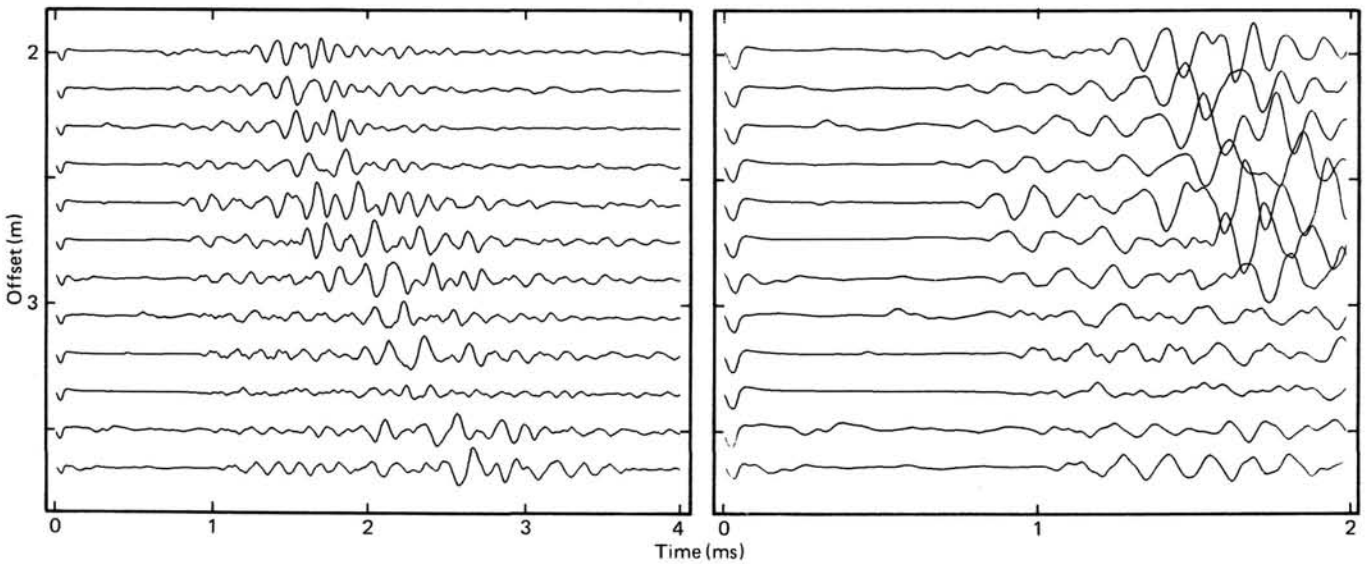

Figure 18. Waveform suite recorded in the breccia of Subunit 6A, at 512 mbsf.

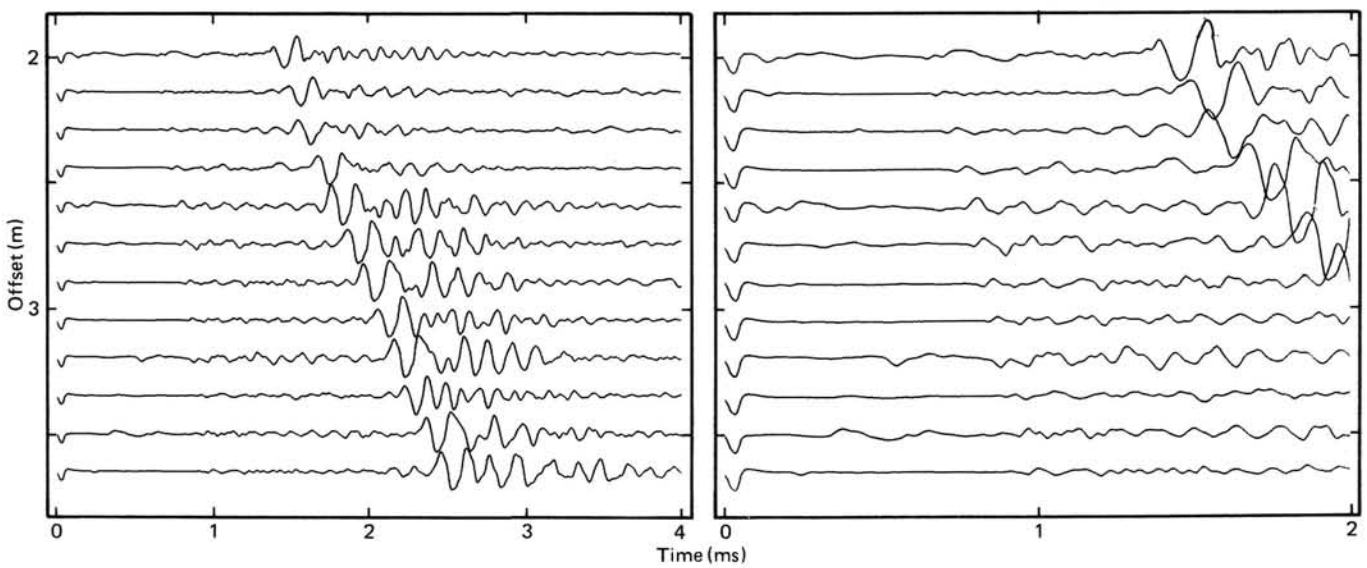

Figure 19. Waveform suite recorded in altered pillows at 486 mbsf.

depth scales are slightly different, which accounts in part for the small depth discrepancies between the unit boundaries determined from the logs and from the cores. Most of the remaining discrepancy can be ascribed to the occasionally poor core recovery. The up- and downgoing logs are similar. Above about 490 mbsf, the semblances are low; compressional velocities are about 4.5 km/s or less, and shear velocities are less than 2.5 km/s. However, these results are not reliable owing to the low semblance. Compressional velocity in the rest of the well ranges between 5 and 6 km/s, and shear velocity between 2.6 and 3.4 km/s; both velocities increase somewhat with increasing depth. Throughout the well, Vp/Vs is variable, between 1.7 and 2.1. A few sections are notable, however. The Subunit 6A breccia appears at 503–514-m log depth and has a shear velocity of 2.2 km/s and a compressional velocity of 4.5, resulting in Vp/Vs of 2.0–2.1. The massive flow at 679–687 mbsf has Vp = 6.0, Vs = 3.3, and Vp/Vs = 1.75. The interval between 733 and 741 mbsf has Vp = 5.9–6.2, Vs = 3.0–3.3, and Vp/Vs about 1.8.

Semblance in most of the well is above 0.5, indicating that these velocities are generally reliable. Depths above about 490 mbsf have very low semblance. The interval from 527 to 587 mbsf also has a semblance of less than 0.5, and the semblance is also intermittently low in the next 40 m. Interestingly, the Schlumberger logs also suggest that the formation is heterogeneous in this interval. Density is highly variable and much lower in the upper part of the interval, suggesting that this interval (which spans most of Subunit 6B) is anomalous. (See "Conventional Logging Results" for plots of the Schlumberger logs and for further discussion.)

Conclusions

The MCS tool performed well in Hole 418A, recording more than 2200 waveforms. Compressional velocities range between 4.5 and 6 km/s throughout most of the logged interval. Shear velocities are generally between 2.1 and 3.4 km/s. Vp/Vs values range between 1.7 and 2.1 and appear to vary systematically

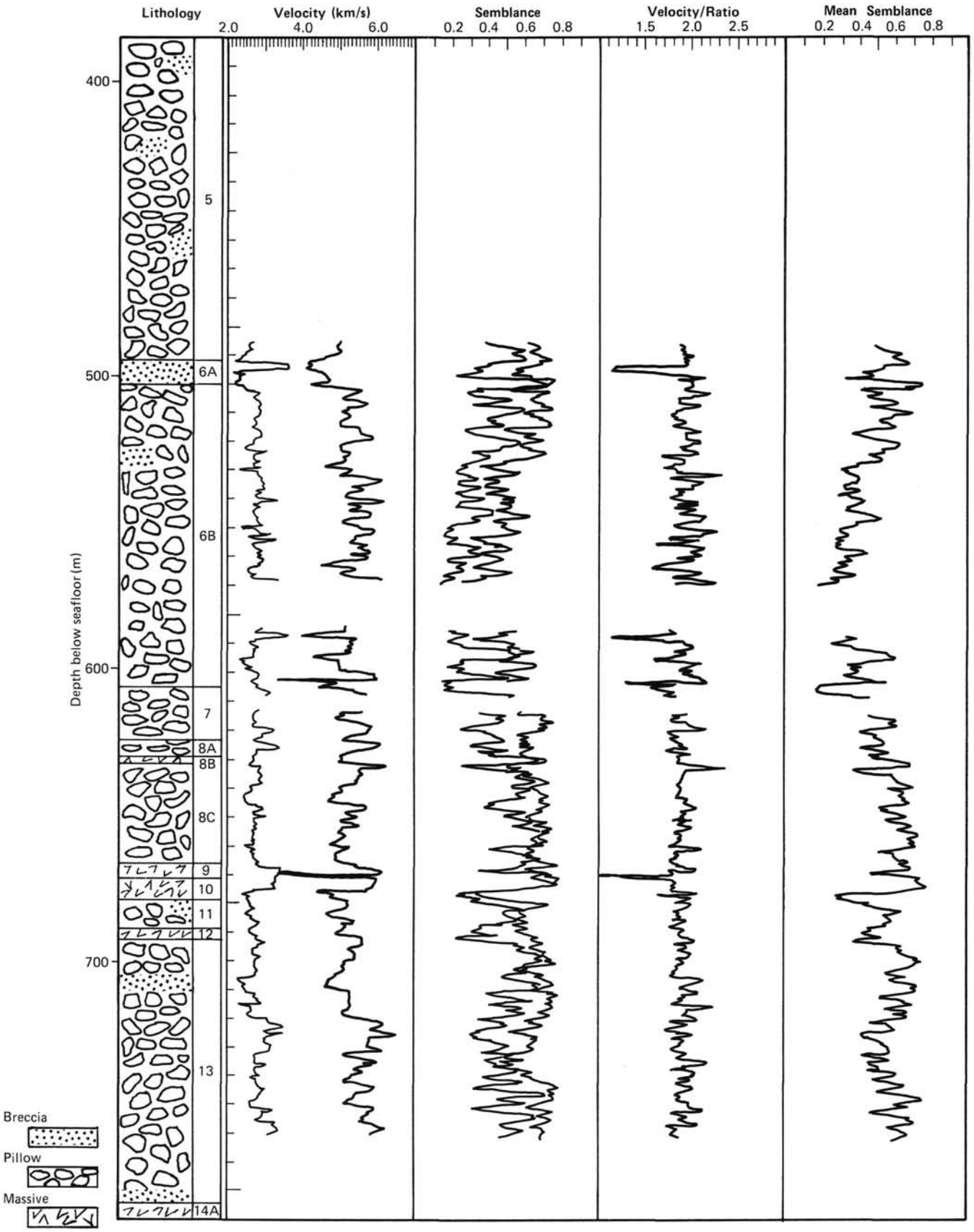

Figure 20. Semblance analyses of the downgoing log, showing compressional and shear velocity, semblance, Vp/Vs, and mean semblance. The lithologic column determined from the core is shown for reference.

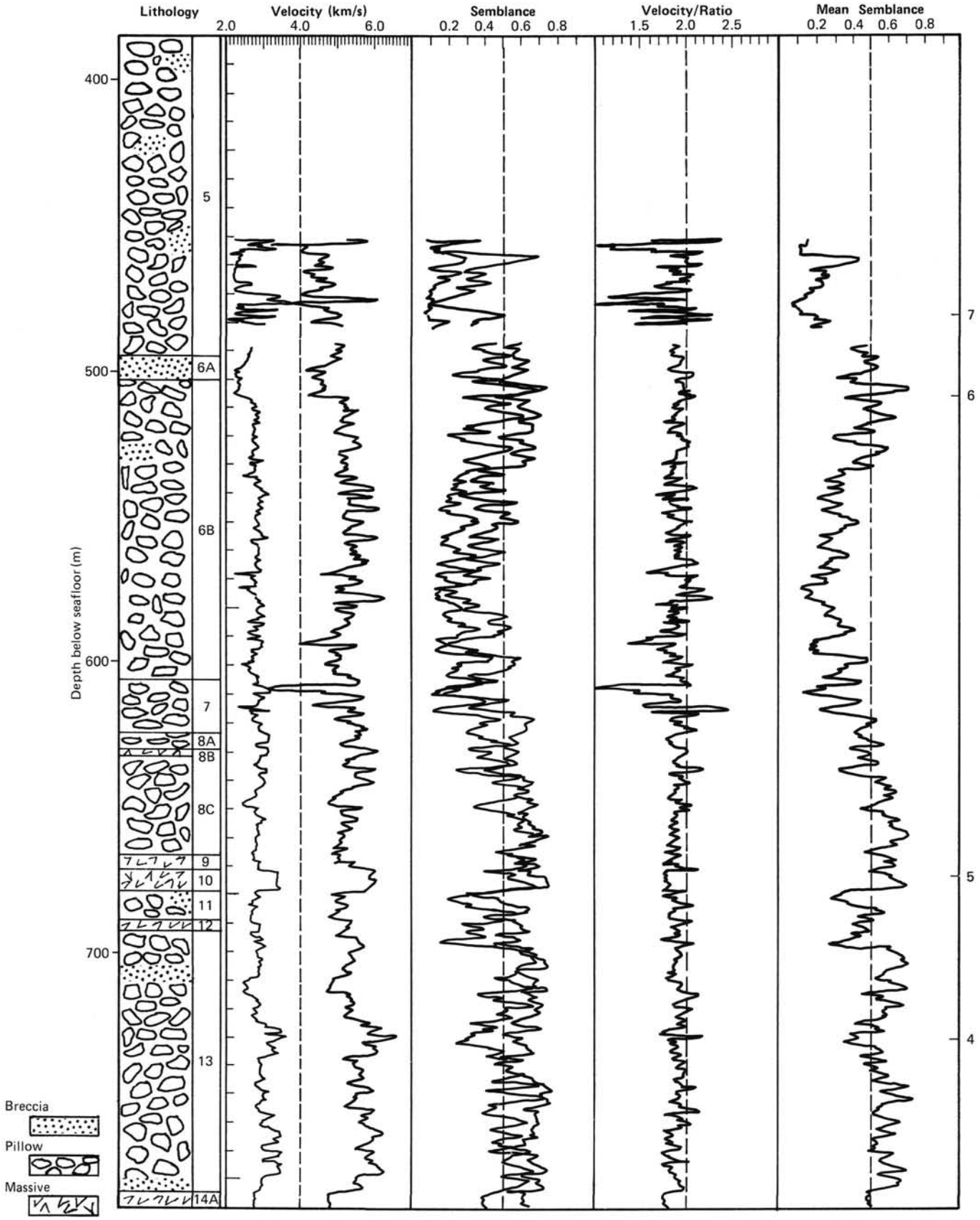

Figure 21. Semblance analyses of the upgoing log, showing compressional and shear velocity, semblances, Vp/Vs, and mean semblance. The positions of the tool with which the data in Figures 16 through 19 were recorded are also shown. The lithologic column determined from the core is shown for reference. These data are reproduced at expanded scale along with a variable density plot of waveform 3 in Plate 5.

from unit to unit. In general, both compressional and shear wave velocities increase from top to bottom in this interval. Finally, local variations can be systematically related to differences between lithologic units observed in the core and in other logs.

BOREHOLE SEISMIC EXPERIMENT RESULTS

Introduction

The R/V *Fred H. Moore* joined the *JOIDES Resolution* at Site 418 to study the uppermost velocity structure, including seismic anisotropy and lateral heterogeneity, in old crust in the Atlantic. The crustal age at Site 418 (25°02.08′N, 68°03.44′W) is 110 m.y.

The cruise consisted of three parts: (1) detailed reflection profiling near the site to determine depth to basement, (2) borehole seismic experimentation, and (3) sonobuoy refraction-line work at the site to study deep structure. Significant dates are outlined in Table 10, and the participating personnel are listed in Table 11.

Reflection Profiling

While waiting for borehole seismometer deployment on the *JOIDES Resolution*, the R/V *Fred H. Moore* carried out a reflection-profiling survey near DSDP Sites 417 and 418. The pattern in Figure 22 (2-km line spacing, out to 8 km from the hole) was made with lines running 110°–290° (in the spreading direction) and orthogonally to this at 020°–200°. Additional coverage was obtained north of this survey to complete the region around Site 417. A total of 370 km of profiling was obtained.

The source was a 90-in.^{3} water gun (from U.S. Geological Survey, Woods Hole). The data were received on a single-channel streamer (from Woods Hole Oceanographic Institution) and on a five-channel streamer (from the University of Texas at Galveston). The data were real-time digitized on a DFS-IV acquisition system on the R/V *Fred H. Moore*. Examples of the data and a preliminary analysis of some significant features are outlined in the "Geophysical Profiling, ODP Leg 102" chapter and the seismic-line interpretation in the hole summary (this volume).

Table 10. Schedule of events for borehole seismic experiment.[a]

Date	*Resolution*	*Moore*
14 March	Arrive Miami port call (0800 hr)	
19 March	Depart Miami (0800 hr)	Depart Galveston (1030 hr)
21 March	Arrive Site 418 (1900 hr)	
23 March		Arrive Miami to load explosives (1930 hr)
24 March	Reenter Hole 418 (1900 hr)	Depart Miami (1130 hr)
26 March	Start logging (1400 hr)	
27 March		Arrive Site 418 (1800 hr)
28 March		Start reflection profiling (0600 hr)
30 March		End reflection profiling (1000 hr)
	Start OSE (1830 hr)	Start OSE (1830 hr)
4 April	End OSE (0430 hr)	End OSE (0430 hr)
5 April	Begin sonobuoy refraction work (0900 hr)	Begin sonobuoy refraction work (0900 hr)
6 April	Pause sonobuoy refraction work (0300 hr)	Pause sonobuoy refraction work (0300 hr)
		Depart Site 418 (1530 hr)
	End sonobuoy refraction work (1930 hr)	End sonobuoy refraction work (1930 hr)
8 April	Depart site 418	
9 April		Arrive Miami (1300 hr)
10 April		Depart Miami
11 April	Arrive Norfolk (1130 hr)	

[a] Times given are in local time.

Table 11. Personnel for borehole seismic experiment.

Personnel	Vessel
[a]Ralph Stephen—P.I.	*Resolution*
Hartley Hoskins—borehole seismologist	*Resolution*
Lee Gove—digital and analog data acquisition technician	*Resolution*
Jim Broda—shooter	*Moore*
Gordon Glass—shooter	*Moore*
Archie Roberts—shooter	*Moore*
Wayne Spencer—watchstander/Del Norte technician	*Moore*
Tom Bolmer—data-acquisition technician	*Moore*
Ken Griffiths—elec. engineer	*Moore*
Mike Campbell—elec. technician	*Moore*
Oscar Febres-Cordero—mech. technician	*Moore*
George Pearcy—mech. technician	*Moore*
Dave Senske—powder monkey/watchstander	*Moore*

[a] Transferred to and from Site 418 on *Moore*.

Borehole Seismic Experiment

For the borehole seismic experiment, a three-component seismometer was clamped at five depths in Hole 418A, while the R/V *Fred H. Moore* fired explosive charges and air guns on circle and radial line patterns out to 8-km range. The experiment had the following objectives:

1. To determine, *in situ*, the velocity structure of the crust intersected by the hole at seismic frequencies (~10 Hz).
2. To determine the large-scale fracture density and fracture orientation in the upper crust by measuring the direction and magnitude of the seismic anisotropy.
3. To determine the magnitude and scale of the lateral variations within the upper oceanic crust. These variations are caused predominantly by changes in porosity and large-scale fracturing in the crust.
4. To look ahead of the bit to determine the depth of discontinuities such as the Layer 2B/Layer 2C boundary (the bound-

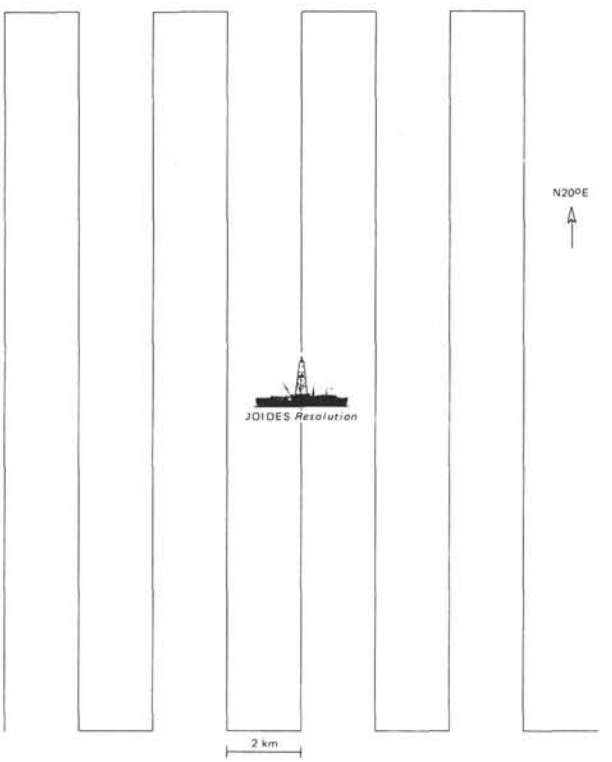

Figure 22. Shooting pattern for reflection profiling at the site. This pattern was shot along the spreading direction (110°–290°) and perpendicular to this direction (20°–200°).

ary between extrusive and intrusive basalts) and the deeper reflectors.

The fundamental question addressed by the experiment is: How typical of the area is the crust intersected by the hole (and analyzed by core samples and logging)? The seismic experiment effectively increased the diameter of the hole from centimeters to hundreds of meters and bridged the gap between the small-scale sample analysis and logging and the large-scale geophysical measurements, which to date have defined the structure of oceanic crust.

The borehole seismic experiment addressed these questions and used several innovative techniques:

1. Compressional wave velocity at the receiver was determined from the inflection point of the first-arrival times, as plotted against range.
2. Seismic anisotropy was investigated, using particle-motion diagrams of three-component data to reveal "split" shear waves. In anisotropic media, shear waves propagate in two polarizations, here resolved as vertical and horizontal. The two shear waves travel at different velocities, which are functions of the azimuth of propagation. This analysis was carried out in addition to the usual measurement of compressional wave arrival times as a function of azimuth.
3. Upper crustal velocities were estimated from the decay with depth into basement of the direct wave. This is a new technique, which had not been used previously because of inadequate data.
4. The circular stack, a new technique, was used to enhance the signal-to-noise ratio of deep reflectors by summing traces shot on a circle of constant range from the borehole.

This data set has higher density and is of better quality than that produced by any previous borehole seismic experiment. Three component seismograms (vertical, horizontal 1, and horizontal 2) were obtained for more than 3300 shot locations within 8-km range. The seismometer was clamped with a motor-driven, spring-loaded arm at five depths in the hole: three deep positions (754, 654, and 554 mbsf) for polarization analysis and two shallow positions (405 and 365 mbsf) for analysis of the direct wave root.

The R/V *Fred H. Moore* has the capability of firing two 2000-in.^{3} air guns at a 30-s repetition rate. Air-gun shots (two 2000-in.^{3} guns) and explosive charges (15 lb) were intermixed in the experiment. The data were acquired digitally in real time using the Highres data-acquisition system on the *JOIDES Resolution* Masscomp computer. The real-time digital-acquisition system provides much greater dynamic range than did the analog recording used previously and alleviates the need of months of post-real-time analog-to-digital conversion.

Field tapes written in SEG-Y format were transcribed on the ship's VAX 11/750 computer system, where data processing (filtering, stacking, plotting, arrival-time picking, etc.) could be carried out within hours of acquisition. This rapid turnaround allowed acquisition parameters to be adjusted as the experiment progressed.

Ranges were determined to within 10 m, using Del Norte radar transponders, and bearings to the R/V *Fred H. Moore* were obtained by a watch of ODP marine technicians on the bridge from the ship's radar. Shot instants were transmitted using dual-tone multifrequency (DTMF) encoding from the R/V *Fred H. Moore* to the *JOIDES Resolution* via VHF radio. Both ships monitored National Bureau of Standards Universal Coordinated Time (UTC) transmitted on the National Oceanic and Atmospheric Administration GOES satellite using Kinematics True Time satellite receivers. Each ship tied its acquisition computer system to an accurate local chronometer, which was periodically rated against the satellite time. Timing accuracy should have been to a millisecond.

Operations

The R/V *Fred H. Moore* of the Institute for Geophysics, University of Texas, was used as the shooting ship. It arrived at Site 418A at 2100 hr UTC on 27 March 1985. Radar transponders necessary for the experiment were transferred. Between 1100/28 and 1400/30 hr UTC, the R/V *Fred H. Moore* carried out the reflection-profiling survey, using an 80-in.^{3} water gun, on a 2-km grid of the immediate vicinity of sites 417 and 418.

The borehole seismometer was tested on deck at 0100/31 hr UTC and lowered to its first depth (754 mbsf) and clamped at 0207 hr. The preamplifier has a low output impedance, and its gain for the experiment was either 48 or 60 dB. The strategy was to bring the signal up the 30,000-ft seven-conductor logging cable at a high level (2–20 volts) to maintain a good signal-to-noise ratio.

An eight-spoke pattern oriented 020°, 065°, 110°, 155°, 200°, 245°, 290°, and 335° was shot, together with concentric circles at 2-, 4-, 6-, and 8-km radii. The 020°–200° heading is approximately parallel to the magnetic anomaly pattern, and the 110°–290° heading is parallel to the fracture zones in the area. Most or all of this pattern was repeated for each clamping of the seismometer. In the entire program, 943 explosive shots were fired, generally on a 3-min schedule, and 2,345 air-gun shots were fired, generally on a 1-min schedule (Figs. 23 through 27 and Tables 12 and 13). Total shooting time was about 92 hr. Total time in the hole was 106 hr.

Numerous higher frequency arrivals were observed, which are probably due to falling debris in the hole. At three of the unclampings, closure of the arm required repeated flexing, an indication of debris lodged around the instrument. This was corroborated by the encounter of the drill pipe with sediment and rock bridges and its removal of 30 m of fill from the bottom of the hole. The nearly continuous pumping of water down the drill pipe and the periodic raising and lowering of the drill pipe to distribute the bending stress probably also dislodged material from the wall of the hole.

The experiment ended at 0610/4 hr UTC because of shorts in the logging cable 4 m above the seismometer caused by mechanical abrasion from the uncompensated heave of the logging-cable suspension. The tool, which showed no damage, was brought to the rig floor at 0930/4 hr UTC.

After the borehole experiment, the R/V *Fred H. Moore* shot four 40-km-long unreversed refraction profiles, at 020°, 200°, and 290°, to sonobuoys drifting near the *JOIDES Resolution*. There were 230 shots using 15–120-lb explosive charges. After transfer of equipment and personnel, the R/V *Fred H. Moore* departed for Miami at 0040/7 hr UTC.

The Data

Examples of the data are given in Figures 28, 29, and 30; all the data and the shot locations are given in the Appendix. Figure 28 shows clearly the advantages and disadvantages of air guns and explosives. Air guns have a more consistent waveform, are fired at a shorter spacing, and have less uncertainty in depth and range than do explosives. However, the first P-wave energy drops below the background noise level at about 6-km range. Explosives, which are about 12 dB larger in signal strength than the two 2000-in.^{3} air guns, are required for longer range work.

Preliminary analysis gives a compressional wave velocity of 4.9 k/s and a shear wave velocity of 2.7 k/s in the area. This agrees reasonably well with sonic-logging results and is consistent with the hypothesis that porosity in the upper crust has

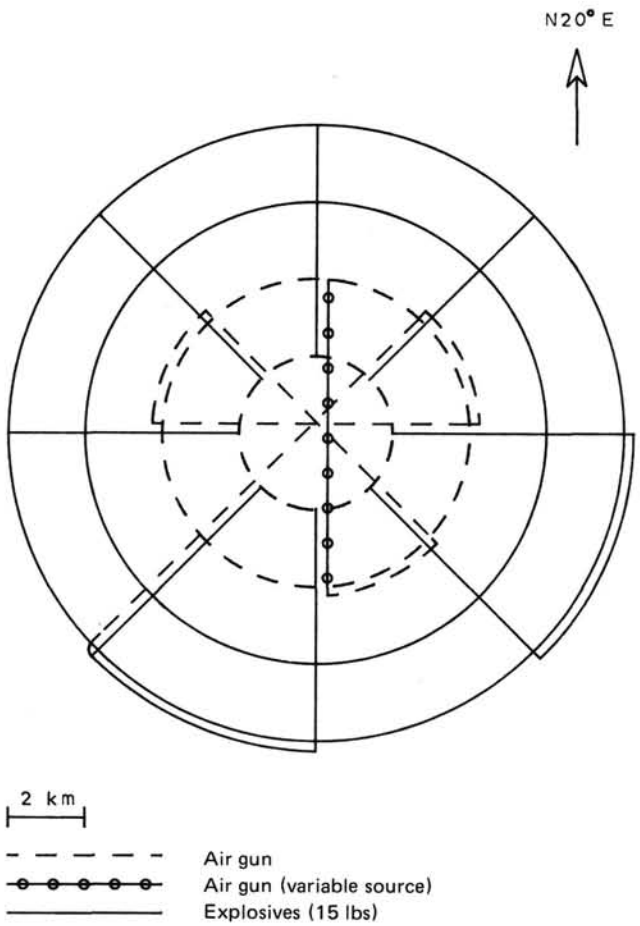

Figure 23. Shooting pattern shot to the borehole geophone at 754 mbsf (430 m into basement).

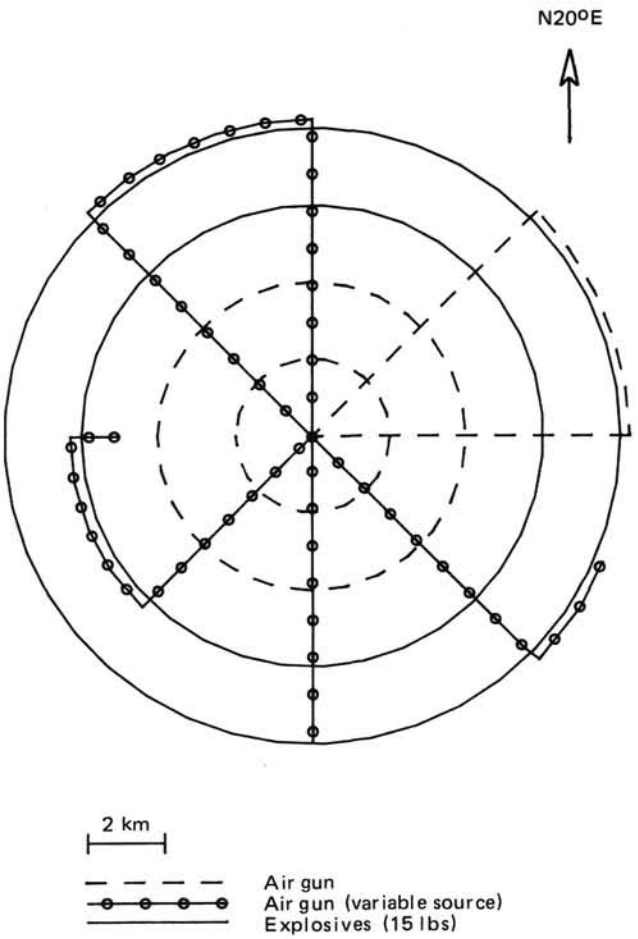

Figure 24. Shooting pattern shot to the borehole geophone at 654 mbsf (330 m into basement).

been reduced by secondary mineralization. Analysis of anisotropy and lateral heterogeneity must wait for further processing of the data.

Background-noise measurements were acquired at all five depths (Fig. 29). At the shallow-position borehole, noise was observed with and without the heave compensator (Fig. 30). Levels were significantly quieter when the heave compensator was deployed. Apparently most of the background noise was caused by the pipe banging in the hole.

Sonobuoy Refraction Work

The sonobuoy refraction part of the program was not planned. It was carried out after the borehole seismic experiment, while we waited for the opportunity to do more shooting to the borehole seismometer, and consumed the rest of the explosives.

Two refraction lines were run to 40 km, 20° from the site, and one line each was run to 200° and 290°. The latter line ran out to 55 km. The data should be adequate to study Layer 3 and the Mohorovičić discontinuity (Moho) at the site and will provide further survey data, should more drilling be attempted.

THREE-AXIS BOREHOLE MAGNETOMETER MEASUREMENT RESULTS

The main components of the borehole magnetometer (Bosum and Rehli, 1985) are as follows:

1. A three-axis Foersterprobe Fluxgate system, which measures the Earth's magnetic field in three mutually perpendicular directions, one parallel and two perpendicular to the borehole (sensitivity 1 nT).

2. A gradiometer, which measures the gradient of the magnetic field parallel to the borehole (sensitivity 2 nT/40 cm).

3. A directional unit, consisting of a gyroscope used as a directional reference (mean drift 0.6°–1°/hr), and two inclinometers (accelerometers) (sensitivity 5×10^{-3} degrees). This unit is fixed to the magnetometer, thus defining its position.

4. The electronic unit, consisting of a signal-processing, data-transmission unit and a power supply.

Measurements are taken continuously downward and upward in the borehole (magnetometer log) and with the probe held stationary at discrete points at increments of 5–10 m. The magnetometer log yields detailed information on magnetic characteristics of the drilled rock sections, stationary measurements on the (total) magnetization directions, and magnetic source bodies near magnetically undisturbed drill-hole sections.

In the case under discussion, the magnetometer log recorded the vertical component Z of the Earth's magnetic field at a spacing of about 8 cm. The azimuth of the gyroscope was also read to allow more accurate measurement of the probe's motion during logging (in relation to the gyroscope reference).

The vertical-component magnetometer log is shown together with the susceptibility log in Plate 6 (back pocket). The normal value of the vertical component of the Earth's magnetic field is about 37,200 nT at Site 418.

The most conspicuous feature of the magnetometer log is the change of the sign of the anomaly of the vertical component Z

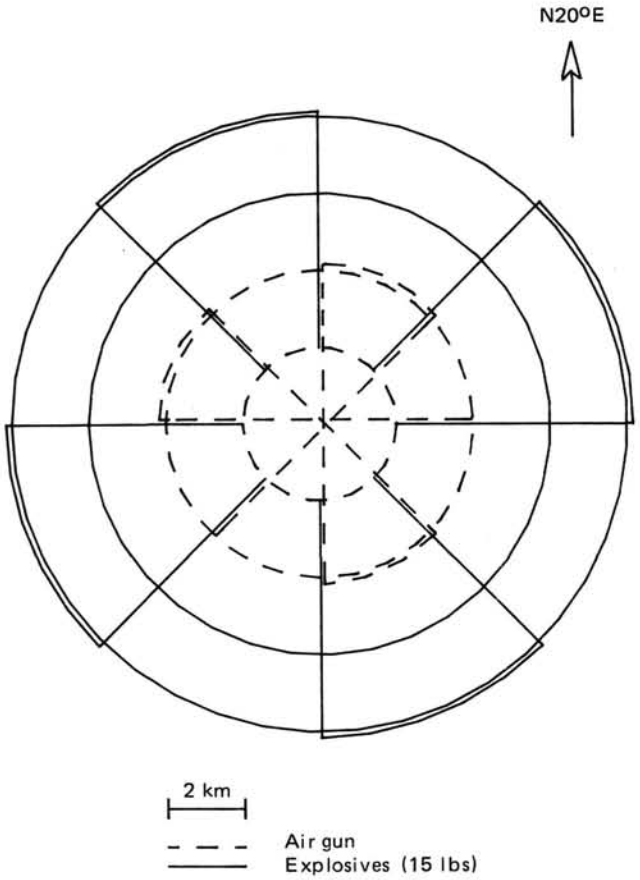

Figure 25. Shooting pattern shot to the borehole geophone at 554 mbsf (230 m into basement).

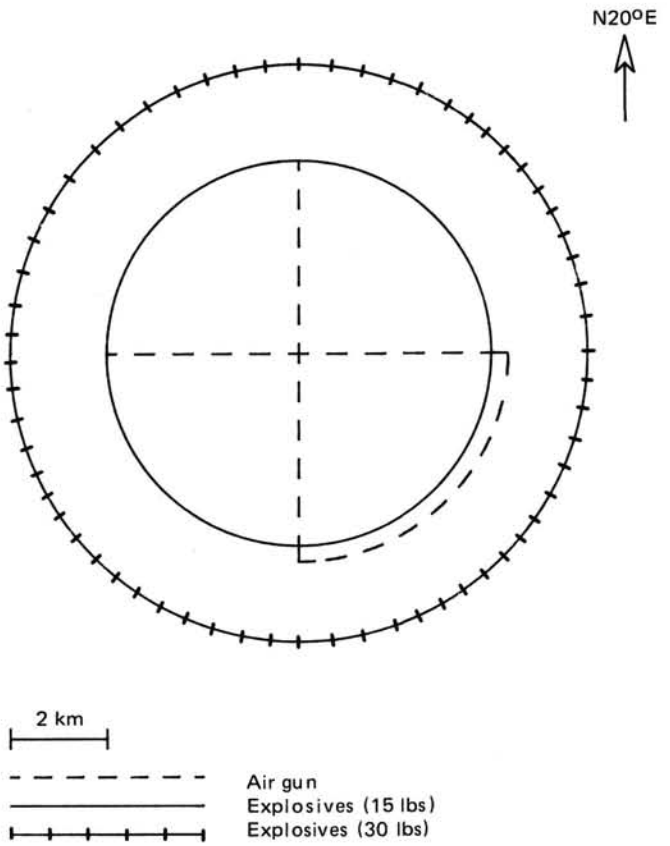

Figure 26. Shooting pattern shot to the borehole geophone at 405 mbsf (81 m into basement).

from about −8000 nT to +6000 nT (with respect to the normal field value) at a depth of about 503 mbsf. This change is caused by a reversal of polarization of the upper and lower basalt units and is also indicated by investigations of magnetic properties of core samples from the borehole (Levi, 1979). The reversal coincides with the breccia zone, shown on the lithologic log at 503–514 mbsf.

Below the breccia zone, the magnetometer log can be subdivided by the anomaly pattern and/or field strength into different units. The strongest fields—i.e., the strongest magnetizations and most homogeneous composition—occur in the sections between about 514 and 565 mbsf, 565 and 610 mbsf, and below about 725 mbsf. The sections between 610 and 645 mbsf and between 645 and 725 mbsf are characterized by a more heterogeneous behavior, in accordance with the lithologic profile, which shows numerous intercalations of massive basalt in pillow basalt. The magnetic and petrographic boundaries typically coincide approximately. It should be mentioned that the estimated accuracy of the depth determination is ±2 m because of cable stretch, ship's heave, and uncertainty in the depth-measuring system. Below about 785 mbsf, the magnetic field becomes smoother and declines, as does the natural remanent magnetization (NRM) of drill cores.

Some sections in the magnetometer log indicate thin zones of low field levels caused by lower magnetizations. A magnetic reversal indicated by core measurements (NRM) at a depth of about 675 mbsf, reported by Levi et al. (1979), is not indicated by the magnetometer log.

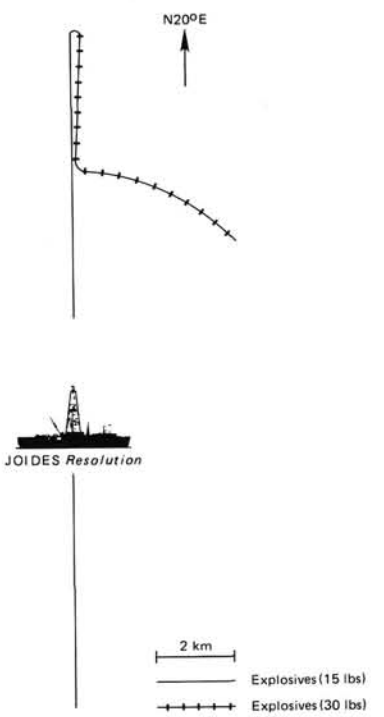

Figure 27. Shooting pattern shot to the borehole geophone at 365 mbsf (41 m into basement).

Table 12. Shooting program.

Resolution heading	Description	Shot no.	Time (UTC)	Comments	Shooting source[a]
754 mbsf (430 m into basement)					
126–127	20° line	20–32	90/0436–0512	2–8 km, 48 dB geophone gain	E
126–127	335° line	33–44	0522–0555	60 dB geophone gain from here on	E
126–127	290° line	45–57	0637–0713		E
126	245° line	58–68	0724–0754		E
126	245°–200° arc	69–86	0757–0845	At 8 km	E
126–127	200° line	87–97	0848–0915		E
126–127	155° line	98–110	0930–1006		E
126	155°–110° arc	111–122	1009–1042	At 8 km	E
126–127	110° line	123–134	1045–1118		E
127	65° line	135–146	1133–1206		E
126–127	8-km circle	148–232	1218–1630	046°–065° gap	E
126–127	6-km circle	233–303	1648–2024	042°–017° overlap	E
126	20°–200° lines	305–374	2137–2228	0–4 km one gun partly	A
126	100°–155° arc	375–396	2230–2250	Two guns(?) at 4½ km	A
126–127	155°–335° line	397–440	2251–2334	Two guns(?)	A
126–127	335°–290° arc	441–463	2335–2358	Two guns(?) at 5 km	A
127	290°–110° lines	464–516	2359–91/0050	Two guns(?)	A
127	110°–65° arc	517–552	0052–0105	Two guns(?) at 3–5 km	A
127	65°–245° lines	553–621	0127–0236	Out to 8 km	A
127	249°–224° arc	622–656	0237–0310	Back to 4-km circle	A
126–127	4-km circle	670–813	0325–0548	206°–205° overlap	A
126–127		814–835	0549–0610	Between circles	A
126–127	2-km circle	836–917	0611–0731	143°–116° overlap	A
654 mbsf (330 m into basement)					
		989–1010	0901–0953	False start on line 1	A
126	200°	1011–1046	0954–1029	Lines to 8 km	A
		1047–1084	1030–1107	Circling *Resolution*, problems	A
127	20° line	1085–1136	1108–1159		A
127	20°–335° arc	1140–1169	1203–1232	At 8 km	A
126–127	335°–155° lines	1170–1280	1233–1423	Intermittent guns	A
126	155°–110° arc	1281–1295	1424–1438	Intermittent guns at 8 km	A
126–222	8-km circle	1297–1383	1527–1945	82°–84° gap	E
232–233	6-km circle	1384–1455	2006–2339	64°–47° overlap	E
232–233	4-km circle	1456–1601	92/0015–0240	Two air guns	A
		1602–1622	0241–0301	Between circles, 343°	A
212–146	2-km circle	1623–1699	0302–0418	343°–289° overlap	A
		1700–1730	0419–0449	Between circle and line	A
146–147	110° line	1731–1777	0450–0535	8-km lines, 2 guns	A
146–147	110–65° arc	1778–1808	0536–0607	At 8 km	A
147	65° lines	1809–1899	0608–0738	1 and 2 guns	A
147	6-km arc	1900–1944	0739–0819	Poor air guns	A
554 mbsf (230 m into basement)					
141–162	8-km circle	1945–2033	0930–1357	224°–210° overlap	E
		2034–2037	1358–1414	Between lines	E
151–162	6-km circle	2038–2104	1415–1733	208°–197° overlap	E
166–167	155° line	2106–2116	1818–1848	High res. problems, 8 km lines	E
167	110° line	2117–2129	1900–1936		E
166–167	110°–65° arc	2130–2142	1937–2017	At 8 km	E
167–169	65° line	2143–2154	2018–2048		E
167	020° line	2155–2164	2100–2127		E
167–172	020°–335° arc	2165–2175	2133–2203	At 8 km	E
172	335° line	2176–2186	2206–2236		E
172	290° line	2187–2197	2251–2321		E
172	290°–245° arc	2198–2209	2324–2357	At 8 km	E
172	245° line	2210–2220	93/0000–0030		E
166–173	200° line	2221–2232	0042–0115		E
167–170	200°–155° arc	2233–2244	0118–0151	At 8 km	E
156–172	335° line	2245–2254	0154–0221		E
157–172	2-km circle	2255–2334	0243–0403	60°–40° overlap	A
171–205	40°–270° arc	2345–2390	0414(?)–0459	At 4 km, timing no good	A
205–207	4-km circle	2391–2545	0500–0734	269°–267° overlap	A
207	245°–065° lines	2560–2612	0749–0841	From/to 4 km	A
207	065°–020° arc	2614–2637	0843–0906	At 4 km	A

[a] A = air gun; E = explosives.

Table 12 (continued).

Resolution heading	Description	Shot no.	Time (UTC)	Comments	Shooting source[a]
554 mbsf (cont.)					
208–166	20°–200° lines	2641–2710	0910–1019	From/to 4 km	A
166–167	200°–155° arc	2711–2780	1020–1129	At 4 km *Moore* turned right instead of left to start line	A
140–172	155°–335° lines	2782–2825	1131–1214	From/to 4 km	A
161–172	335°–290° arc	2826–2852	1215–1241	At 4 km	A
161–172	290°–110° lines	2853–2916	1242–1345	From/to 4 km	A
405 mbsf (81 m into basement)					
161–172	20°–200° line	2925–3006	1421–1542	From/to 6 km	A
171–172	200°–110° arc	3008–3044	1544–1620	At 6 km	A
171–177	110°–290° line	3045–3015	1621–1721	From/to 6 km	A
179–185	4-km circle	3106–3121	1722–1737	Aborted air-gun failure	A
184–185	4-km circle	3123–3169	1857–2115	257°–251° overlap	E
187–342	6-km circle	3170–3240	2154–94/0210	30 lb, 165°–154° overlap	E
365 mbsf (41 m into basement)					
2–(359)	70°–10° arc	3244–3255	0218–0248	30 lb, at 6 km	E
2–(346)	20° radial line	3257–3264	0300–0321	To 10 km, 30 lb, shot-instant transmission problem	E
(345)–9	020°–200° lines	3267–3296	0339–0526	From/to 10 km (no shots within 2 km) 15 lb	E
342 mbsf (18 m into basement)					
			094/0610 Z	Logging-cable malfunction	E

Table 13. Shooting statistics for Leg 102 oblique seismic experiment.

Shooting source	Duration	Number of shots	Time (hr)	Shot numbers
Explosives	15 hr 48 min	303	90/0436–2024	1–303
Air gun	17 hr	991	2137–91/1438	304–1295
Explosives	8 hr 12 min	158	1527–2339	1297–1455
Air gun	8 hr 34 min	488	2340–92/0814	1456–1944
Explosives	16 hr 51 min	309	0930–93/0221	1945–2254
Air gun	14 hr 54 min	866	0243–1737	2255–3121
Explosives	10 hr 29 min	173	1857–94/0526	3123–3296

The data of the stationary measurements carried out every 5 m show that the computed directions of the anomalous fields clearly form clusters that indicate a reversal of the direction of magnetization above and below the breccia zone. The average inclination of the (total) magnetization changes from about $+30°$ to $-30°$, as do the laboratory magnetic measurements of drill cores. The average declination of the magnetization vector also changes at this boundary and points to about 180° below 530 m. It should be stressed that the determination of declination of the magnetization is the great advantage of borehole magnetics in comparison with the investigation of drill samples the azimuthal orientation of which normally is unknown. Using data from the susceptibility log, the Q-factor (ratio of remanent to induced magnetization) was calculated, which amounted to about 9–34 (average for individual layers).

By knowing the declination and inclination, we were able to calculate for the first time paleopole positions from ocean drilling surveys. The calculation considered the induced magnetization calculated from the susceptibility log, which, however, in this experiment did not influence the results significantly because of the large Q-factor. Figure 31 shows the result for different depth ranges of the borehole in comparison with the apparent polar wandering path (Landolt-Börnstein, 1985); to indicate the statistical accuracy of these results, Fisher circles are also plotted. On the average, the locations of these points agree well with the pole positions of the Cretaceous (K).

As a byproduct of the borehole magnetometer measurements, the results of the gyroscope-inclinometer directional unit indicate an almost vertical borehole (inclination $\leq 2°$). The total gyroscope drift was 10° for 15 hr and 40 min.

MAGNETIC-SUSCEPTIBILITY LOGGING RESULTS

Introduction

Magnetic logging was attempted previously on DSDP Legs 68, 69, and 78B (Holes 501, 504B, 505B, and 395A) by a team of scientists from the U.S.S.R., using a three-component fluxgate magnetometer without orientation sensors, combined with a magnetic susceptibility meter (Ponomarev and Nechoroshkov, 1983, 1984). Because the holes were nearly vertical, the magnetometer probe was not stabilized by contact with the borehole wall. The probe lacked a means of orientation, rendering meaningless the horizontal component measurements of the magnetic field. The magnetometer logs of ODP Leg 102, however, were made with an oriented probe of West German design, so that the direction as well as the intensity of the magnetic field could be determined (see "Three-Axis Borehole Magnetometer Measurement Results" section, this volume).

To compute the remanent vector from the magnetometer data, the Earth's main field near the site and the magnetic susceptibility of the rock layers penetrated by the borehole must be known. The magnitude of the Earth's magnetic field can be estimated from recent surveys in the area or from charts and maps. The magnetic susceptibility of the rock in the borehole can be obtained from the logging results described in this section.

Equipment

The U.S. Geological Survey's susceptibility probe used to obtain the logs in Hole 418A was described in detail by Scott et al.

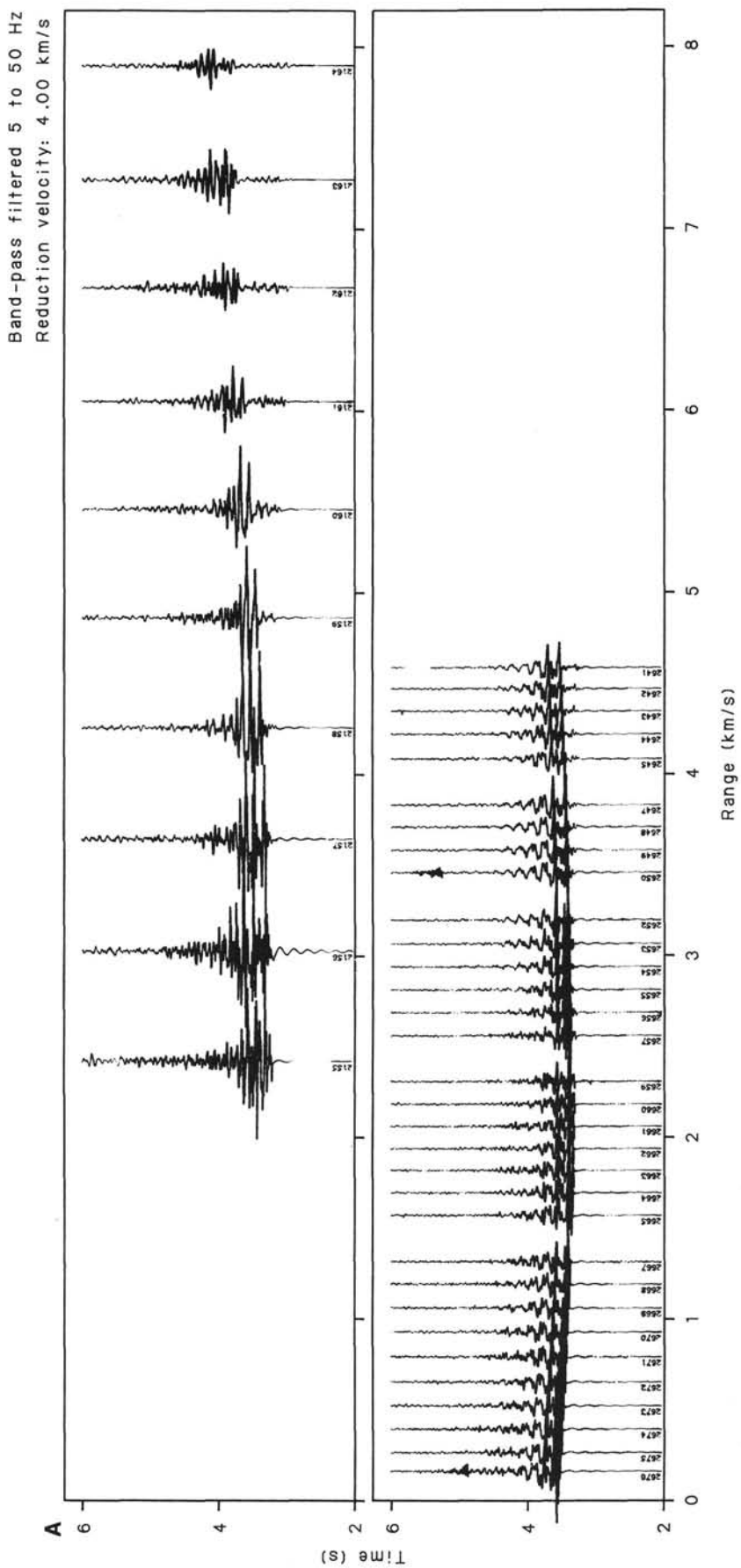
Band-pass filtered 5 to 50 Hz
Reduction velocity: 4.00 km/s
A
Time (s)
Range (km/s)

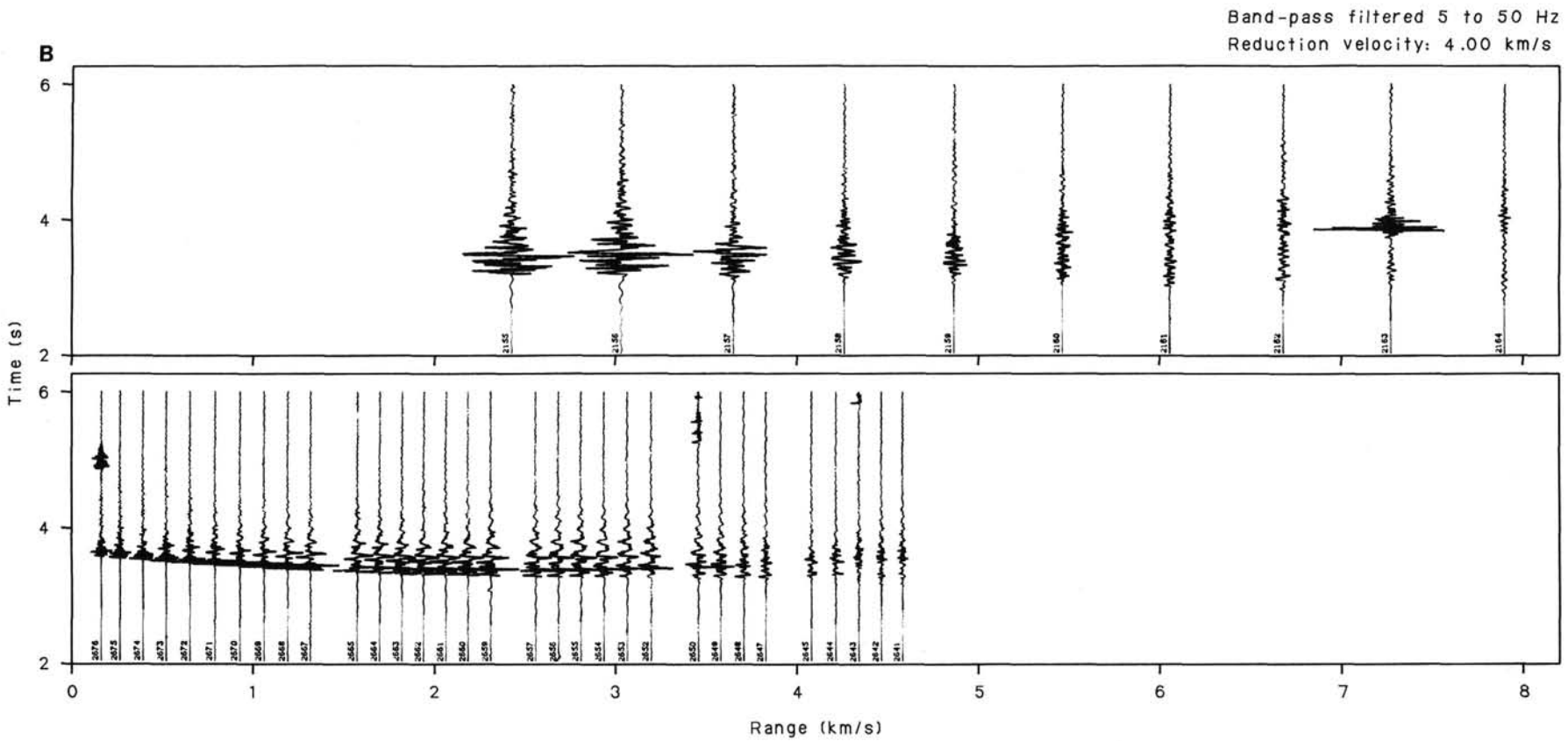

Figure 28. Comparison of explosive (top) and air-gun (bottom) records for the 20° line shot to the geophone at 554 mbsf. The 2–2000 in.^{3} air guns give a more consistent source at a closer shot spacing. However, signal strength is about 6–12 dB lower for the air guns, and compressional wave arrivals are at the background noise level about 6 km. A. Vertical component. B. Horizontal 1 component. C. Horizontal 2 component.

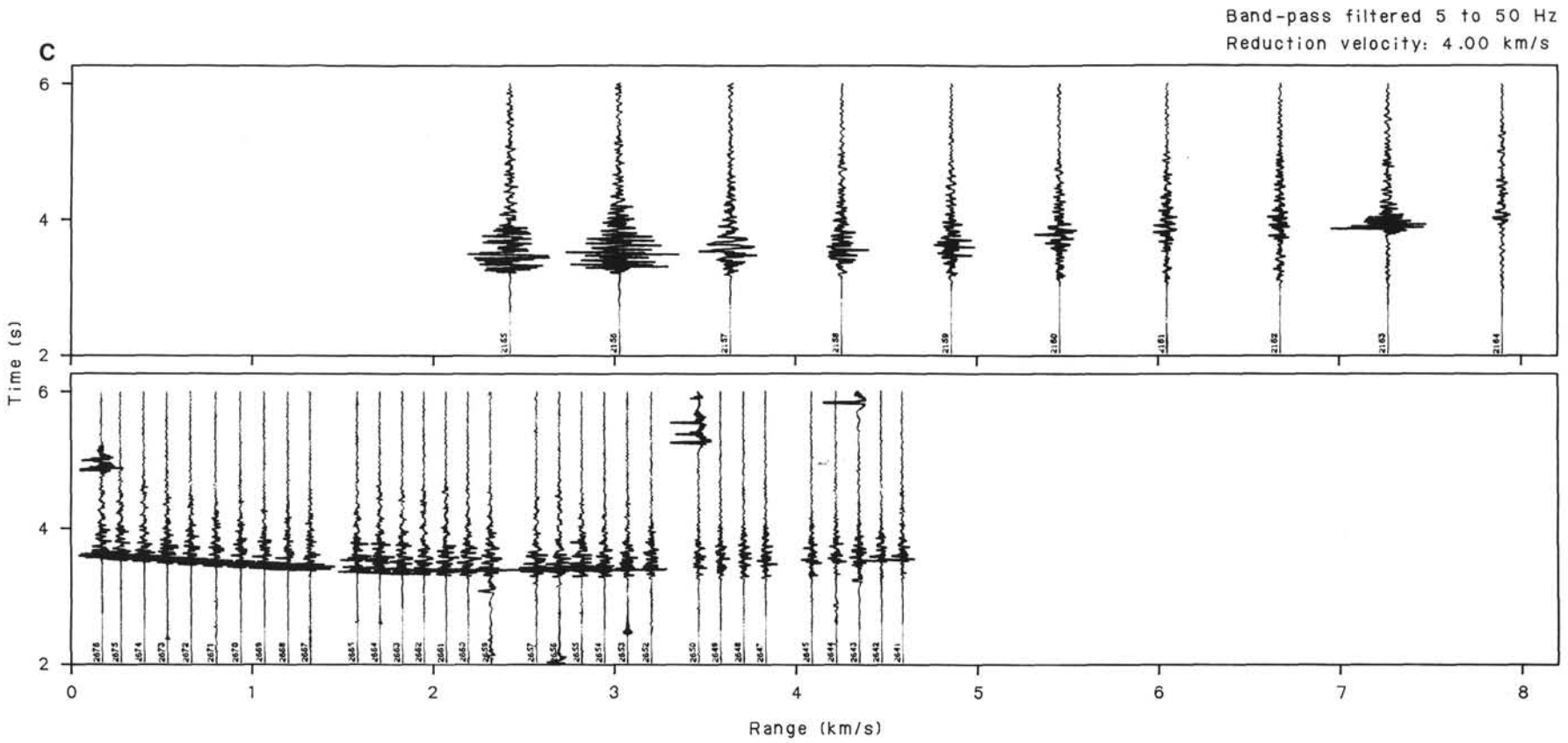

Figure 28 (continued).

(1981). The probe contains a solenoid sensing coil connected in a Maxwell induction bridge (Fig. 32). Before logging, the Maxwell bridge is nulled in a zero-susceptibility environment, having air but no conductive or magnetic objects within 1 m of the probe sensing coil. The 30-cm-long solenoid is in a heated chamber in the lower section of the probe, where the temperature is maintained at a constant level by a proportional electronic regulator (Fig. 33). The lower section of the probe is housed in a thick-walled fiberglass shell of laminar construction designed to withstand pressures of 15,000 psi. The coil temperature is monitored at the surface and is recorded along with the susceptibility and conductivity measurements obtained from the sensing coil and its associated electronic circuitry (Fig. 34). Because the measurement frequency is low (1000 Hz), the conductivity channel is insensitive to variations in the normal range of rock resistivity (1–1000 ohm-m) and is useful only for detecting concentrations of massive metallic sulfides, graphite, or other materials having resistivities on the order of 0.1 ohm-m and lower. The reason for using such a low frequency is that it increases the sensitivity of the sensing coil to susceptibility variations, making possible the detection of anomalies as small as a few μcgs units (cgs $\times$ 10^{-6}). This level of sensitivity is desirable for tracing alteration zones in sedimentary rock. Induction-logging probes that are designed to measure rock resistivity in the range 1–1000 ohm-m use a frequency of 20–50 kHz, but at these frequencies the measurement is relatively insensitive to susceptibility.

Geological Significance

Basalts typically have susceptibilities in the range of a few hundred to several thousand μcgs, and significant anomalies are commonly 100 μcgs or larger with respect to the average or background level. Susceptibility semiquantitatively indicates the concentration of ferromagnetic iron and iron–titanium oxides (e.g., magnetite and ilmenite) in rock surrounding the borehole (Mooney and Bleifuss, 1953). Variations in the susceptibility can be expected to correlate with variations in lithology and with the effects of alteration, which destroys ferromagnetic minerals or converts them to species that have relatively low susceptibilities (e.g., pyrite, hematite, limonite).

Results

The magnetic-susceptibility log of Hole 418A is shown in Plate 6 (back pocket), and laboratory measurements of the susceptibility of drill core obtained on Leg 53 are plotted on the same figure as solid circles (Hamano et al., 1979). The log was made in three separate runs because bridges formed in the hole, making use of the drill pipe necessary to guide the probe through the tight spots. For Plate 6, the three runs were spliced together with a few meters of overlap in the intervals from 321 to 336 and 464 to 480 mbsf. A hole-diameter correction was applied using an average diameter of 10.5 in. obtained from the Schlumberger caliper log. The susceptibility log was smoothed with a five-point Hamming filter, having an effective length of 1 m, to reduce the high-frequency noise thought to have been caused by the ship's heave.

As expected, the lowest susceptibilities occur in the sediments near the top of the hole (above a depth of 323 mbsf), where they average about 0.3 $\times$ 10^{-3} cgs units. Downward through the pillow-basalt section from 323 to 590 mbsf, the susceptibility becomes variable (0.3–2.7 $\times$ 10^{-3} cgs), suggesting the possibility of alteration between pillow layers. In this interval, the basalts are polarized in the normal direction (direction of the Earth's present magnetic field), according to the three-axis magnetometer log made on Leg 102 and the laboratory analyses of cores from Leg 53. In the breccia zone from 503 to 514 mbsf, the susceptibility falls to values almost as low as those of the sediments, suggesting that weathering has altered or destroyed most of the ferromagnetic minerals in the breccia. Below the breccia, the basalt is polarized in the reverse direction with respect to that of the Earth's present field as shown by the three-axis magnetometer log. Low but variable susceptibility values continue downward to about 605 mbsf in the pillow unit below the breccia zone. Note that the neutron and density logs show much variation in this same interval, suggesting differential alteration between pillow layers.

Below 605 mbsf, the susceptibility gradually climbs to the highest values recorded on the log ($\geq$4.0 $\times$ 10^{-3} cgs units) in the interval of 670–720 mbsf. Some high-susceptibility anomalies in this interval correspond to massive basalt units, but others, equally high, occur in the pillow sections between the massive units. This zone of high susceptibility from the top of massive basalt at 676 mbsf to 791 mbsf corresponds to the thick zone of high resistivity, density, velocity, and low porosity indicated by the Schlumberger logs (Plates 1 through 3, back pocket). A pronounced low anomaly (about 1 $\times$ 10^{-3} cgs units) occurs near the bottom of the susceptibility log at 791–797 mbsf. This anomaly correlates with a thin zone of low density and low velocity indicated by the core laboratory data (Salisbury et al., 1979). Unfortunately, none of the other geophysical logs reached this depth. A strong high-susceptibility anomaly (4.0 $\times$ 10^{-3} cgs units) occurs below 797 mbsf and extends to the bottom of the log. This anomaly correlates with the top of the dike zone where the laboratory results of Leg 53 show substantial increases in core velocity and density (Salisbury et al., 1979).

In general, the laboratory measurements of the susceptibility of drill core agree with susceptibility log values to a reasonable degree of accuracy, considering the difference in sample volume of the two measurements. However, in the interval of low susceptibility from the breccia zone downward through the pillow basalts (504–610 mbsf), the core susceptibilities are consistently higher than the log values. We think that this is explained by the tendency of laboratory measurements to reflect the properties of the least altered rock in zones of poor core recovery because most of the highly altered rock is lost.

In summary, the magnetic-susceptibility log indicates that magnetic mineral content of the pillow and massive basalt units is more variable than most of the physical properties shown by the other geophysical logs. Susceptibility appears to be particularly sensitive to alteration and weathering, which attack the magnetic minerals. In addition to indicating lithologic variations, the susceptibility log provides the quantitative information needed to correct the three-axis magnetometer log for the induced magnetic field.

TEMPERATURE-MEASUREMENT RESULTS

Introduction

The return to Hole 418A during ODP Leg 102, over 8 yr after the hole had been drilled, provided a unique opportunity to assess the geothermal state of old oceanic crust. The 8-yr period since Hole 418A was drilled during DSDP Legs 51, 52, and 53 was certainly long enough for the thermal disturbance from drilling to have dissipated and for borehole temperatures to have fully equilibrated to crustal geothermal conditions. Undisturbed borehole temperatures needed to be measured immediately after reentry of the hole, before the thermal equilibrium in the borehole was disturbed by subsequent pumping and pipe movement during the logging and experimentation of Leg 102.

Temperature measurements in Hole 418A were planned for two specific purposes:

1. To determine the geothermal gradient at Site 418 and compare it to that predicted by models of a conductively cooling plate. Such models predict that the conductive heat flow for the

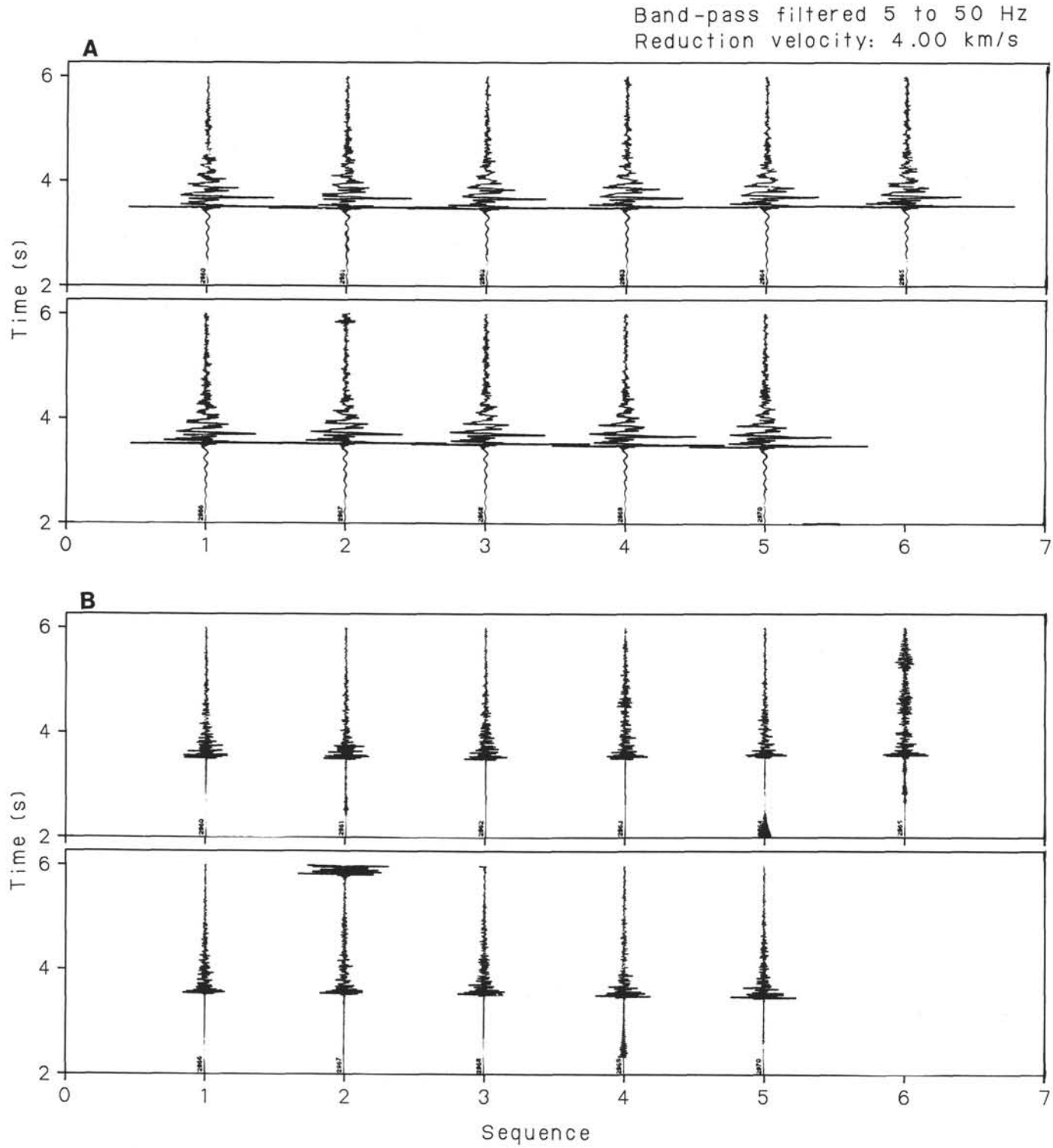

Figure 29. Signal-to-noise levels for the 2–2000 in.^{3} air guns at near-normal incidence can be estimated from these traces. The geophone was clamped 81 m into basement with the pipe between 10 and 15 m into basement. Scattered large-amplitude dispersive arrivals occur, which are due to the pipe banging in the rock. In the absence of these spurious arrivals, signal-to-noise levels are 40 dB or better. A. Vertical component. B. Horizontal 1 component. C. Horizontal 2 component.

110-m.y.-old crust at Site 418 should be 45–48 mw/m^2. Measured temperatures agreeing with the predicted heat flow would verify the expectation that the old crust at Site 418 had cooled enough and is sealed by a sediment cover sufficiently thick that hydrothermal circulation is no longer active and plate heat transfer occurs by purely conductive processes. Measured temperatures different from predicted values would require consideration of the unexpected possibility that hydrothermal circulation might still be active in the crust around Site 418.

2. To assess the possibility that ocean-bottom water might be flowing down the hole and into the upper levels of basement, as has occurred at several other DSDP basement holes, mostly

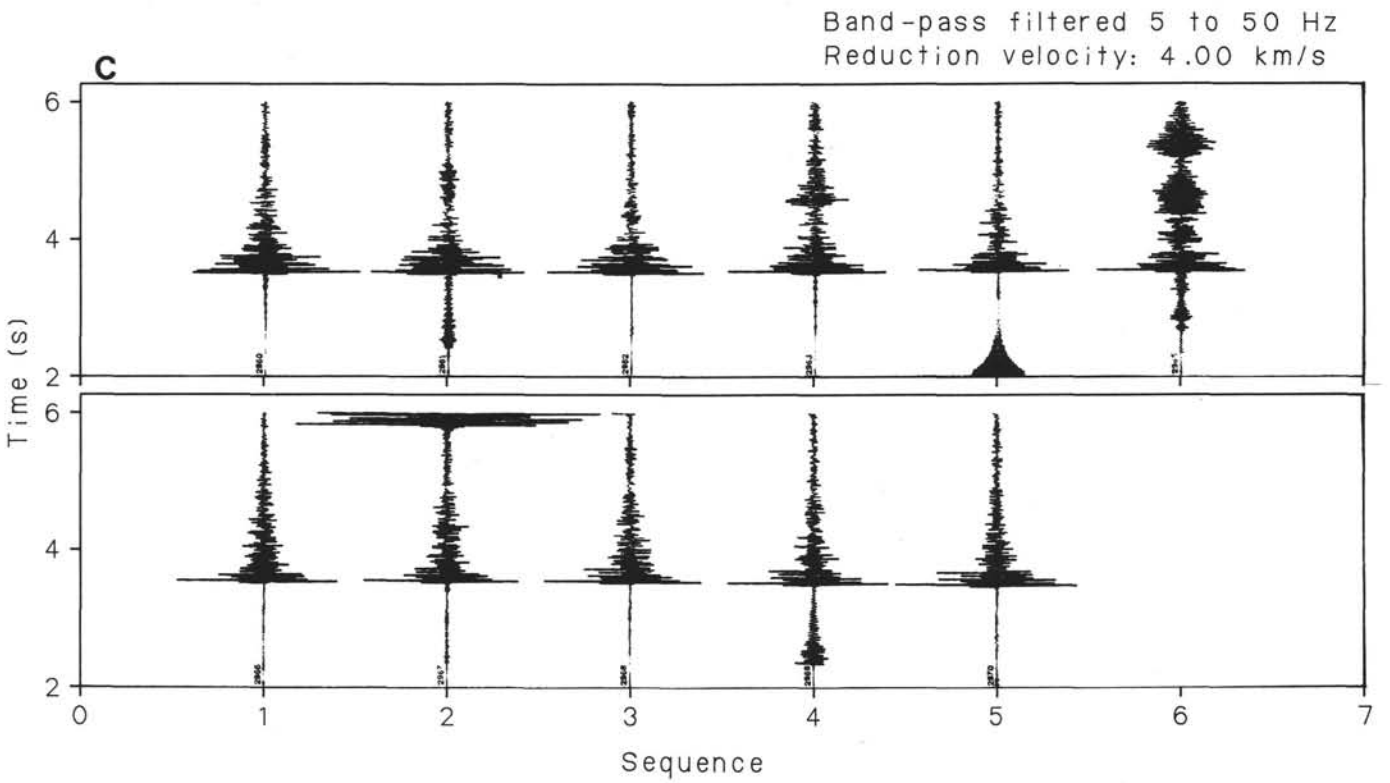

Figure 29 (continued).

in much younger crust. Such downhole flow has been found to be driven by underpressure of basement pore fluids, which may be related to hydrothermal circulation. Thus, as no hydrothermal circulation was expected at Site 418, no downhole flow was expected, but this expectation needed testing.

The Leg 102 temperature-measurement program in Hole 418A was limited by time constraints to the minimum required to fulfill the two aforementioned objectives. For two stations, the temperature tools were deployed during the initial operation of running pipe to the bottom of the hole immediately after reentry: (1) a station in the lower part of the cased section, to determine either the geothermal gradient through the sediments or the downhole flow rate, if downhole flow were occurring; and (2) a station deep within the basement, to determine the geothermal gradient in the basaltic crust.

The first station had to be run in the cased section because, if downhole flow were occurring, the flow rate could be reliably determined only from temperatures in the casing, in which any flow must remain uniform with depth. If the first station had indicated downhole flow, a third station would probably have been required, involving a new hole to measure the undisturbed gradient in the sediments. (The undisturbed gradient is the essential boundary and initial condition required to estimate flow rate from measured temperatures.)

Methods

For both temperature measurements, the Von Herzen hydraulic piston corer (HPC) temperature shoe and the Barnes-Uyeda temperature/pore-water sampler (T-probe) were run in tandem to ensure collection of data in the event of a tool failure. Each of these devices monitors the resistance of a single thermistor. Relevant tool properties are summarized in Table 14.

Each lowering was run on a wireline, as opposed to being released, to minimize damage to the T-probe upon landing into the bit and because of uncertainties about the location of the lost logging tool and about the condition of the hole. This limited the depth range of each measurement to 29 m, the length of the single stand of pipe that could be drawn up in the derrick before the tool and wireline were run into the pipe. During each lowering, the tool was run down the pipe without pumping, stopped for about 5 min roughly 100 m above the seafloor, and then lowered until it latched into the bit for the first temperature-reading point. Temperatures were measured for about 10 min at each of four depths: the starting depth, and after lowering the pipe to each of the three joints that made up the single stand originally drawn up in the derrick. The last stop was held longer than the others to allow time to take a pore-water sample.

Before the first lowering (52–81 mbsf), the pipe had been run the length of two stands into the hole without any pumping. Therefore, (1) the water in the pipe at mud-line level should have accurately represented bottom-water temperature, and (2) the temperatures of the water in the borehole should have been little disturbed. Before the second lowering (624–648 mbsf), pipe was run into the hole to a depth of about 605 m, with rotation and pumping to clean the hole and "feel" for the lost logging tool. The pumps were stopped while the pipe was run in from 605 m to the measurement-taking depth of 623 m, but the data suggest that the pumping above 605 m affected the temperatures in the measurement interval of 624–648 m.

Measurement Results

The temperature–time records for the two tools during the two lowerings are shown in Figures 35 through 38. In general, the T-probe data read about 0.2°C higher than the HPC data, and the T-probe digital thermistor resistance data were degraded by some losses of digits. Because the HPC thermistor had been calibrated more recently than the T-probe thermistor, the HPC tool probably gave more accurate temperature readings. For these reasons, and because the HPC tool samples thermistor resist-

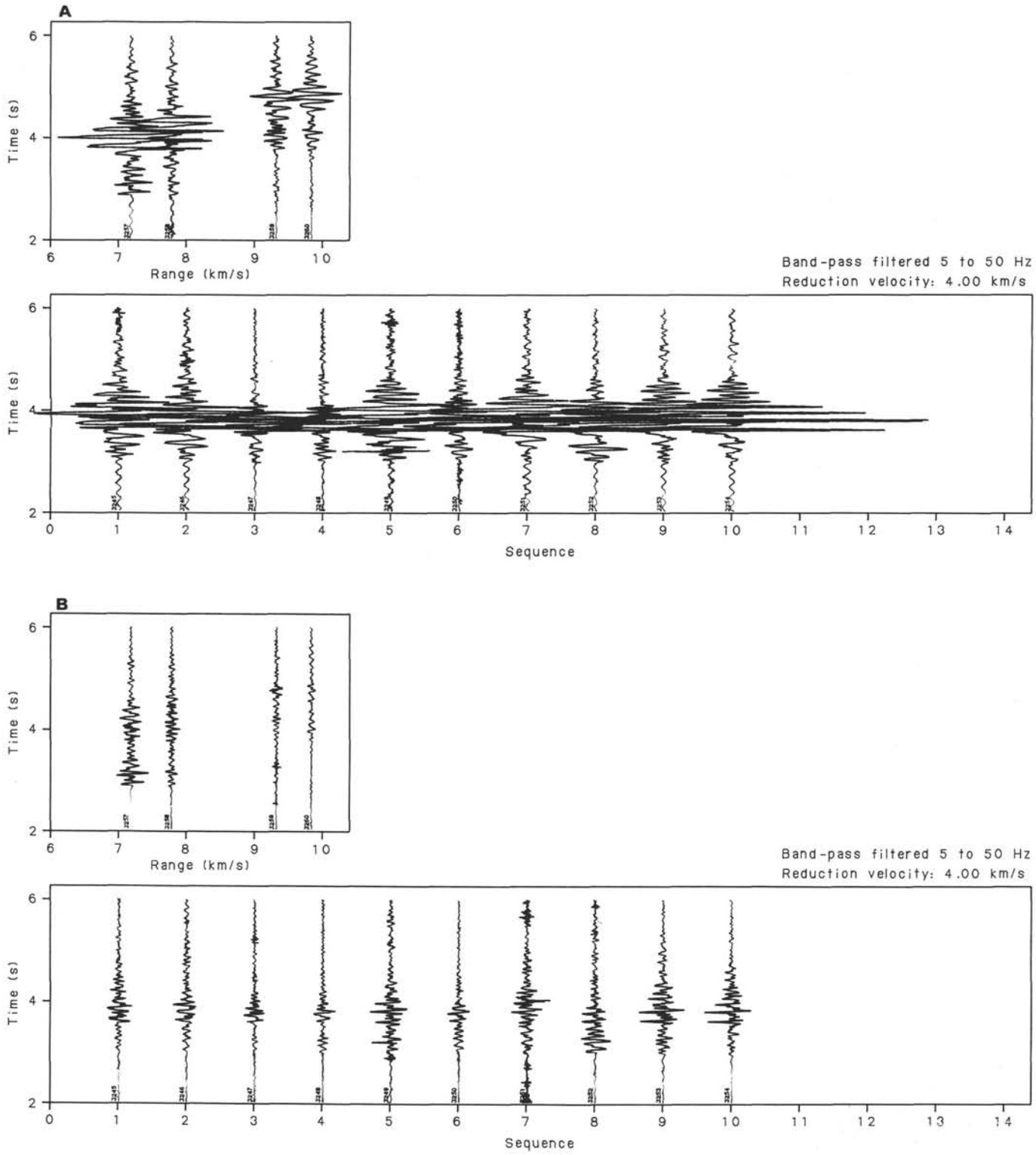

Figure 30. Comparison of noise levels, with the heave of the pipe compensated (left) and uncompensated (right), can be judged from these plots. The shots are 30-lb explosive charges fired at ranges greater than 6 km. The geophone was clamped at 41 m into basement within 30 m of the end of the pipe. The number of spurious arrivals decreases and the general background noise is reduced with heave compensation. This evidence suggests that the dominant source of noise in our experiment is generated by the pipe banging in the hole. A. Vertical component. B. Horizontal 1 component. C. Horizontal 2 component.

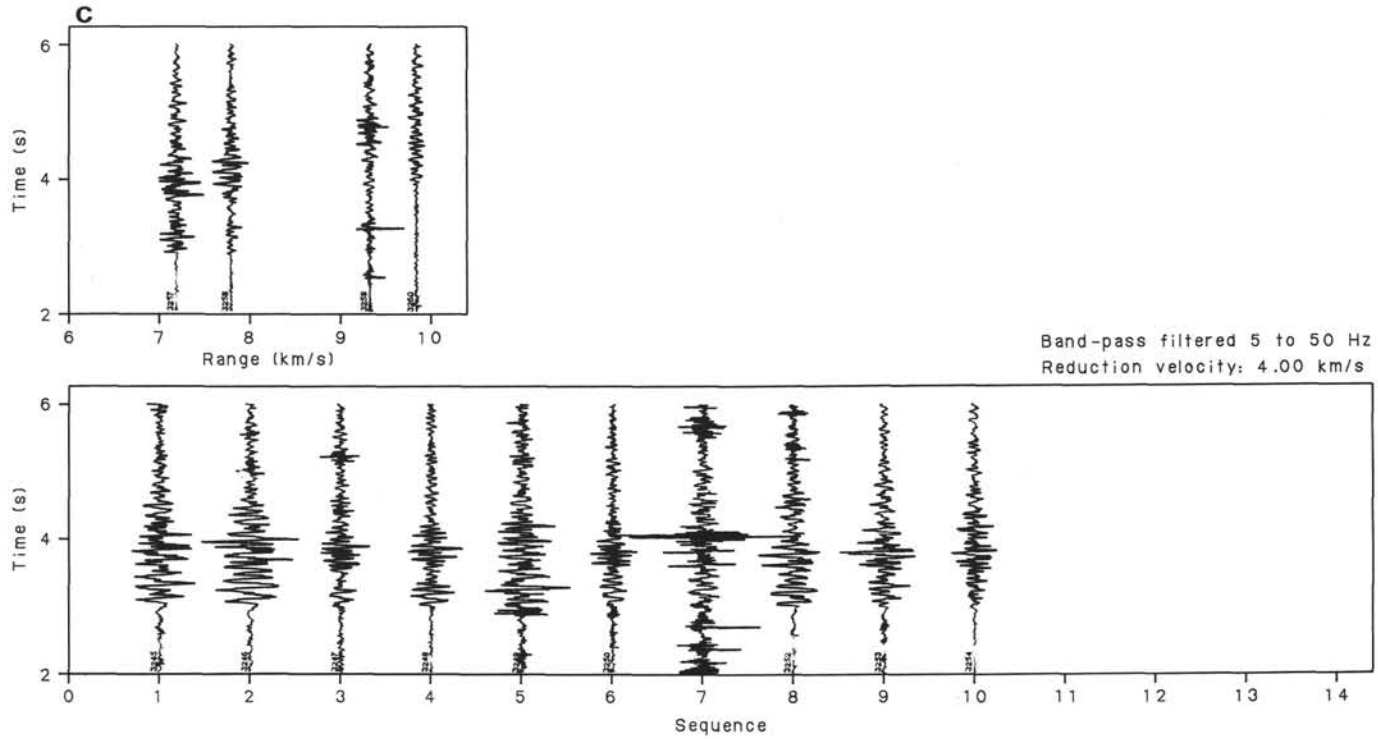

Figure 30 (continued).

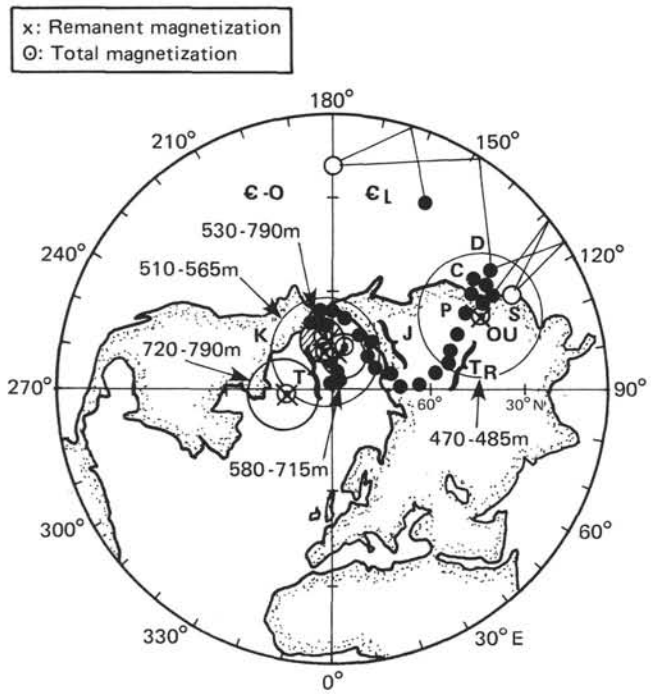

Figure 31. Apparent polar-wandering paths (solid circles) and pole positions calculated from the results of magnetic logging of Leg 102. Small open circles indicate pole positions according to total magnetization (three-axis magnetometer). The *X* indicates pole position on basis of remanent magnetization (calculated using the susceptibility log). Large Fisher circles represent areas in which the pole positions may occur at the 95% confidence level. T = Tertiary; K = Cretaceous; T_R = Triassic; P = Permian; C = Carboniferous; D = Devonian; S = Silurian; O_U = Upper Ordovician; ϵO = Cambrian–Ordovician; ϵ_L = Lower Cambrian.

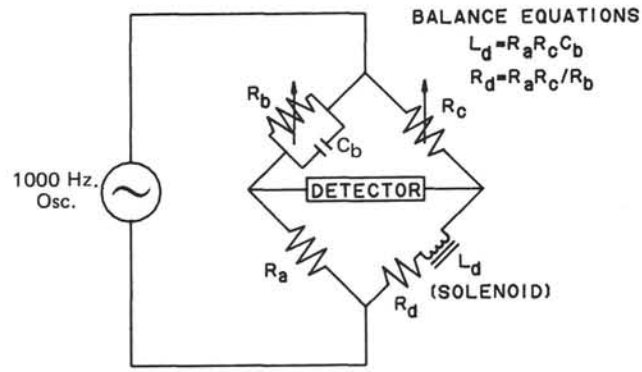

Figure 32. Schematic diagram of the Maxwell bridge used in the magnetic-susceptibility well-logging system. The lower right arm of the bridge is the sensing coil with inductance, L_d, and effective resistance, R_d. The upper left arm contains a capacitor, C_b, which balances the reactance of the solenoid. Variable resistors, R_b and R_c, are used to null the bridge in air so that the signal measured by the detector is zero. Resistor R_a is fixed at a resistance equivalent to the reactance of the sensing coil.

ance at a much denser rate, the HPC temperatures were used as the primary data set in interpreting the measurement results.

The downhole temperature–depth data are summarized in Table 15. The tabulated temperatures are mean values for the most stable segments of the measurement periods. Errors are estimated at ±0.02°C for HPC values and ±0.05°C for T-probe values. For good-quality temperature measurements in a seawater-filled borehole, one would expect the probe to rapidly equilibrate (<5 min) with ambient temperatures and produce stable readings thereafter. These criteria were met only at the first and

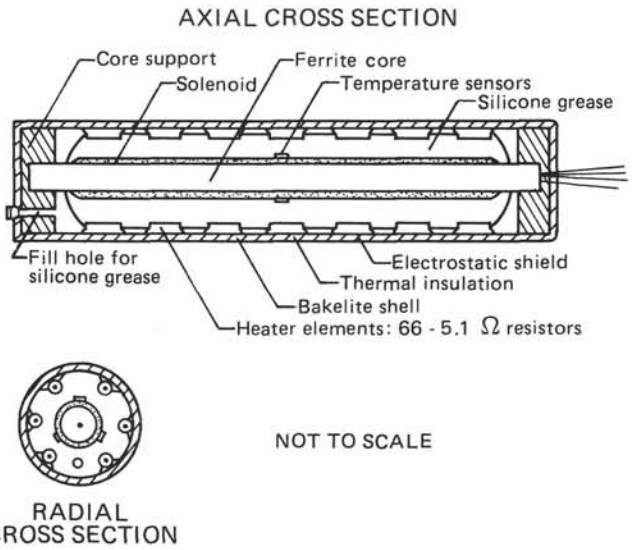

Figure 33. Diagrammatic cross sections of magnetic-susceptibility sensing coil, showing relative positions of components. The overall length of the package is 33.5 cm, and its diameter is 3.6 cm.

second temperature–depth points of the first lowering and by the first and third points of the second lowering (Figs. 35 through 38).

During the third stop of the first lowering, the probe apparently sank through some sediment in the hole, as indicated by the steadily increasing temperatures, interpreted to have resulted from frictional heating of the probe. When it was recovered, the probe was covered with sticky sediment. The early part of the fourth point in the first lowering may be a reliable value, followed by more frictional effects on the probe as it contacted more sediment.

The temperature records for the second, third, and fourth points of the second lowering also suggest the decay of pulses of frictional heating owing to probe penetration of sediments, but this is unlikely because the second lowering was conducted about 300 m into basement. Instead, the wide range of measured temperatures at these points may have resulted from mixing of borehole fluids ahead of the bit. Extensive pumping was used in cleaning out the section of hole to 19 m above the starting depth of the second lowering. This may have cooled a zone of unknown extent ahead of the bit and contributed to unstable temperatures at the temperature-reading depths.

Data Interpretation and Conclusions

The HPC temperatures, plotted against depth in Figure 39, indicate the following:

1. Temperatures in the upper 100 m (first lowering) are relatively co-linear with the bottom water. This suggests a linear, conductive gradient of about 0.05°C/m, consistent with the plate heat transfer predicted for 110-m.y.-old crust having no indication of downhole flow of bottom water.
2. Temperatures measured during the second lowering in the basement are also co-linear, but the value of the apparent gradient is unreasonably high. This is interpreted to indicate cooling of the borehole water or displacement of cooler borehole fluids from above into the measurement interval, which probably resulted from the circulation and pipe movement during cleaning of the hole above. Given this interpretation, the only useful information from the second lowering is that the highest measured temperature of about 24°C, which must be a minimum, is bound to the value of the undisturbed temperature at 648 m.

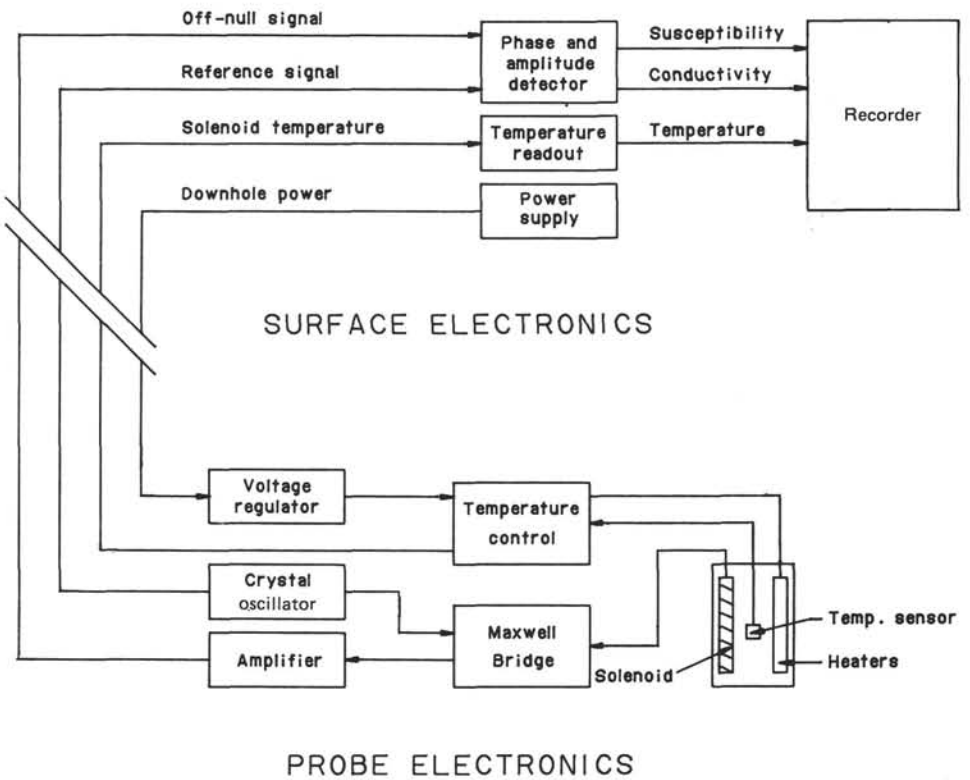

Figure 34. Block diagram of surface electronics and probe electronics for the magnetic-susceptibility well-logging system.

Table 14. Properties of temperature tools as deployed during Leg 102.

Tool	Thermistor housing	Thermistor number	Thermistor to bit (m)[a]	Recorder program
HPC tool	Steel annular cylinder 1.435-cm wall	8	0.47	Delay 30 min 1080 samples at 10 s
T-probe	Steel probe 0.95-cm dia.	6	0.96	128 samples at 2 min

[a] Distance that the thermistor extended ahead of the bit.

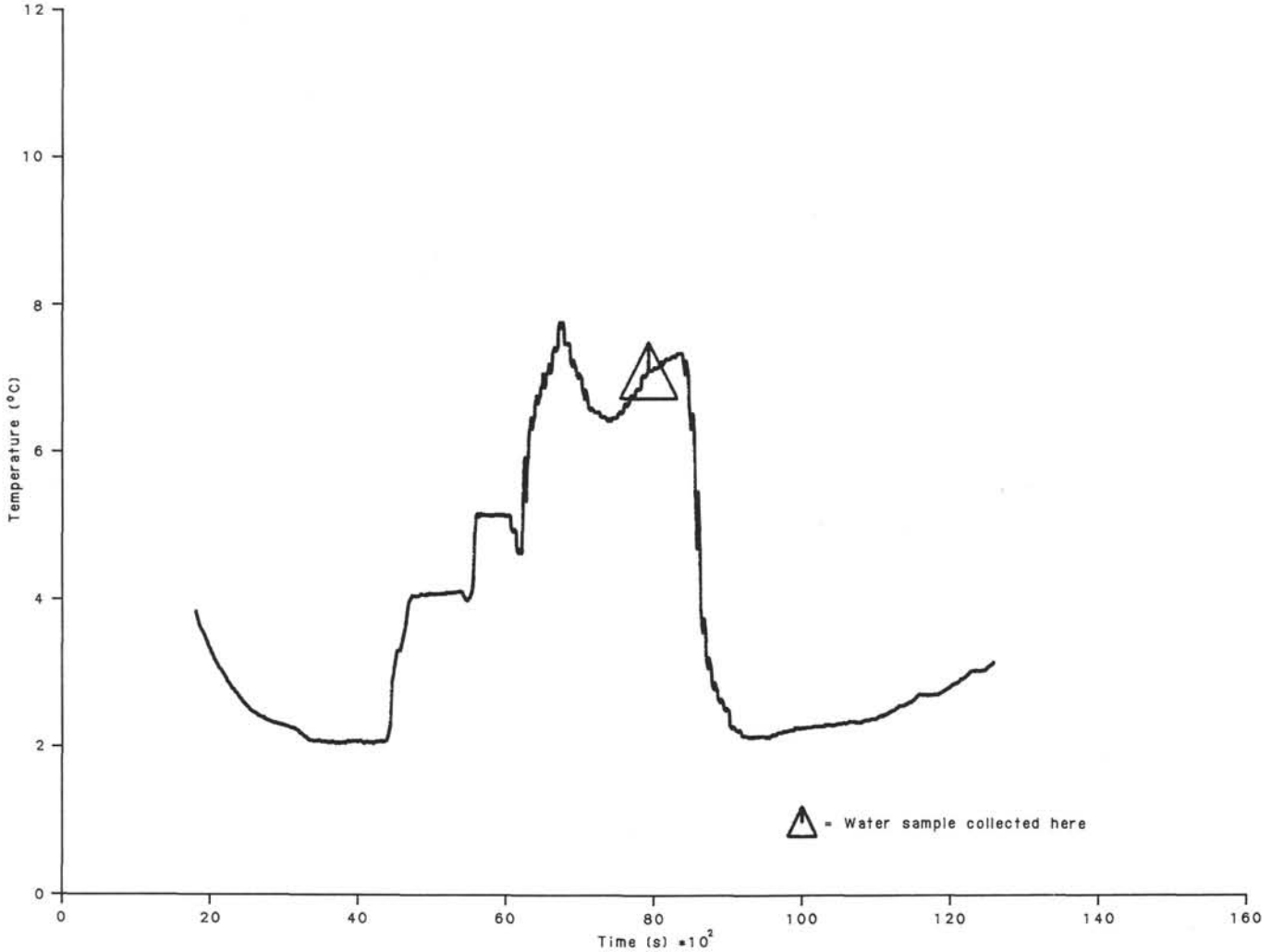

Figure 35. Temperature-time record for the HPC tool, first lowering.

The temperatures measured in the upper 100 m were fit in a least-squares sense to a linear model forced through the measured bottom-water temperature at the seafloor. The results indicate a gradient of 0.050°–0.053°C/m, the higher value being obtained by omitting the somewhat low temperature at 51.9 m. Assuming an average thermal conductivity of 0.9 w $m^{-1}s^{-1}$ in the sediments, a conductive heat flow of 45–48 mw $m^{-2}s^{-1}$ is indicated.

The temperatures measured about 300 m into basement were disturbed but do not contradict the conclusions from the measurements in the upper 100 m of Hole 418A. Downward continuation of the conductive heat flow indicates (1) a temperature of about 18.4°–19.3°C at the sediment/basement contact, and (2) a gradient of about 0.023°–0.024°C/m in the basement, assuming a thermal conductivity of 2.0 w $m^{-1}s^{-1}$.

The calculated heat flow of 45–48 mw $m^{-2}s^{-1}$agrees completely with the heat flow predicted for a conductively cooling 110-m.y.-old plate and verifies our expectations that (1) heat transfer occurs only by conductive processes around Site 418, (2) hydrothermal circulation is no longer active around Site 418, and (3) cold ocean-bottom water does not flow down Hole 418A.

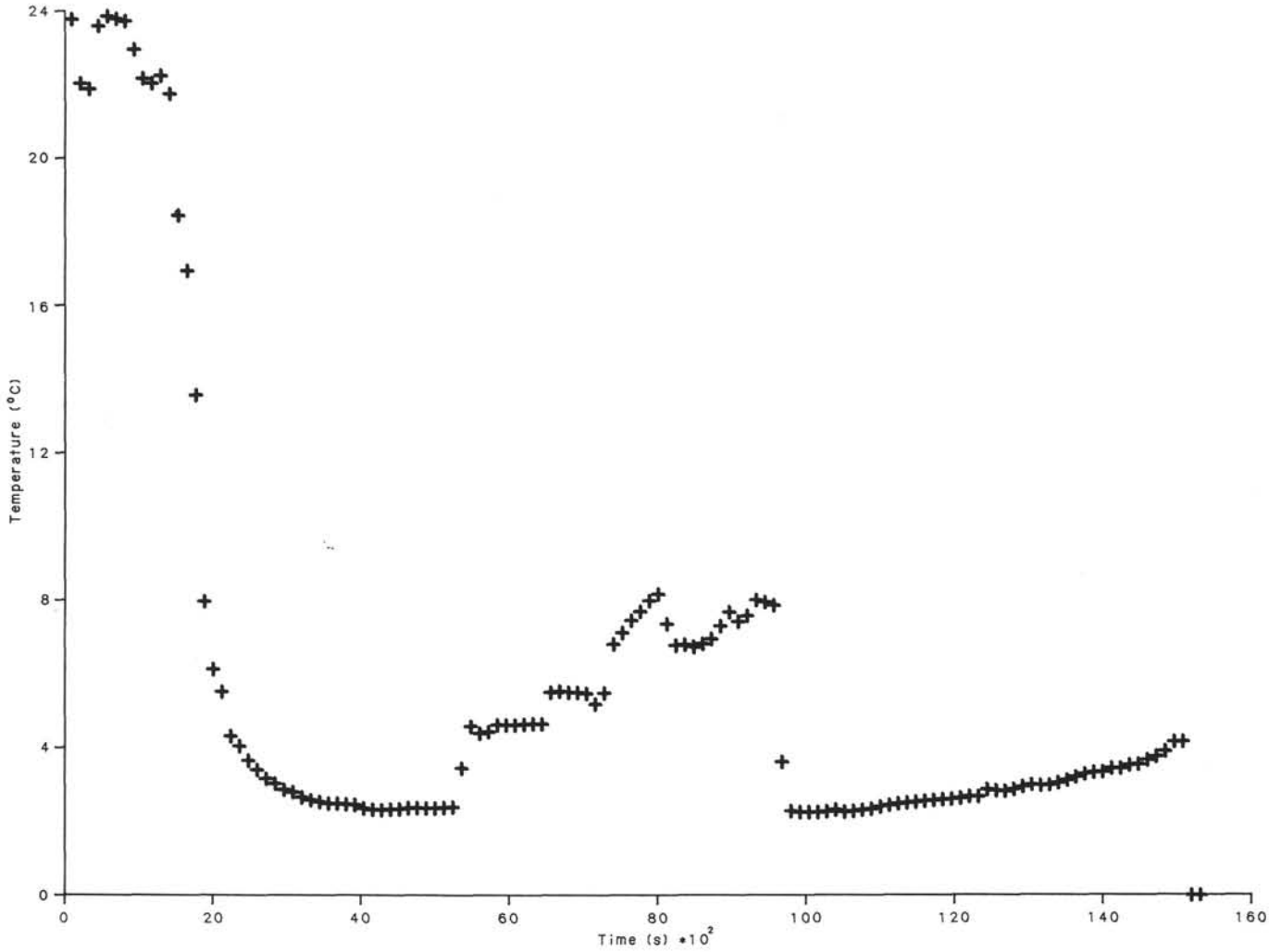

Figure 36. Temperature-time record for the T-probe, first lowering.

BOREHOLE-WATER STUDIES

Introduction

During the last 12 yr of the Deep Sea Drilling Project, a large body of information had been collected on the chemical composition of the dissolved solids in the interstitial waters of marine sediments. The concentration–depth gradients, especially of major constituents such as Ca^{2+}, Mg^{2+}, K^+, and Na^+, have indicated that changes in these constituents are commonly the result of low-temperature alteration of the underlying Layer 2 basalts. These basalts are a sink for K^+, Mg^{2+}, and Na^+, as well as for $^{18}O(H_2O)$, whereas they serve as a source for Ca^{2+} (Lawrence et al., 1975; Gieskes and Lawrence, 1981; Lawrence and Gieskes, 1981; Gieskes, 1983). McDuff (1981) argued that, to maintain these concentration gradients, circulation of formation waters must start when ocean crust is of a considerable age—i.e., well beyond the period that so-called sealing of the crust occurs by the accumulation of a thick, impermeable (to flow) sediment cover (Anderson et al., 1977). After this sediment sealed the crust, transport of ions through Layer 1 to/from the ocean from/to Layer 2 becomes diffusive (McDuff, 1981). Lawrence and Gieskes (1981), using oxygen isotope mass-balance considerations, also concluded that substantial alteration of Layer 2 must occur over a long period, again in agreement with observations of Muehlenbachs and Clayton (1976).

Hitherto, few opportunities arose to study the chemistry of the basalt formation waters to verify some of the aforementioned ideas developed on the basis of the interstitial-water data. However, during the last few years, reentry into abandoned holes, in particular DSDP Hole 395A near the Mid-Atlantic Ridge and Hole 504B near the Costa Rica Rift, has enabled the study of the composition of borehole waters of relatively young age (1–5 yr) deep in the oceanic crust. We thought that these studies might yield inferences on composition of formation waters surrounding the holes.

McDuff (1984) described the chemical composition of a borehole sample obtained in Hole 395A at a sub-bottom depth of 543 m—i.e., in the zone where no further drawdown of bottom water has been observed (Becker et al., 1984). McDuff inferred from the changes in Ca^{2+} (small increase) and in Mg^{2+}, K^+, and SO_4^{2-} (relatively large decreases) that these changes were caused by reactions in basement and that the chemical signals of basement waters were transferred to the pumped-down surface waters that fill the basement by advective and/or diffusive transport. Relatively small increases in calcium were associated with calcium carbonate precipitation, which was observed extensively

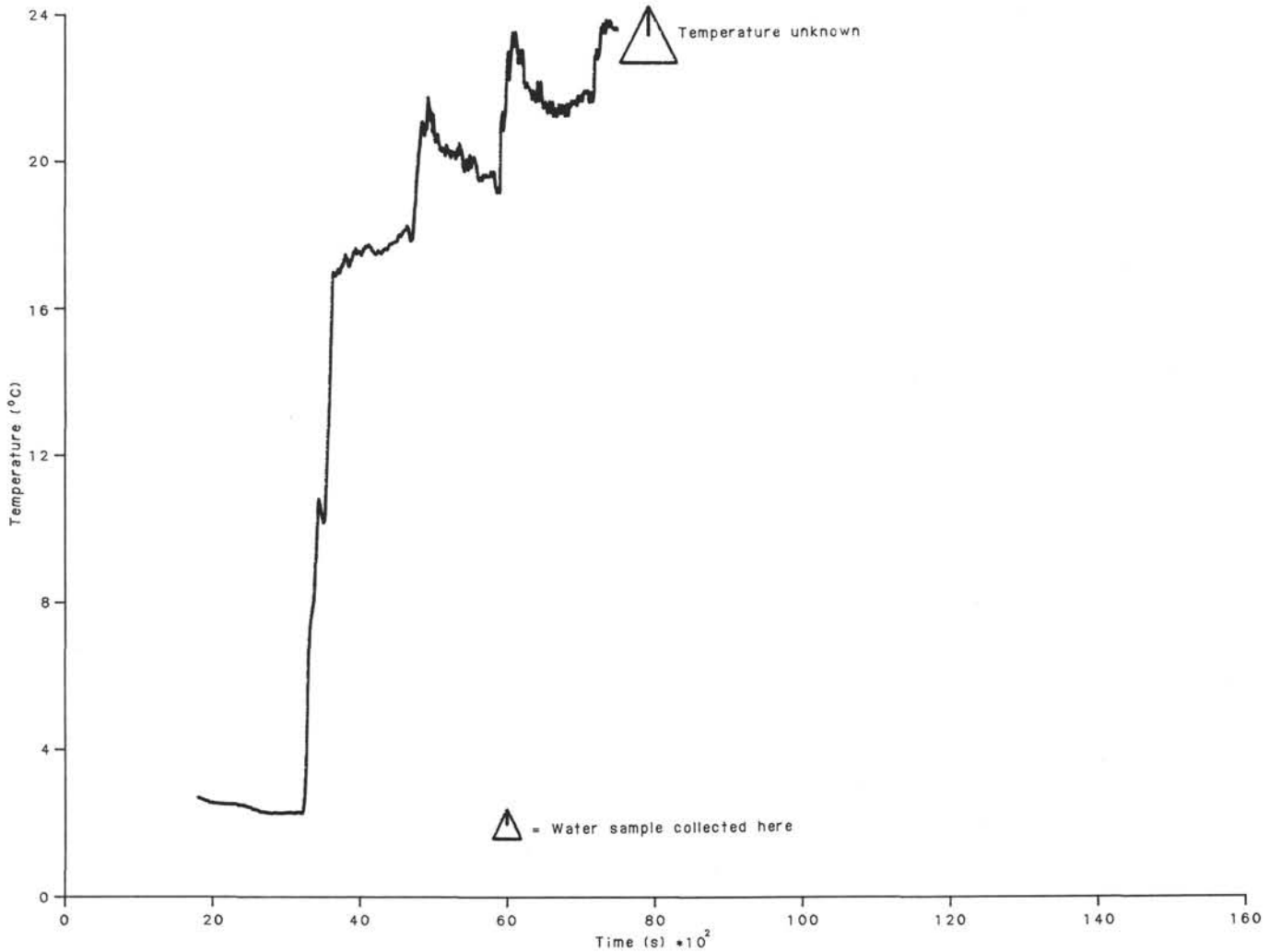

Figure 37. Temperature–time record for the HPC tool, second lowering.

as vein fillings at Site 395. Decreases in sulfate could not be explained readily and were considered to be due to sulfate-reduction processes occurring in overlying sediment through which percolating seawaters flowed before entering the basalts. However, sediments of Site 395 do not now show significant depletions in sulfate.

Hole 504B was visited several times since it was originally drilled, and extensive studies of the borehole fluids have been made (Mottl et al., 1983, 1985; Gieskes et al., in press). Though great changes in the major ion composition were observed, the evidence of the causes of these changes is still considered ambiguous. Gieskes et al. (in press) proposed various scenarios ranging from interchange with the surrounding rocks by transport of formation waters to reaction between borehole waters and wall rocks. These authors, however, could not reach any definite conclusions about the actual causes of the observed changes in chemistry.

A visit to Hole 418A was considered an important addition to the holes studied until now, particularly because it was thought to be closed off from the overlying seawaters by sediment bridges in the deeper, uncased sections of the hole in the sediment. Thus, a closed system would have existed in which pumped-down surface seawater has remained in the hole for the last 8 yr, ample time for reaction and/or exchange with the surrounding rocks. Herein, we present data on two samples of borehole fluids obtained during ODP Leg 102.

Previous Hydrogeochemical Studies at Sites 417 and 418

During Leg 51, samples were obtained for interstitial-water studies in both Sites 417 and 418. The data obtained for dissolved calcium and magnesium are summarized in Figure 40 (Gieskes and Reese, 1980; Holland, 1984). Gieskes and Reese (1980) suggested that the gradients of Ca^{2+} and Mg^{2+} were essentially diffusive in nature, i.e., that the major source for Ca^{2+} and the major sink for Mg^{2+} were located not in the sediments but rather in the underlying basalts of Layer 2.

Figure 41 correlates plots for Ca^{2+} and Mg^{2+}, showing that typically the ratio of the change in these constituents is $\Delta Ca/\Delta Mg \sim -1.45$ at both sites. With the slight observed decreases in dissolved sulfate at these sites, the charge balance requires depletions of Na^+ (and K^+, as observed). This observation is typical for older sites (McDuff, 1978, 1981) and has been explained in terms of uptake of Na^+ in alteration products after the depletion of Mg^{2+} in the formation waters (McDuff, 1981).

Lawrence and Gieskes (1981) observed that at most DSDP sites, a good correlation exists between changes in dissolved calcium and the changes in $\delta^{18}O(H_2O)$ of the interstitial waters.

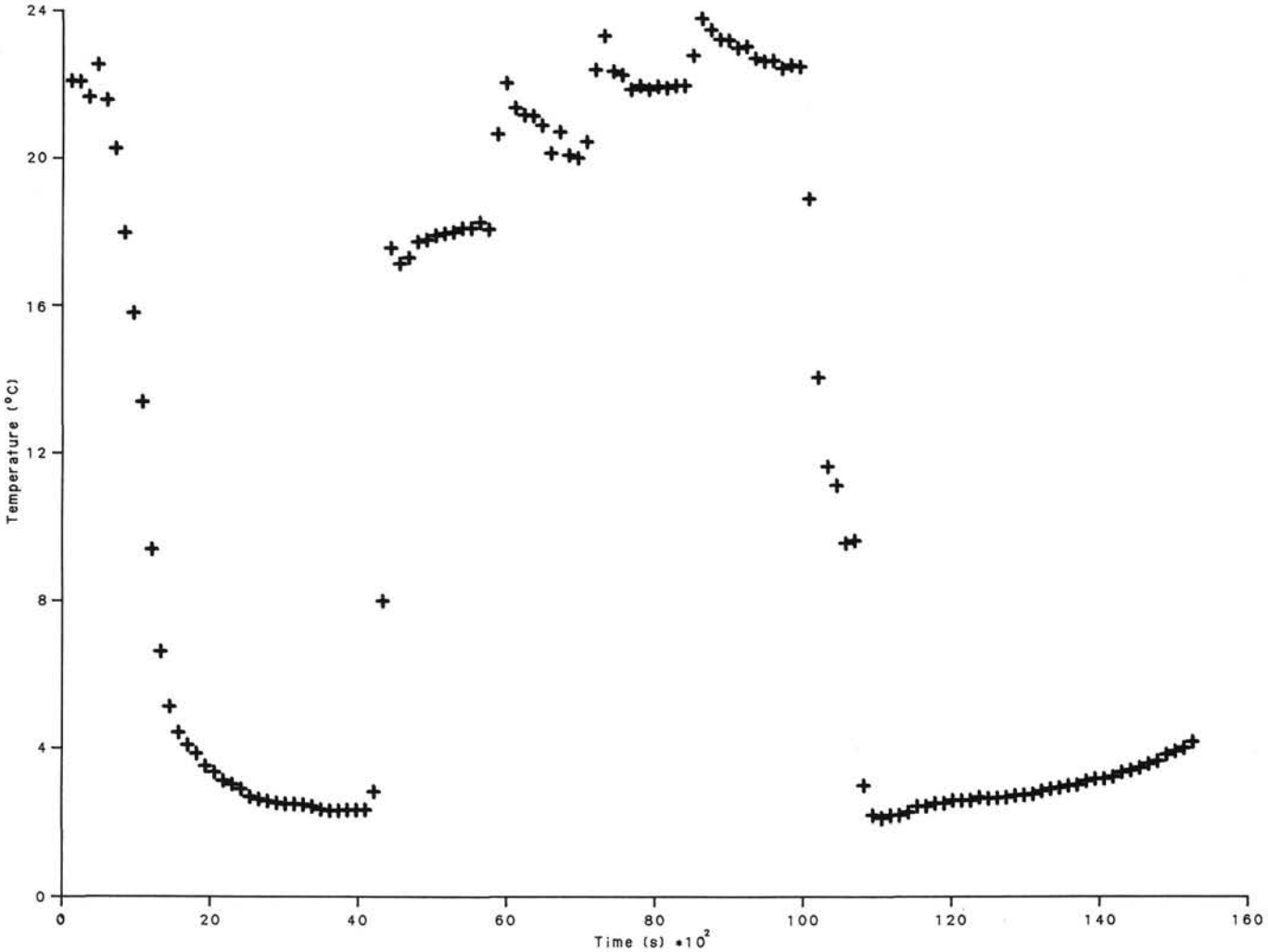

Figure 38. Temperature-time record for the T-probe, second lowering.

Table 15. Temperature-depth data for five temperature readings, lowering numbers 1 and 2.[a]

	Bit depth (mbrf)	HPC depth (mbsf)	HPC temp. (°C)	T-probe depth (mbsf)	T-probe temp. (°C)
Lowering no. 1					
T_{bw}	5400	—	2.068	—	2.32
T_1	5570.90	51.9	4.094	52.4	4.60
T_2	5580.55	61.5	5.153	62.0	5.46
T_3	5590.20	71.2	not good	71.7	not good
T_4	5599.85	80.8	6.503	81.3	6.75
Lowering no. 2					
(T_{bw})	5400	—	(2.28)	—	(2.30)
T_1	6142.78	623.8	18.056	624.2	18.08
T_2	6152.44	633.4	(19.81)	633.9	(20.23)
T_3	6162.10	643.1	21.782	643.6	21.87
T_4	6167	648	(23.72)	648.5	(23.37)

[a] Seafloor is taken to be 5519.5-m pipe length below rig floor, on the basis of the 0.5-m difference between rig-floor heights on *JOIDES Resolution* and *Glomar Challenger* and the 5519-m pipe length required to touch bottom from *Glomar Challenger* during Leg 52. Temperatures in parentheses are dubious values.

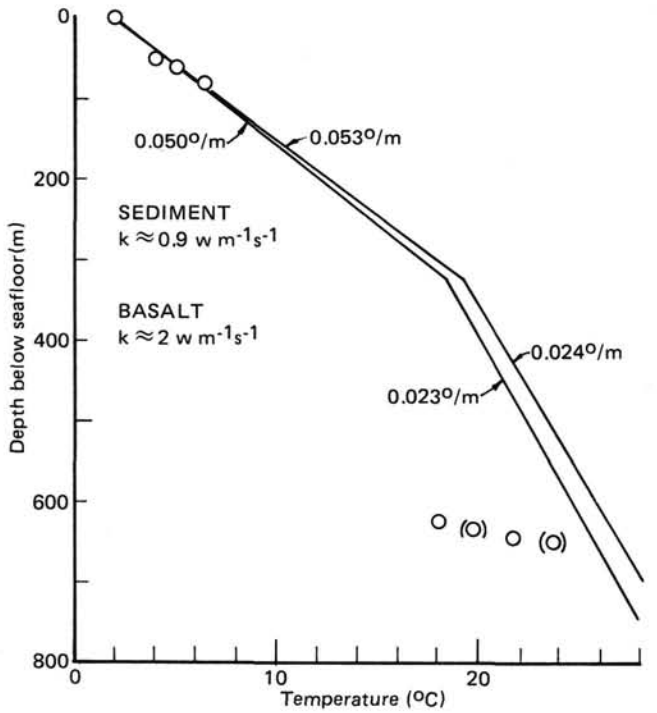

Figure 39. Temperatures measured with the HPC tool during first and second lowerings, plotted against depth into Hole 418A.

Data have been obtained for $\delta^{18}O$ for the pore waters of Sites 417 and 418 (J. R. Lawrence, pers. comm., 1977). The correlation between Ca^{2+} and $\delta^{18}O$ is presented in Figure 42. Although the data quality is not outstanding, little doubt exists about a tendency to decrease $\delta^{18}O$ with increasing Ca^{2+} with $\delta^{18}O/\Delta Ca^{2+} = -0.06$ ‰/mM, slightly less than the average correlation of -0.08 ‰/mM suggested by Lawrence and Gieskes (1981). Nevertheless, mass-balance calculations based on similar depletions in $\delta^{18}O$ at other sites (Lawrence and Gieskes, 1981) require substantial alteration of basaltic material in Layer 2 and cannot be explained by carbonate or clay-mineral diagenesis in the sediments.

We conclude, therefore, that underlying basalts are the main source of dissolved Ca^{2+} and are the sink for Mg^{2+} in Sites 417 and 418, and that because of the observed decrease in $\delta^{18}O$, a substantial alteration signal is still present in the fluids of Layer 2.

Sampling Methodology

For the sampling procedure on Leg 102, the Barnes-Uyeda *in-situ* interstitial-water sampler was used, in conjunction with the temperature tool associated with this sampler and the Von Herzen thermometer device.

Two samples were obtained. The first sample was taken just below the open casing at a sub-bottom depth of approximately 81 m. Upon retrieval of the probe, we found evidence that the sampler had entered soft sediments, presumably associated with mud collapse in the upper part of the sediment column. The second sample was obtained, again associated with temperature measurements, at a depth of approximately 325 m into basement. Only in the overflow tube of the sampling device did some fine suspended mud appear, but both the stainless-steel-coil samples were essentially free of particulates. The suspended material consisted of a mixture of calcite and the clay minerals smectite, kaolinite, and illite (M. A. Holmes, pers. comm., 1985). Especially because of the careful lowering of the tool on the sand line and the subsequent lowering of the pipe after the device was

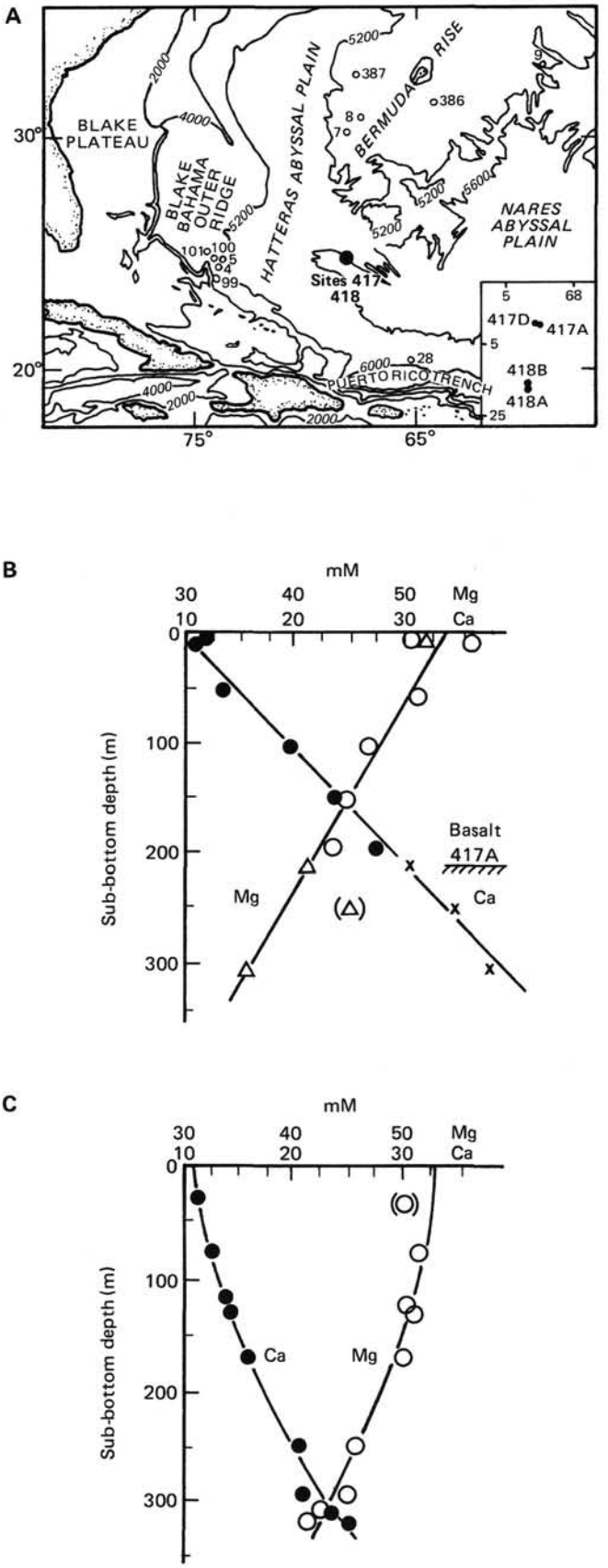

Figure 40. A. Location of DSDP Sites 417 and 418. B. Ca^{2+} and Mg^{2+} concentration depth profiles—Holes 417A and 417D. C. Ca^{2+} and Mg^{2+} concentration depth profiles—Hole 418.

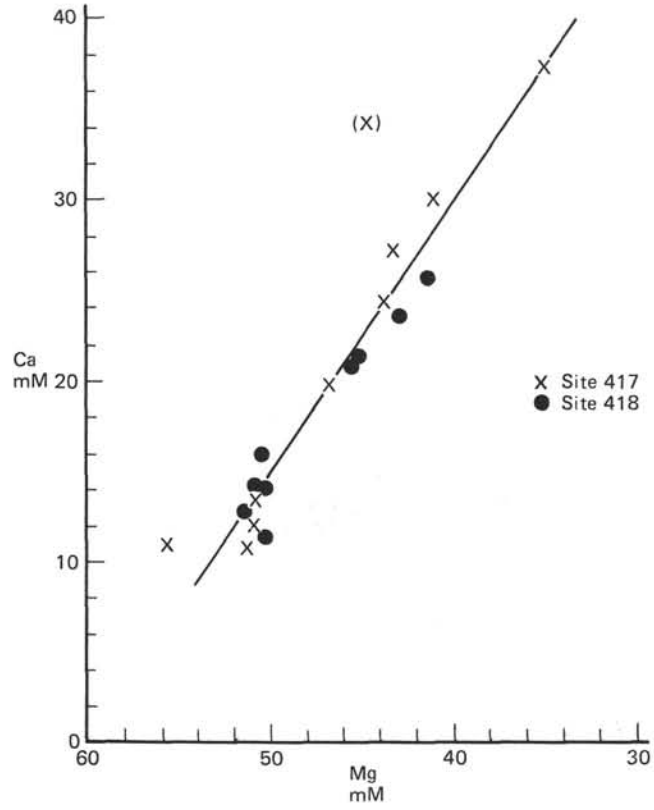

Figure 41. Correlation between Ca^{2+} and Mg^{2+} in interstitial waters of Sites 417 and 418 (Gieskes and Reese, 1980); $\Delta Ca/\Delta Mg = -1.45 \pm 0.1$.

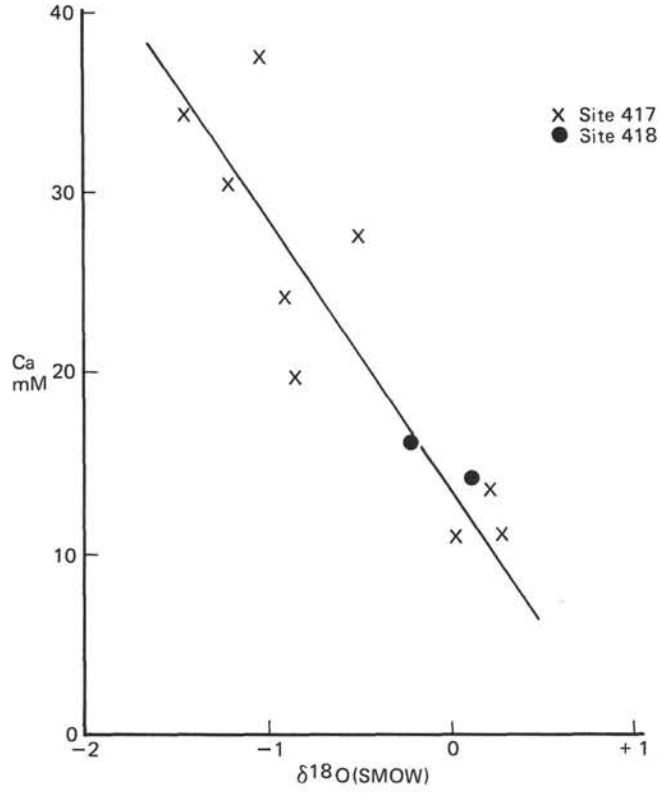

Figure 42. $\delta^{18}O(H_2O)$ vs. Ca^{2+} in interstitial waters of Sites 417 and 418. SMOW = standard mean ocean water.

seated in the bottom of the pipe, we are convinced that we obtained two representative samples. Temperature measurements in the deeper part of the hole, however, suggest that some downhole mixing may have occurred as a result of surface seawater having been pumped to a depth of 50 m above the sampling depth.

Chemical Analyses

Methodologies included the following:

pH, alkalinity	Semiautomatic titration in Metrohm titrator; alkalinity ±3%
Ca	EGTA titration (Gieskes, 1974), but with >95% of EGTA added as an extra precaution before buffer addition; accuracy ±1%
Mg	EDTA titration for total alkaline earths (Gieskes, 1974) and subsequent subtraction of Ca; accuracy ±1%
SO_4	Dionex ion chromatography; accuracy ±3%
NO_3	Colorimetry using Cd reduction and subsequent determination of NO_2 by diazotization; accuracy ±2 μM using 0.5-cm^3 samples
SiO_2	Colorimetry with molybdate blue method; accuracy ±2%
Cl	Mohr titration with silver nitrate; accuracy ±0.3%
Fe	Colorimetry using orthophenantroline method; accuracy 3%
NH_4	Colorimetry with phenol-hypochlorite method; accuracy ±3 μM using 0.5-cm^3 samples

We were successful only in determining potassium tentatively by Dionex ion chromatography.

Results

In this study, we analyzed five samples: surface seawater, which is relevant because the original hole was filled with surface seawater; Barnes No. 1 (BAW-1); and Barnes No. 2 (BAW-2), which was sampled from the first stainless-steel coil (A), from the second stainless-steel coil (B), and from the overflow tube (diluted with distilled water).

The data for these samples are presented in Table 16. In Table 17 we present the differences in the chemistry of present-day surface seawater and borehole waters. Note that surface seawater has a considerably higher chlorinity than bottom water (Cl = 590 mM vs. Cl = 557 mM, a difference of about 5.9%) and is thus readily distinguishable from bottom water. In the diluted BAW-2 sample, dissolved silica values are too low, probably as a result of uptake on the clay present in this sample.

Discussion

Sample BAW-1

The BAW-1 sample was taken in soft mud, about 9 m below the casing of the hole. Before reentry, surface seawater was pumped down the pipe, but pumping was halted upon reentry. After initially lowering the pipe approximately 40 m, the Barnes-Uyeda tool was lowered on the sand line and seated in the bottom of the pipe. Subsequently the pipe was lowered to below the casing. The sample showed evidence of having been in soft mud, presumably caused by a previous flow-in of the hole. Temperature data taken in the pipe show little evidence of downward displacement of water during lowering of the tool. Thus, we can assume that a valid sample was taken.

A substantial amount of dissolved iron occurs, presumably from iron contamination in the cased section by corrosive release from the casing. Therefore, either downward mixing of pipe water could have occurred before reentry, or such mixing could have been induced by the lowering of the pipe and tool.

Table 16. Chemical composition of borehole waters, Site 418.

Sample	pH	Alkalinity meq/dm^{-3}	Ca mM	Mg mM	Cl mM	SO_4 mM	NO_3 μM	NH_4 μM	Fe μM	H_4SiO_4 μM
Surface seawater	8.2	2.35	11.05	56.8	590	30.5	0	5	—	0
BAW-1	6.88	5.35	12.17	55.4	576	28.5	12.5	36	[c]167	31
BAW-2-A	7.69	1.66	47.0	39.1	585	28.0	3	4	0	130
BAW-2-B	8.07	1.65	48.7	37.6	585	27.5	4	6	—	142
BAW-2-overflow	—	—	32.6	27.8	425	19.4	—	10	—	50
BAW-2-corrected to Cl = 585	—	—	44.9	38.3	(585)	26.7	—	—	—	69
Bottom water	—	—	10.50	53.8	[a]575	28.8	22.5	—	—	[b]55
IAPSO standard seawater			10.55	54.0	559	28.9	—	—	—	—

[a] Estimated from salinity profile of Broecker and Peng (1983).
[b] Estimated from Broecker and Peng (1983) and GEOSECS data.
[c] Sample showed visible precipitation of $Fe(OH)_3$.

Table 17. Differences in concentration between deep borehole waters of Hole 418A and surface seawater.

Sample	ΔCa mM	ΔMg mM	ΔCa/ΔMg	ΔCl mM	ΔSO_4 mM	ΔNO_3 μM	ΔH_4SiO_4 μM	Δ(Na+K)[a] mM
BAW-2-A	+36.0	−17.7	−2.03	−5	−2.5	+3	+130	−48
BAW-2-B	+37.7	−19.0	−1.98	−5	−2.9	+4	+140	−49

[a] By charge balance calculation.

Lowering the pipe alone would cause little mixing because the outside diameter of the pipe is considerably smaller than the inside diameter of the casing (G. Foss, pers. comm., 1985). However, the Barnes-Uyeda tool may have pushed down some pipe water, though presumably little. For instance, under similar operating conditions, good samples were obtained during Leg 92 (Gieskes et al., in press). We will assume, therefore, that a pristine sample was taken.

The chlorinity of the sample is between that of surface water and bottom water. Similarly dissolved NO_3^- is, at 12.5 μM, about 50% of the bottom-water value, and dissolved silica roughly 50% of the bottom-water concentration. Using a number of 50%, we calculate a chlorinity of Cl = 574 mM, i.e., near the observed value of Cl = 576 mM. We interpret this observation in terms of a gradual downhole mixing of bottom seawater into the cased section, which was originally filled with surface seawater. That such mixing may occur was demonstrated by Luheshi (1983), although, of course, the density of surface seawater at bottom-hole temperatures is greater than that of bottom water.

The slightly increased concentration of Ca^{2+} is matched by that of alkalinity and is probably the result of $CaCO_3$ dissolution at the relatively low pH of the water. A change in Mg^{2+}, if any, is not significant.

Again, the sample does not indicate any significant change in major ion chemistry, but NO_3^-, H_4SiO_4, and Cl^- concentrations suggest possible downhole mixing of bottom water during the life of the hole. Indeed, the lack of any sediment signal in the water composition suggests that the sediment may have collapsed owing to the reintroduction of the pipe. However, we see no evidence that actual downhole flow of water has occurred in the past.

Sample BAW-2

Because circumstances dictated that we had only one chance to obtain basement water, we decided to obtain a sample at about 325 m into basement. Again, the sampling for BAW-2 was carried out in conjunction with temperature measurements in a manner similar to the sampling in the upper part of the hole. Any contamination from bottom waters can be ruled out because surface water was pumped in to a depth of only about 50 m above sampling depth. If anything, contamination would have been due to mixing with surface water during vigorous pumping of surface seawater to a depth of 50 m above our sampling depth. This surface water would have mixed to a certain unspecified extent with bottom-hole water. Thus, any observed changes in chemistry should constitute minimum values.

An intriguing problem is the small amount of NO_3^- present in the sample. Surface waters generally have no NO_3^- (Table 16), or, if they do, the concentrations are at least well below 0.5 μM. Could the concentration of NO_3^-, therefore, indicate downhole mixing of NO_3^- to a degree that 10%–15% of the originally pumped-in surface water was replaced by bottom water? This would mean that the hole must have been open for a considerable amount of time before sediment collapse sealed it off. Certainly, sample BAW-1 appears to show evidence of downhole mixing. Unfortunately we do not have a precise estimate of the chlorinity of the originally introduced surface water or of the original dissolved nitrate, but the slightly lower Cl = 585 mM in BAW-2, when compared with present surface water of Cl = 590 mM, is compatible with a 10% bottom-water component. Naturally, these arguments are highly speculative.

The most striking aspect of the water-sample chemistry is the relatively large increase in Ca^{2+} when compared with the decrease in Mg^{2+}. The change in calcium is more than twice as large as in the lowermost interstitial-water sample in the sediment column (Fig. 40). The ratio of the concentration changes is $\Delta Ca/\Delta Mg = -2.0$, larger than at either Site 417 or 418. The decrease in sulfate is very small (Table 17). From application of charge-balance considerations, a decrease in $(Na^+ + K^+)$ of about 50 mM is then expected. Preliminary data indicate small decreases in K^+, so that the cation balance is mostly made up by the loss of Na^+.

Dissolved silica concentrations range from 130 to 142 μM, i.e., near the value of quartz solubility. This observation is intriguing because of the only sporadic occurrence of quartz in the basalt and the higher than expected dissolved silica in an environment dominated by basaltic materials (c.f. Hole 395A, McDuff, 1984).

In the following, we present two scenarios that may explain these observations. Without data on the $\delta^{18}O$ of the water and the $^{87}Sr/^{86}Sr$ of the dissolved strontium, quantification of water/rock ratios is extremely difficult.

Reaction in the Hole

Though at low temperatures, reaction rates involving basalt alteration should be extremely small, reaction could have occurred with volcanic material in the hole, either suspended or in the wall of the hole. Thus, one expects the reaction to occur at high water/rock ratios. Indeed, assuming a 12% CaO content in the basalts and an increase in Ca^{2+} of 37 mM in the solution, a water/rock ratio of about 58 is obtained. This estimate assumes no precipitation of $CaCO_3$ or of any other Ca mineral phase. Significant precipitation of carbonate is ruled out because of the low alkalinity of the surface water. Of course, this calculation assumes complete release of all Ca^{2+} by the rock. If only 10% of the rock is altered, which is a more common observation from bulk chemical analyses, the actual water/rock ratio would be about 6 or perhaps lower. If this is true, then for every cm^3 of water, about 0.17 kg (about 65 cm^3) of rock must have undergone alteration. In a 30-cm-diameter hole, a 1-cm-thick layer would require about 45 cm^3 of rock to be altered to 10%, implying that only about 1.5 cm of the surrounding basalts have been altered. This is, of course, purely a mass-balance calculation, and for complete alteration (and total loss of CaO), a much thinner layer of rock is required. At these high water/rock ratios, the effect on the $\delta^{18}O$ of the borehole waters would hardly be noticeable (Lawrence et al., 1976) and would cause a change of no more than $-0.5‰_o$ and probably less.

As mentioned, the dissolved silica values are curiously low, especially because control by quartz is unlikely. For instance, McDuff (1984) notes a value of >700 μM in the sample obtained from Hole 395A. One way of interpreting this observation is that the noted changes are not the result of reactions in the hole but rather are due to exchange by transport through formation fluids in the rocks.

Exchange with Surrounding Rocks

Before discussing the possibility of exchange of dissolved constituents with the surrounding rocks by transport of dissolved constituents from or into the potential water reservoir in the rocks, it will be appropriate to estimate whether diffusive processes could be the main cause for the exchange. If the average porosity of the formation is between 5% and 10%, the bulk diffusion coefficient can be approximated by the formula

$$D_b = p^2 D_o,$$

where p = porosity, and D_o = pure solution diffusion coefficient ($\sim 10^{-5} cm^2/s$). For the aforementioned porosity values, this yields $D_b = 0.3 \times 10^{-7} cm_b^2/s$ to $1.0 \times 10^{-7} cm_b^2/s$, where the subscript b denotes the bulk formation. McDuff (1984) assumed a value of $10^{-6} cm_b^2/s$ for Site 395, corresponding to a porosity of 30%.

For the range of diffusion coefficients of $0.3 - 1.0 \times 10^{-7}$ cm_b^2/s, we calculate an average diffusive path length of $X = (2D_b t)^{9/2}$ of 4–7 cm_b over the 8-yr period since the hole was drilled.

McDuff (1984), assuming diffusion from a porous bed into a well-stirred reservoir (the hole), solved the diffusion equation and derived a relation between the concentration in the hole and in the formation (Crank, 1970):

$$C_{hole} = (C_{formation} - C_{initial})(1 - \exp\Omega \operatorname{erfc}\Omega) + C_{initial},$$

where $\Omega = D_b t/r^2$, r is the radius of the hole, and $\Omega < 1$. Applying this formula for the dissolved calcium, we obtain

$$\begin{aligned} \text{for} \quad & D_b = 10^{-6} cm_b 2/s \; C_{formation} = 85 \text{ mM}; \\ & D_b = 10^{-7} cm_b 2/s \; C_{formation} = 130 \text{ mM}; \\ & D_b = 3 \times 10^{-8} cm_b 2/s \; C_{formation} = 210 \text{ mM}. \end{aligned}$$

These concentrations do not appear impossible, especially according to our own observations of sediments intercalated in basalts (e.g., Site 446, Gieskes and Johnson, 1981, 120 mM; Site 528, Gieskes et al., 1984, 80 mM; as well as at other sites). In these investigations, concentration gradients in the overlying sediments were diffusive in nature—i.e., diffusive transport through the sediments could explain the essentially linear gradients. Thus much of the calcium signal could indeed stem from the surrounding rocks owing to transport processes rather than to reaction with borehole waters.

If this is true, then the $\delta^{18}O$ should show a considerable decrease. Assuming $\Delta\delta^{18}O/\Delta Ca^{2+}$ for the overlying sediments, a change in $\delta^{18}O$ of $-2.2‰_o$ might be expected. This change would be much larger than that of high water/rock ratio interactions in the hole itself.

Often, increases in chloride have been observed in conjunction with large concentration changes in Ca^{2+}, presumably as a result of water lost to alteration minerals. Thus the presence of a Cl^- concentration similar to that of surface seawater may not necessarily mean that exchange does not occur with the surrounding rocks.

Chemical Changes

Unfortunately, little is known about the quantitative aspects of exchange of ions during low-temperature alteration of basaltic materials, at least in an experimental setting. Undoubtedly, during early alteration of basalts, Ca^{2+} is released and $CaCO_3$ is precipitated, especially when fresh seawater flows through basalts having high water/rock ratios, thus supplying a source of CO_3^{2-} ions for $CaCO_3$ precipitation. Debate occurs about release or uptake of Mg^{2+} by the rock during early alteration, but the loss of dissolved K^+ is well recorded, though little evidence exists on the fate of Na^+. McDuff (1981), in his analysis of DSDP interstitial-water Ca^{2+} and Mg^{2+} gradients, showed that younger sites commonly show $|\Delta Ca^{2+}/\Delta Mg^{2+}| \leq 1$ (c.f. his observation in Site 395; McDuff, 1984). With age and total disappearance of Mg^{2+} in underlying basement, this ratio will exceed 1.0, as in the interstitial waters of Sites 417 and 418 (Gieskes and Reese, 1980). The correlation in sample BAW-2 yields a ratio of $\Delta Ca^{2+}/\Delta Mg^{2+} = -2$. This high ratio would classify the change in Ca^{2+} and Mg^{2+} as being characteristic of older sites or, rather, as being Mg^{2+} depleted. Thus the end-member ($C_{formation}$) would presumably be devoid of Mg^{2+} and should show complete depletion in K^+ and a large depletion in Na^+.

In Figure 43, we have extrapolated our data to $Mg^{2+} = 0$ mM, yielding concentrations of $Ca^{2+} = 120$ mM, $H_4SiO_4 = 400$ μM, and $K^+ \sim 0$ mM, as predicted. Real increases in Ca^{2+} may well exceed these concentrations and fall in the range predicted for low porosities.

Conclusions

The sample obtained at 350 m into basement of Hole 418A shows considerable changes in chemical composition when compared with originally introduced seawater (about 8 yr ago). Two possibilities were presented to explain these changes, but further work on the oxygen isotope composition of this water may help to delineate which mechanism is the more realistic. Small changes in ^{18}O are predicted if reactions in the hole are responsible; larg-

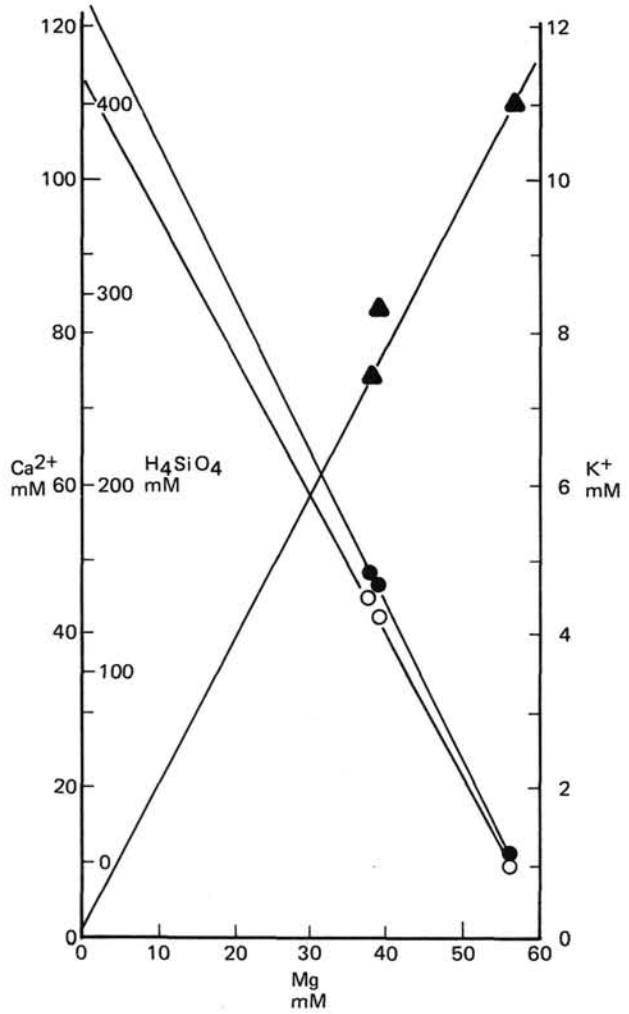

Figure 43. Extrapolation of Ca^{2+} (·), K^+ (Δ), and H_4SiO_4 (o) to Mg^{2+} = 0 mM; end-member concentrations: Ca^{2+} = 125 mM; K^+ = 0 mM; H_4SiO_4 = 400 μM.

er changes are predicted if exchange occurs with fluids having large concentration anomalies trapped in the surrounding rocks. Studies of $^{87}Sr/^{86}Sr$ will also distinguish these mechanisms.

SUMMARY AND CONCLUSIONS

Eight years after it was originally drilled on DSDP Leg 53, Hole 418A was reentered to retrieve a logging tool lost in the hole and to conduct logging and geophysical experiments in the hole to determine for the first time the *in-situ* geophysical behavior of old oceanic basement. Specific scientific objectives were as follows:

1. To determine the *in-situ* velocity structure at a site in old crust and to determine whether Layers 2A, 2B, and 2C are present and if they correspond to the same lithologies as those in Hole 504B.
2. To determine permeability of the old oceanic crust.
3. To determine the porosity vs. depth function for the site. These data, together with data from Hole 504B, would make it possible to determine whether or not the extrusive section had become sealed by alteration products and to determine the porosity–velocity systematics for Layer 2.
4. To determine the thickness of the magnetic layer in old crust.
5. To determine whether or not convection and underpressures persist in old crust.
6. To sample and determine the chemistry of water in equilibrium with old basement.
7. To determine the direction and magnitude of *in-situ* stress.
8. To determine the temperature profile in old crust, and from this, to infer whether heat transfer in old oceanic basement is by convection or conduction.
9. To determine the eruptive history of the Layer 2 extrusive pile from variations in magnetic susceptibility and natural remanent magnetization intensity, inclination, and declination vs. depth values.
10. To determine the magnitude, direction, and origin of seismic anisotropy in Layer 2.
11. To determine whether or not sub-basement seismic reflectors are present in the crust.

To these ends, the ship returned to Hole 418A, which was drilled through pillow basalts, massive basalts, and into the top of the dike-transition zone to a sub-basement depth of 544 m on Legs 52 and 53 (Figs. 1 and 4). The hole was thought to have a logging tool lodged in the overlying sediments. After reentering the hole, we found that extensive bridges had developed in the uncased sediments during the interim but that the tool was not lodged in the hole, so we eventually succeeded in reopening it to total depth (878 mbsf, 544 m sub-basement) for further experiments and drilling. During the following 2 weeks, we conducted 14 separate runs in the hole with 11 tools (Fig. 5 and Table 18), including three that had never been run before in a marine environment (the U.S. Geological Survey susceptibility tool, the German three-axis magnetometer, and the TAM packer).

The hole was nearly to gauge (10.25 in.) throughout, which is itself unusual, allowing virtually all the tools to operate flawlessly. The only exceptions were the deep Laterolog, which was improperly calibrated; the packer, which failed to seat; and the borehole televiewer, which caught on a ledge just outside the pipe. The only limitations experienced were those imposed by a bridge at 479 mbsf, which required that the hole be logged in stages, and those imposed by time constraints, which prevented us from running several tools in the upper third of the basement and in the lower 79 m after the hole was reopened toward the end of the leg.

Results

Since the hole was thought to have been isolated from the water column by cavings for the past 8 yr, a limited temperature-measurement and water-sampling program was conducted in the hole immediately after reentry. The temperature measurements,

Table 18. Summary of depths and measurements made with various borehole tools, ODP Leg 102, Hole 418A.

Tools run	Sub-bottom interval (mbsf)
Temperature probes; water sampler	52–81; 81
Temperature probes; water sampler	624–649; 649
Velocity; induction; natural gamma; spherically focused log; caliper	327–788
Density; porosity; spectral gamma	0–462; 462–790
Resistivity; natural gamma	490–785
Magnetic susceptibility; conductivity	295–800
Three-axis magnetometer; gradiometer	465–790
Multichannel sonic: Vp, Vs	365–800
Borehole seismometer	343; 366; 406; 555; 655; 755
Packer	347; 465; 517
Borehole televiewer	360

conducted in the sediments between 52 and 81 mbsf and in the basement between 624 and 649 mbsf, indicate that heat transfer is conductive at the site. The water sample taken in the basement at 649 m is strongly enriched in Ca^{2+} and depleted in Mg^{2+} and K^+, suggesting exchange with basement water. A remote possibility exists that these chemical changes are due to reaction with the basalts lining the borehole, but this cannot be determined until oxygen isotope studies are completed in shore-based laboratories.

In general, the logs confirm and refine the lithologic units defined on Legs 52 and 53 on the basis of petrology (Fig. 44); the log values of velocity, density, porosity, and magnetic susceptibility often approach or match laboratory values obtained on core material. In particular, the massive basalts between 676 and 687 mbsf display compressional wave velocities of 4.2 and 6.3 km/s, shear wave velocities as high as 3.3 km/s, Vp and Vs semblance values greater than 0.5, densities as high as 2.89 g/cm^3, apparent porosities as low as 7.5%, and resistivities exceeding 1000 ohm-m.

On the other hand, the pillow basalts, which compose 85% of the section logged, display compressional and shear wave velocities ranging, respectively, from 2.9 to 7.0 km/s and from 2.6 to 3.4 km/s; lower values of semblance; densities of 2.00–2.97 g/cm^3; apparent porosities ranging from 6% to 48%; and resistivities of 6–2000 ohm-m. The pronounced difference in velocity and frequency content of multichannel waveforms in pillow and massive basalts is shown in Figure 45. Although distinct from massive basalts, the pillow basalts in Hole 418A also behave differently from pillow basalts in young crust: the velocities and densities are much higher and the porosities are lower, indicating the infilling and sealing of interpillow voids by alteration products. Since the compressional wave velocity throughout the section matches that of Layer 2B, but the natural gamma count from the top 190 m is high, we conclude that the upper part of the section was once much more porous and represents paleo-Layer 2A. Interestingly, the boundary between this unit and the rest of the section is also marked by a thick smectite-sealed breccia (Subunit 6A), a sharp magnetic polarity reversal (Fig. 44), and a pronounced decrease in magnetic susceptibility from an average apparent value of about 1.5×10^{-3} cgs units to about 0.5×10^{-3} cgs units. Below 605 m, however, the susceptibility climbs sharply again to values averaging 2.0×10^{-3} cgs units and exceeding 4.0×10^{-3} cgs units in several thin zones (Fig. 44). Positions computed from the borehole magnetometer measurements in the lower basalt units show general agreement with Cretaceous polar-wandering paths, determined from land-based paleomagnetic data.

In addition to measurements of the borehole wall, a major two-ship seismic experiment was conducted on Leg 102, using the R/V *Fred H. Moore* as a shooting ship and a three-component geophone clamped sequentially at five different depths in the basalt section of Hole 418A. Specifically, an oblique seismic experiment was conducted, shot points being along radial lines and circles centered at the borehole, to determine the velocity structure of the upper crust and to determine azimuthal variations in velocity and attenuation. A close-spaced seismic-reflection survey was also made in this area to obtain basement topographic correction, and a long-range sonobuoy survey was made around the site to search for deep layers. According to preliminary results, the old crust is anisotropic in its transmission of seismic waves, as indicated by both the particle motions and the amplitudes of waveforms received in the borehole from shot points at different azimuthal positions (Fig. 46). This anisotropy may be related to *in-situ* stress or to structural features in the basement. The quality and dynamic range of the digitally recorded waveforms are vastly superior to those of previous surveys of this type. If deep reflectors exist in the crust or at the Moho, bringing them into sharp focus should be possible by processing the high-quality field data with beam-steering and stacking techniques.

REFERENCES

Anderson, R. H., Langseth, M. G., and Sclater, J. G., 1977. The mechanism of heat transfer through the floor of the Indian Ocean. *J. Geophys. Res.*, 82:3391–3409.

Anderson, R. N., Honnorez, J., et al., 1985. *Init. Repts. DSDP,* 83: Washington (U.S. Govt. Printing Office).

Aumento, F., Melson, W. G., et al., 1977. *Init. Repts. DSDP,* 37: Washington (U.S. Govt. Printing Office).

Becker, K., Langseth, M. G., and Hyndman, R. D., 1984. Temperature measurements in Hole 395A, Leg 78B. *In* Hyndman, R. D., Salisbury, M. H., et al., *Init. Repts. DSDP,* 78B: Washington (U.S. Govt. Printing Office), 689–698.

Bosum, W., and Rehli, H.-J., 1985. Bau und Erprobung eines 3-D-Bohrlochmagnetometers. *Geol. Jahrb.,* E28, 191–217.

Broecker, W. S., and Peng, T. H., 1983. *Tracers in the Sea:* Palisades, NY (Eldigio Press).

Cann, J. R., Langseth, M. G., Honnorez, J., Von Herzen, R. P., White, S. M., et al., 1983. *Init. Repts. DSDP,* 69: Washington (U.S. Govt. Printing Office).

Crank, J., 1970. *The Mathematics of Diffusion* (1st ed., rev.): London (Oxford Univ. Press).

Davis, R. R., Hall, J. E., and Boutemy, Y. L., 1981. A dual porosity CNL logging system. *Soc. Pet. Eng. AIME Pap.* 10296.

Donnelly, T., Francheteau, J., Bryan, W., Robinson, P., Flower, M., Salisbury, M., et al., 1980. *Init. Repts. DSDP,* 51, 52, 53: Washington (U.S. Govt. Printing Office).

Fertl, W. H., and Frost, E., Jr., 1980. Evaluation of shaly clastic reservoir rocks: *J. Pet. Technol.,* 32:1641–1646.

Gieskes, J. M., 1973. Interstitial water studies, Leg 15. Alkalinity, pH, Mg, Ca, Si, PO_4 and NH_4. *In* Heezen, B. C., McGregor, I. G., et al., *Init. Repts. DSDP,* 20: Washington (U.S. Govt. Printing Office), 813–829.

_____, 1974. Interstitial water studies, Leg 25. *In* Simpson, E. S. W., Schlich, R., et al., *Init. Repts. DSDP,* 25: Washington (U.S. Govt. Printing Office), 361–394.

_____, 1983. The chemistry of interstitial waters of deep sea sediments: interpretation of deep sea drilling data. *Chem. Oceanogr.* 8: 221–269.

Gieskes, J. M., and Johnson, J., 1981. Interstitial-water studies, Leg 58. *In* Larson, R. L., Schlanger, S. O., et al., *Init. Rpts. DSDP,* 61: Washington (U.S. Govt. Printing Office), 607–611.

Gieskes, J. M., Johnston, K., and Boehm, M., 1984. Interstitial-water studies, Leg 74. *In* Moore, T. C., Jr., Rabinowitz, P. D., et al., *Init. Repts. DSDP,* 74: Washington (U.S. Govt. Printing Office), 701–711.

Gieskes, J. M., Kastner, M., Erzinger, J., Boulegue, J., and Hart, S. R., in press, Geochemical studies in Hole 504B, Leg 92. *In* Leinen, M., Rea, D. K., et al., *Init. Repts. DSDP,* 92: Washington (U.S. Govt. Printing Office).

Gieskes, J. M., and Lawrence, J. R., 1981. Alteration of volcanic matter in deep sea sediments: evidence from the chemical composition of interstitial waters from deep sea drilling cores. *Geochim. Cosmochim. Acta,* 45:1687–1703.

Gieskes, J. M., and Reese, H., 1980. Interstitial water studies, Legs 51–53. *In* Donnelly, T., Francheteau, J., Bryan, W., Robinson P., Flower, M., Salisbury, M., et al., *Init. Repts. DSDP,* 51, 52, 53, Pt. 2: Washington (U.S. Govt. Printing Office), 747–751.

Hamano, Y., Nishitani, T., and Kono, M., 1979. Magnetic properties of basalt samples from Deep Sea Drilling Project Holes 417D and 418A. *In* Donnelly, T., Francheteau, J., Bryan, W., Robinson, P., Flower, M., Salisbury, M., et al., *Init. Repts. DSDP,* 51, 52, 53, Pt. 2: Washington (U.S. Govt. Printing Office), 1391–1405.

Holland, H. D., 1984. *The Chemical Evolution of the Atmosphere and Oceans:* Princeton, NJ (Princeton Univ. Press).

Honnorez, J., Von Herzen, R. P., et al. 1983. *Init. Repts. DSDP,* 70: Washington (U.S. Govt. Printing Office).

Houtz, R., and Ewing, J., 1976. Upper crustal structure as a function of plate age. *J. Geophys. Res.,* 81: 2490–2498.

Hyndman, R. D., Salisbury, M. H., et al., 1984. *Init. Repts. DSDP,* 78B: Washington (U.S. Govt. Printing Office).

Landolt-Börnstein, 1985. Numerical data and functional relationships in science and technology, new ser., group V. *In* Fuchs, K., and Soffel, H., *Geophysics of the Solid Earth, the Moon and the Planets*, subv. B of *Geophysics and Space Research*, v. 2: Heidelberg (Springer-Verlag).

Larson, R. L., Schlanger, S. O., et al., 1981. *Init. Repts. DSDP*, 61: Washington (U.S. Govt. Printing Office).

Lawrence, J. R., and Gieskes, J. M., 1981. Constraints on water transport and alteration in the oceanic crust from the isotopic composition of pore water. *J. Geophys. Res.*, 86:7924–7934.

Lawrence, J. R., Gieskes, J., and Anderson, T. F., 1976. Oxygen isotope material balance calculations, Leg 35. *In* Hollister, C. D., Craddock, C., et al., *Init. Repts. DSDP*, 35: Washington (U.S. Govt. Printing Office), 507–512.

Lawrence, J. R., Gieskes, J. M., and Broecker, W. S., 1975. Oxygen isotope and cation composition of DSDP pore waters and alteration of Layer 2 basalts. *Earth Planet. Sci. Lett.*, 27:1–10.

Leinen, M., Rea, D. K., et al., in press, *Init. Repts. DSDP*, 92: Washington (U.S. Govt. Printing Office).

Levi, S., 1979. Paleomagnetism and some magnetic properties of basalts from the Bermuda triangle. *In* Donnelly, T., Francheteau, J., Bryan, W., Robinson, P., Flower, M., Salisbury, M., et al., *Init. Repts. DSDP*, 51, 52, 53, Pt. 2: Washington (U.S. Govt. Printing Office), 1363–1378.

Levi, S., Bleil, U., Smith, B. M., and Rigotti, P. A., 1979. Compilation of paleomagnetic and rock magnetic results of basalt samples from Deep Sea Drilling Project Legs, 51, 52, and 53. *In* Donnelly, T., Francheteau, J., Bryan, W., Robinson, P., Flower, M., Salisbury, M., et al., *Init. Repts. DSDP*, 51, 52, 53, Pt. 2: Washington (U.S. Govt. Printing Office), 1337–1350.

Luheshi, M. N., 1983. Estimation of formation temperature from borehole measurements. *Geophys. J. R. Astron. Soc.*, 74:749–776.

McDuff, R. E., 1978. Conservative behavior of calcium and magnesium in the interstitial waters of marine sediments: identification and interpretation [Ph.D. thesis], Univ. California, San Diego.

_____, 1981. Major cation gradients in DSDP interstitial waters: the role of diffusive exchange between seawater and upper ocean crust. *Geochim. Cosmochim. Acta*, 45: 1705–1713.

_____, 1984. The chemistry of interstitial waters from the upper ocean crust, Site 395, DSDP Leg 78B. *In* Hyndman, R. D., Salisbury, M. H., et al., *Init. Repts. DSDP*, 78B: Washington (U.S. Govt. Printing Office), 795–799.

Matthews, D. J., 1939. Table of velocity of sound in pore water and in seawater: London (Admiralty, Hydrographic Dept.).

Melson, W. G., Rabinowitz, P. D., et al., 1978. *Init. Repts. DSDP*, 45: Washington (U.S. Govt. Printing Office).

Moberly, R., Schlanger, S. O., et al., in press, *Init. Repts. DSDP*, 89: Washington (U.S. Govt. Printing Office).

Mooney, H. M., and Bleifuss, R., 1953. Magnetic susceptibility measurements in Minnesota, Part II: Analysis of field results. *Geophysics*, 18:383–393.

Mottl, M. J., Anderson, R. N., Jenkins, W. J., and Lawrence, J. R., 1983. Chemistry of waters sampled from basaltic basement in Deep Sea Drilling Project Holes 501, 504B, and 505B. *In* Cann, J. R., Langseth, M. G., Honnorez, J., Von Herzen, R. P., White, S. M., et al., *Init. Repts. DSDP*, 69: Washington (U.S. Govt. Printing Office), 475–483.

Mottl, M. J., Druffel, E. R. M., Hart, S. R., Lawrence, J. R., and Saltzman, E. S., 1985. Chemistry of hot waters sampled from basaltic basement in Hole 504B, Deep Sea Drilling Project Leg 83, Costa Rica Rift. *In* Anderson, R. N., Honnorez, J., Becker, K., et al., *Init. Repts. DSDP*, 83: Washington (U.S. Govt. Printing Office), 315–328.

Muehlenbachs, K., and Clayton, R. N., 1976. Oxygen and isotope composition of the oceanic crust and its bearing on sea water. *J. Geophys. Res.*, 82:4365–4369.

Ponomarev, V. N., and Nechoroshkov, V. L., 1983. First measurements of the magnetic field within the ocean crust: Deep Sea Drilling Project Legs 68 and 69. *In* Cann, J. R., Langseth, M. G., Honnorez, J., Von Herzen, R. P., White, S. M., et al., *Init. Repts. DSDP*, 69: Washington (U.S. Govt. Printing Office), p. 271–279.

_____, 1984. Downhole magnetic measurements in oceanic crustal Hole 395A on the Mid-Atlantic Ridge. *In* Hyndman, R. D., Salisbury, M. H., et al., *Init. Repts. DSDP*, 78B: Washington (U.S. Govt. Printing Office), 731–739.

Rabinowitz, P. D., Hoskins, H., and Asquith, S. M., 1979. Geophysical site summary results near Deep Sea Drilling Project Sites 417 and 418 in the Central Atlantic Ocean. *In* Donnelly, T., Francheteau, J., Bryan, W., Robinson, P., Flower, M., Salisbury, M., et al., *Init. Repts. DSDP*, 51, 52, 53, Pt. 1: Washington (U.S. Govt. Printing Office), 629–669.

Salisbury, M. H., Stephen, R., Christensen, N. I., Francheteau, J., Hamano, Y., Hobart, M., and Johnson, D., 1979. The physical state of the upper levels of Cretaceous oceanic crust from the results of logging, laboratory studies, and the oblique seismic experiment at Deep Sea Drilling Project Sites 417 and 418. *In* Donnelly, T., Francheteau, J., Bryan, W., Robinson, P., Flower, M., Salisbury, M., et al., *Init. Repts. DSDP*, 51, 52, 53, Pt. 2: Washington (U.S. Govt. Printing Office), 1579–1597.

Sayles, F. L., Manheim, F. T., and Chan, K. M., 1970. Interstitial water studies on small core samples, Leg 4. *In* Bader, R. G., Gerard, R. D., et al., *Init. Repts. DSDP*, 4: Washington (U.S. Govt. Printing Office), 401–414.

Schlumberger, Inc., 1972. *Log Interpretation: Vol. 1, Principles:* New York (Schlumberger).

Scott, H. D., Flaum, C., and Sherman, H., 1982. Dual porosity CNL count rate processing. *Soc. Pet. Eng. AIME Pap.* 11146.

Scott., J. H., Seeley, R. L., and Barth, J. J., 1981. A magnetic susceptibility well-logging system for mineral exploration. SPWLA 22nd Ann. Logging Symp. June 23–26, 1981, *Trans.*, Pap. CC.

Vogt, P. R., and Johnson, G. L., 1971. The morphology of the Bermuda Rise, *Deep Sea Res.*, 18: 605–617.

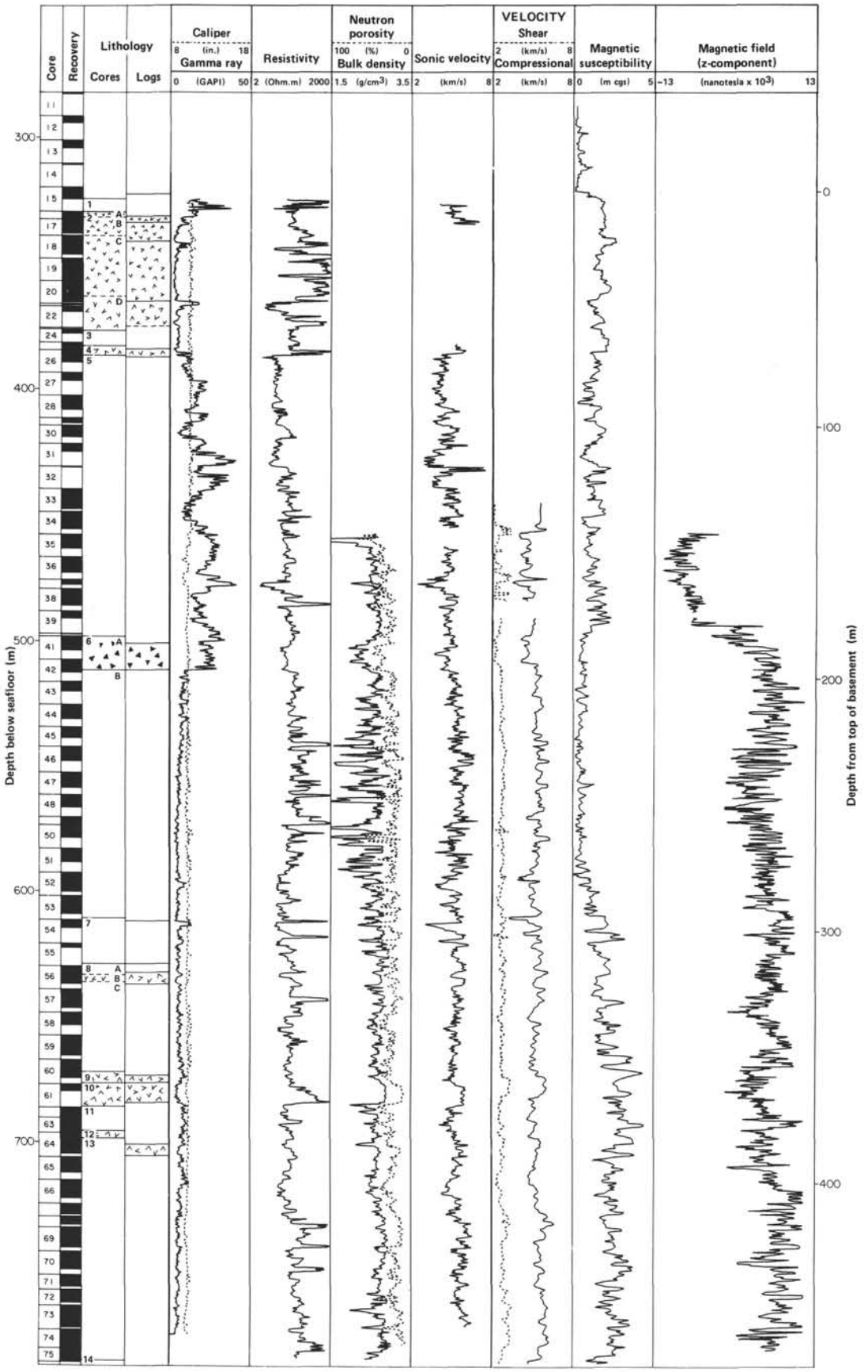

Figure 44. Hole 418A lithology and borehole geophysical measurements made on Leg 102.

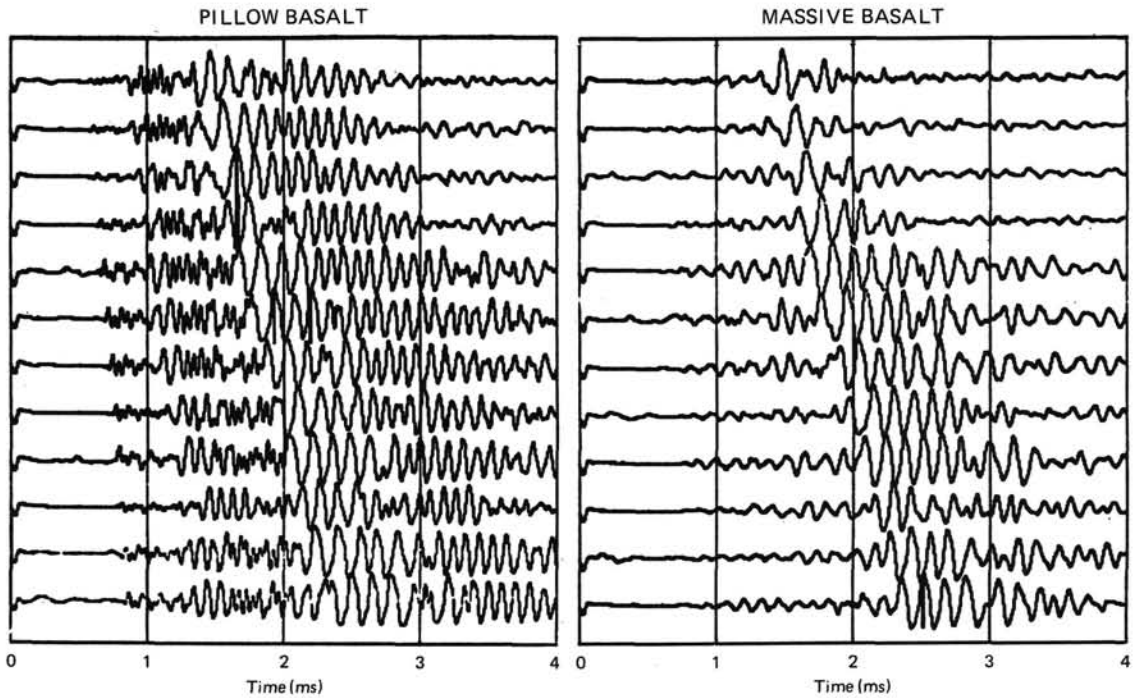

Figure 45. Multichannel sonic waveforms obtained in massive basalt and pillow basalt, Hole 418A, Leg 102.

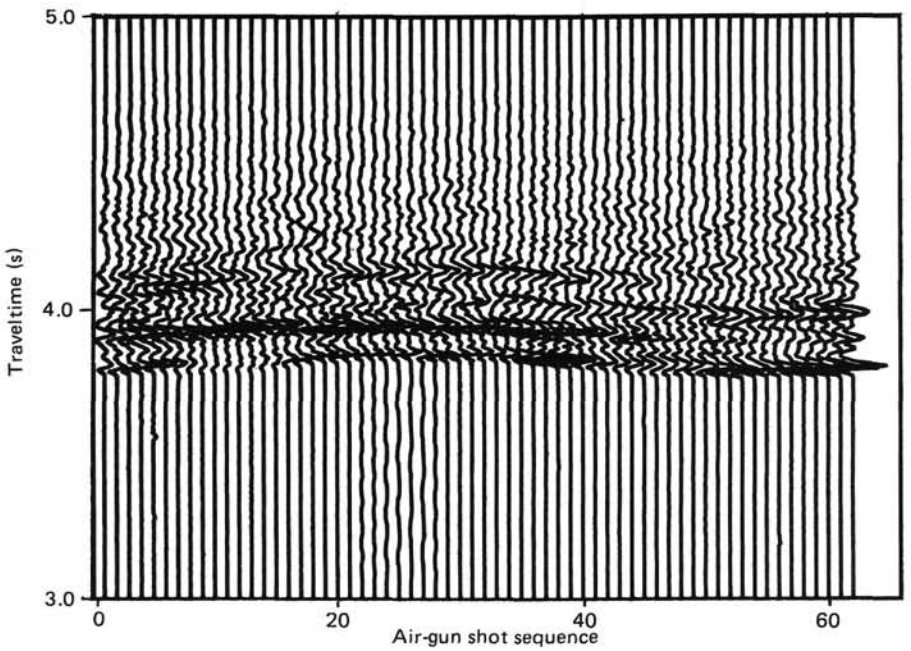

Figure 46. Example of vertical-component waveforms received by a geophone clamped in Hole 418A from an air-gun source deployed by the shooting ship R/V *Fred H. Moore* as it followed a circular course around the *JOIDES Resolution* at a distance of 2 km.